UCSF
UC San Francisco Electronic Theses and Dissertations

Title

Molecular mechanisms that regulate synaptic efficacy at the Drosophila neuromuscular junction

Permalink

https://escholarship.org/uc/item/5w50p18r

Author

Albin, Stephanie D

Publication Date

2006

Peer reviewed|Thesis/dissertation

eScholarship.org
Powered by the California Digital Library
University of California

Molecular Mechanisms that Regulate Synaptic Efficacy at the Drosophila Neuromuscular Junction

by

Stephanie D. Albin

DISSERTATION

Submitted in partial satisfaction of the requirements for the degree of

DOCTOR OF PHILOSOPHY

in

Neuroscience

in the

GRATUATE DIVISION

of the

UNIVERSITY OF CALIFORNIA, SAN FRANCISCO

[redacted]

Date University Librarian

Degree Conferred:..

Copyright 2006

by

Stephanie D. Albin

Acknowledgements

I am very grateful for the people – family, friends, colleagues, and faculty – who have supported me during graduate school. I would first like to thank Grae Davis for being an enthusiastic mentor. He taught me much about science, as well as how to see the "big picture." I can't imagine having completed my Ph.D. without Grae's positive outlook and endless encouragement to back me up.

I would also like to thank everyone, past and present, in the Davis Lab. I have never before worked with such clever, open-minded and stimulating individuals. Not only was lab a fun place to go to everyday, but also our stimulating scientific discussions helped me through all phases of my graduate career.

The graduate program at UCSF is an amazing collection of people. The faculty are friendly and accessible. In addition to my thesis committee, Roger Nicoll, Lily Jan, Cori Bargmann and Kristin Scott, I would like to thank all of the faculty I've been lucky to have interacted with during my time here.

Most of all, I would like to thank my caring family. My parents and my husband have been endlessly supportive and I am lucky to have these people on my side.

Preface

Some of the material contained in this dissertation has been published elsewhere. Chapter 2, *Coordinating Structural and Functional Synapse Development: Postsynaptic Pak Kinase Independently Specifies GluR Abundance and Postsynaptic Morphology*, was published in the *Journal of Neuroscience* (2004) 24, 6871-6879 (Albin and Davis, 2004).

Involvement of Co-authors

Thesis Advisor's Statement

Chapter 2 and chapter 3 of this dissertation contain experiments that were done solely by Stephanie Albin in my laboratory. Chapter 4 contains experiments that Stephanie Albin did in collaboration with Peter Clyne. Stephanie performed the immunofluorescent imaging of the third-instar NMJ and CNS. In addition Stephanie performed all of the S2 cell work and half of the electrophysiology.

Graeme W. Davis, Ph.D.

Molecular Mechanisms that Regulate Synaptic Efficacy at the Drosophila Neuromuscular Junction

by

Stephanie D. Albin

Lily Jan

Chair, Thesis Committee

Abstract

The homeostatic regulation of synaptic efficacy is a mechanism by which the nervous system maintains stability despite changes in cellular excitability that ocurr during development or various types of plasticity. The Drosophila neuromuscular junction

(NMJ) has been used as a model glutamatergic synapse to study two types of homeostatic compensation. The first involves the regulation of synaptic efficacy by increasing postsynaptic glutamate receptor function in response to defects in presynaptic neurotransmitter release. The second type of homeostatic compensation involves the retrograde regulation of presynaptic neurotransmitter release in response to decreases in postsynaptic muscle excitability. This work describes experiments that further characterize the molecular mechanisms that underlie the regulation of postsynaptic receptors and presynaptic neurotransmitter release.

The p21-activated kinase (Pak) signaling pathway has been described as a regulator of postsynaptic glutamate receptor abundance at the NMJ. Here we examine how postsynaptic Pak signaling controls glutamate receptor abundance. In addition, we identify a second genetically separable function of Pak signaling which controls muscle membrane development. Pak signaling is thus required postsynaptically for the coordination of multiple aspects of postsynaptic maturation.

To understand the dynamics of glutamate receptor trafficking at the NMJ, we describe the creation of a modified glutamate receptor subunit that is capable of binding fluorescently conjugated α-bungarotoxin. α-bungarotoxin should only bind surface receptors, and by imaging tagged glutamate receptors over time we can visualize the internalization and insertion of these receptors into the membrane.

The molecular mechanisms underlying the retrograde control of presynaptic neurotransmitter release at the NMJ are not well understood. Here we describe the identification of the first known inhibitor of synaptic homeostasis. Identification of the

pathways through which this inhibitor act may eventually lead to a greater understanding of the mechanisms that regulate homeostasis.

Table of Contents

ACKNOWLEDGEMENTS III

PREFACE IV

ABSTRACT V

TABLE OF CONTENTS IX

LIST OF TABLES AND FIGURES X

CHAPTER ONE: GENERAL INTRODUCTION 1

- REGULATION OF SYNAPTIC EFFICACY DURING SYNAPSE DEVELOPMENT 2
- CONTROL OF SYNAPTIC EFFICACY INDEPENDENT OF DEVELOPMENT 4
- HOMEOSTATIC CONTROL OF EFFICACY: SYNAPTIC SCALING. 5
- HOMEOSTATIC CONTROL OF EFFICACY: RETROGRADE CONTROL OF PRESYNAPTIC RELEASE 7

CHAPTER TWO: COORDINATING STRUCTURAL AND FUNCTIONAL SYNAPSE DEVELOPMENT: POSTSYNAPTIC PAK KINASE INDEPENDENTLY SPECIFIES GLUR ABUNDANCE AND POSTSYNAPTIC MORPHOLOGY 10

- SUMMARY 11
- INTRODUCTION 12
- RESULTS 14
- DISCUSSION 28
- FIGURES AND TABLES 33

CHAPTER THREE: IMAGING GLURIIA RECEPTORS USING ALPHA-BUNGAROTOXIN BINDING SITE TAGGED RECEPTORS 55

- SUMMARY 56
- INTRODUCTION 57
- RESULTS 60
- DISCUSSION 64
- FIGURES 66

CHAPTER FOUR: CALCULUS IDENTIFIES A NOVEL SECRETED INHIBITOR OF SYNAPTIC HOMEOSTASIS AT THE DROSOPHILA NMJ 74

- SUMMARY 75
- INTRODUCTION 76
- RESULTS 79
- DISCUSSION 88
- FIGURES 92

CHAPTER FIVE: GENERAL CONCLUSIONS 106

- POSTSYNAPTIC SENSOR OF EXCITABILITY. 107
- SYNAPTIC SCALING AND THE REGULATION OF POSTSYNAPTIC RECEPTORS 108
- SYNAPTIC HOMEOSTASIS AND THE REGULATION OF PRESYNAPTIC NEUROTRANSMITTER RELEASE. 109

EXPERIMENTAL PROCEDURES 111

REFERENCES 125

List of Figures and Tables

TABLE 2-1. MUTANT ALLELES OF DOCK AND PAK 33

FIGURE 2-1. DECREASED GLURIIA ABUNDANCE AT THE THIRD INSTAR NMJ IN PAK MUTANT ANIMALS 34

FIGURE 2-2. SIMULTANEOUS DISRUPTION OF CDC42 AND RAC IN MUSCLE LEADS TO DECREASED GLURIIA LEVELS. 36

FIGURE 2-3. DECREASED QUANTAL SIZE AND NORMAL HOMEOSTATIC COMPENSATION AT PAK MUTANT NMJ 38

FIGURE 2-4. SYNAPTIC LOCALIZATION OF DOCK 41

FIGURE 2-5. SYNAPTIC LOCALIZATION OF GLURIIA IS DECREASED IN DOCK MUTANTS 43

FIGURE 2-6. DOCK AND PAK ARE SYNAPTICALLY LOCALIZED INDEPENDENTLY OF EACH OTHER 45

FIGURE 2-7. DOCK AND PAK INTERACT GENETICALLY TO REGULATE SYNAPTIC GLURIIA LEVELS 47

FIGURE 2-8. SYNAPTIC LOCALIZATION OF DLG IS DECREASED IN DOCK AND PAK MUTANTS 49

FIGURE 2-9. THE POSTSYNAPTIC PIX-PAK-DOCK SIGNALING SYSTEM 51

SUPPLEMENTAL FIGURE 2-1. DECREASED GLURIIA ABUNDANCE AT THE NEWLY FORMED NMJ IN PAK MUTANT ANIMALS 53

FIGURE 3-1. GLURIIA$^{\alpha BT}$ *SUBUNITS ARE PROPERLY LOCALIZED AT THE NMJ . 66*

FIGURE 3-2. RECEPTORS CONTAINING THE GLURIIA$^{\alpha BT}$ *SUBUNITS ARE FUNCTIONAL. 68*

FIGURE 3-3. EXPRESSION OF GLURIIA$^{\alpha BT}$ *SUBUNITS AT THE NMJ. 70*

FIGURE 3-4. NO SIGNIFICANT INSERTION OR INTERNALIZATION OF GLURIIA$^{\alpha BT}$ *SUBUNITS IS DETECTED 72*

FIGURE 4-1. SECRETED CALC PROTEIN STRUCTURE AND GENE SEQUENCE ... 92

FIGURE 4-2. CALC EXPRESSION PATTERN. 94

FIGURE 4-3. EARLY CALC OVEREXPRESSION LEADS TO AN ELONGATED CNS 96

FIGURE 4-4. CALC OVEREXPRESSION IN NEURON, FAT BODY OR MUSCLE HAS NO FUNCTIONAL AFFECT 98

FIGURE 4-5. CALC-EXPRESSION IN KIR2.1 ANIMALS IMPAIRS POSTSYNAPTIC DEPOLARIZATIONS 100

FIGURE 4-6. CALC OVEREXPRESSION IN FAT BODIES COMPLETELY BLOCKS GLURIIA^{SP16} *INDUCED HOMEOSTASIS. 102*

FIGURE 4-7. CALC OVEREXPRESSION HAS NO MORPHOLOGICAL EFFECT 104

Chapter One:
General Introduction

Neurons form complex circuits and are connected by synapses which are forming, retracting, strengthening and weakening throughout development, as well as during the adult life of an organism. Neuronal plasticity plays a fundamental role in shaping the strength of synaptic connections in the nervous system. For example, Hebbian correlation based forms of plasticity, such as long-term potentiation (LTP), are though to be a central mechanism underlying processes such as learning and memory. Hebbian plasticity, however, tends to destabilize the activity of neural circuits (Miller, 1996; Turrigiano, 1999). Unchecked LTP, for example, could lead to runaway excitation and a saturation of potentiation at a synapse. While much research has been spent studying the dynamics of the nervous system, recent work indicates that homeostatic mechanisms may exist to maintain an overall level of stability (Destexhe and Marder, 2004; Turrigiano and Nelson, 2004; Perez-Otano and Ehlers, 2005; Davis, 2006). Homeostatic mechanisms are thought to regulate synaptic function such that a "normal" level of activity (the set-point of the cell) is maintained.

Regulation of Synaptic Efficacy during Synapse Development

Pre- and postsynaptic differentiation must be coordinated during development such that a stable synaptic contact is formed. Presynaptic differentiation involves axon guidance to a target cell (Tessier-Lavigne and Goodman, 1996; Yu and Bargmann, 2001; Dickson 2002), a cytoskeletal rearrangement of the presynaptic nerve terminal and the accumulation of synaptic proteins.

Transmembrane proteins, including neuroligin/neurexin and cadherins (Ziv and Garner, 2004), have been found to regulate both presynaptic and postsynaptic assembly.

Presynaptic neurexins and postsynaptic neuroligins are cell adhesion molecules that are sufficient to drive synapse formation. Neuroligins are known to interact with the cytoplasmic postsynaptic density organizing protein PSD-95 (Irie et al., 1997), which in turn can regulate postsynaptic glutamate receptor levels (El-Husseini et al., 2000). Neurexins are the transsynaptic binding partner of neuroligins and are a family of genes which undergo alternative splicing to generate thousands of variants, perhaps to generate specificity during synaptogenesis (Ichtchenko et al., 1995). Neurexins can bind cytoplasmically to the presynaptic scaffold protein CASK (Hata et al., 1996). Expression of neuroligin in non-neuronal HEK293 cells is sufficient to induce morphological and functional presynaptic differentiation in the contacting axons of pontine explants (Scheiffele et al., 2000). In addition to the transsynaptic signaling occurring via neuoligin/neurexins, the cadherins are homophilic Ca^{2+}-dependant cell adhesion molecules found at CNS synapses. Cadherins also undergo extensive alternative splicing (Wu and Maniatis, 1999) and are thought to play a role in the adhesion of the pre-and postsynaptic membranes at a synapse (Fannon and Colman, 1996).

A number of secreted proteins have also been found to play a role in the regulation of synaptogenesis. In the cerebellum, WNT7a (a member of the Wnt family) has been identified as a postsynaptic granule cell secreted factor that can induce axonal remodeling and synaptic differentiation in the presynaptic mossy fibers (Hall et al., 2000). Studies at the Drosophila neuromuscular junction (NMJ) have also demonstrated that Wingless (Wg, another Wnt family member) can regulate synaptogenesis (Packard et al., 2002). In this set of experiments, Wg was found to be presynaptically secreted from motoneurons and, likely, endocytosed by postsynaptic muscles. Low levels of Wg at the

NMJ leads to defective postsynaptic structures and the mislocalization of postsynaptic glutamate receptors, as well as defective presynaptic active zone structures and an overall decrease in the presynaptic terminal elaboration. While the transsynaptic signaling proteins described above clearly play a role in the formation of synaptic connections during development, a subsequent role in the maintenance of synaptic efficacy has not been ruled out.

Control of Synaptic Efficacy independent of Development

A number of transsynaptic signaling molecules have also been identified not as general inducers of differentiation, but as proteins specifically involved in the regulation of synaptic function. Known transsynaptic modulators of synaptic function include retrograde signaling molecules such as endocanabinoids (Wilson and Nicoll 2001) and the secreted neurotrophin BDNF (Zhang and Poo, 2002). In addition, the cell-surface proteins EphB/Ephrin (Takasu et al, 2002) have been found to directly regulate NMDA receptor dependent synaptic function.

Eph receptor tyrosine kinases and their ligands, the membrane bound ephrins, are involved in a transsynaptic signaling cascade regulating cell migration and axon guidance (Mellitzer et al., 2000). In more recent studies, however, these molecules have been found to play a role in synapse function (Takasu et al., 2002). EphB receptors are localized at synapses where they cluster and associate directly with NMDA receptors via the extracellular domains of both receptors. Studies have shown that activation of Eph receptor signaling in cultured neurons, now requiring the intracellular domain of the Eph receptor, results in an increase in synapse number. Blocking Eph signaling has the opposite effect (Dalva et al., 2000). Furthermore, mice lacking the EphB2 receptor completely have reduced hippocampal CA1 and dentate gyrus LTP, a type of long-term plasticity (Henderson et al., 2001). EphrinB2 treatment of cultured cortical neurons potentiates the NMDA receptor-dependent influx of calcium via NMDA receptor phosphorylation (Takasu et al., 2002). Phosphorylation of the NMDA receptor also results in enhanced NMDA receptor-dependent gene expression of a number of genes implicated in synapse development or function, such as BDNF.

Homeostatic Control of Efficacy: Synaptic Scaling

Synaptic scaling is a homeostatic form of plasticity where a multiplicative change in the entire distribution of quantal amplitudes allows a cell to scale the synaptic strength of each individual synaptic input onto that cell while maintaining the relative strength of each input (Turrigiano and Nelson, 2004). Synaptic scaling allows for a global change in synaptic efficacy in response to changes in the overall activity of a cell. For example, a chronic activity blockade of hippocampal or cortical cultured neurons with TTX will lead to a compensatory increase in the amplitude of minature excitatory postsynaptic currents (mEPSCs) as the cell attempts to maintain a set level of activity (Turrigiano et al., 19998; Watt et al., 2000). The opposite perturbation, a block of GABA-mediated inhibition, has an opposite effect on mEPSC size (quantal size). A similar sort of synaptic scaling is also seen *in vivo* in rat visual cortex (Desai et al., 2002). During early post-natal development, the amplitudes of mEPSCs decrease and the frequency of mEPSCs increases. Monocular deprivation prevents these developmental changes, resulting in an overall increase of mEPSC size, demonstrating that synaptic scaling also operates *in vivo*

(Desai et al., 2002). Without synaptic scaling, it is hypothesized that a neural circuit can become unstable (Miller, 1996). Very few of the mechanisms that regulate synaptic scaling have been identified.

Recent work has identified TNF-α as a mediator of synaptic scaling (Stellwagen and Malenka, 2006). Media from cultures experiencing a TTX-induced chronic activity blockade was found to contain high levels of TNF-α. Furthermore, blocking TNF-α signaling by addition of a soluble TNF-α receptor prevented synaptic scaling in TTX-treated cultures. Most convincingly, neurons plated on glia null for TNF-α did not show scaling in response to TTX treatment, whereas neurons plated on wild-type glia did. These experiments indicate that glial-derived TNF-α is a critical component used to maintain synaptic efficacy for this type of synaptic scaling.

At the Drosophila NMJ, a type of plasticity similar to central neuron synaptic scaling has been described. Fasciclin II (FasII), a homophilic cell adhesion molecule, has been shown to be localized both pre- and postsynaptically at the NMJ. Altered levels of FasII can lead to both increases or decreases in synaptic size (Schuster et al., 1996). By manipulating FasII levels, it is possible to create an otherwise normal synapse with fewer presynaptic varicosities (Davis and Goodman, 1998a). By overexpressing FasII on a particular muscle, it is possible to decrease motoneuron innervation by up to 40%. This change in innervation leads to a significant decrease in neurotransmitter release (quantal content). The muscle, however, compensates for decreased innervation and decreased quantal content by upregulating quantal size to enhance synaptic efficacy (Davis and Goodman, 1998a). The increase in quantal size is likely to be due to either an increase in the sensitivity of the postsynaptic glutamate receptors, or an increase in the density of glutamate receptors.

Homeostatic Control of Efficacy: Retrograde Control of Presynaptic Release

In addition to the regulation of postsynaptic receptor function, synaptic homeostasis can modulate synaptic efficacy via the retrograde control of presynaptic neurotransmitter release. Both vertebrate and invertebrate NMJs exhibit the retrograde control of presynaptic neurotransmitter release when muscle excitability is perturbed. Experimental perturbations leading to a decrease in postsynaptic acetylecholine receptor (AChR) sensitivity at the rat NMJ results in compensatory increases in transmitter release. Injection of rats with α-bungarotoxin, an AChR antagonist, led to a gradual increase of presynaptic neurotransmitter release (Plomp et al, 1992). Mice heterozygous for a *neuregulin* deletion have reduced AChR density. The amplitude of postsynaptic evoked depolarizations, however, is unchanged compared to wild-type controls due to an increase in the amount of presynaptic neurotransmitter released (Sandrock et al., 1997). A similar increase in presynaptic neurotransmitter release is seen with the human disease myasthenia gravis. As AChRs are lost from the NMJ, a compensatory increase transmitter release from the motoneurons is seen (Richman and Agius, 2003). At the glutamatergic Drosophila NMJ, three distinct experimental perturbations have been demonstrated to result in synaptic homeostasis via the retrograde control of presynaptic neurotransmitter release.

In the simplest manipulation, a null mutation is the *GluRIIA* glutamate receptor subunit leads to a decrease in quantal size by approximately 50%. Although muscle excitability is impaired, muscle depolarization upon neuronal stimulation is normal. This is accomplished by an increase in presynaptic neurotransmitter release (Petersen et al., 1997). In a second genetic manipulation, overexpression of the activated catalytic subunit of protein kinase A (PKA) in muscle leads to a reduction of mEPSP size via a decrease in the current through the glutamate receptors (Davis et al., 1998). Again, a retrograde signaling cascade from the impaired muscle leads to compensatory increase in transmitter release. A third manipulation, independent of glutamate receptor function, utilizes postsynaptic overexpression of the human Kir2.1 inwardly rectifying potassium channel to impair muscle depolarization (Paradis et al., 2001). Kir2.1 expression reduces the muscle input resistance, leading to a decrease in mEPSP size. Again, presynaptic neurotransmitter release is upregulated in these animals such that depolarization is wild-type. The molecular mechanisms monitoring muscle excitability, the nature of the retrograde transsynaptic signal and the mechanism of increased presynaptic neurotransmitter release are all unknown.

The experiments outline above, including those at the Drosophila NMJ, have lead to two distinct models of synaptic scaling and presynaptic homeostasis. Synaptic scaling involves the regulation synaptic efficacy via the regulation of postsynaptic neurotransmitter receptors. Presynaptic homeostasis involves the regulation of synaptic efficacy via a retrograde signal that modulates presynaptic transmitter release. The molecular mechanisms underlying each of these processes are largely unknown.

As previously mentioned, the Drosophila NMJ has been used as a system to study the regulation of synaptic efficacy. The NMJ is a simple model synapse and, like many vertebrate central synapses, uses glutamate as the main neurotransmitter (Jan and Jan, 1976). The morphological structure of the NMJ has been well characterized and there exist a number of genetic tools to facilitate experimental investigations into the molecular mechanisms that regulate synaptic efficacy. Chapter 2 details a signaling pathway that regulates postsynaptic glutamate receptor abundance and describes how this is coordinated with other aspects of development. Chapter 3 describes the creation of a new genetic tool to study the trafficking of postsynaptic glutamate receptors. Chapter 4 describes a new molecule that can regulate synaptic homeostasis.

Chapter Two:

Coordinating Structural and Functional Synapse Development: Postsynaptic Pak Kinase Independently Specifies GluR Abundance and Postsynaptic Morphology

Summary

Here we show that postsynaptic p21-activated kinase (Pak) signaling diverges into two genetically separable pathways at the Drosophila neuromuscular junction (NMJ). One pathway controls glutamate receptor abundance. Pak signaling within this pathway is specified by a required interaction with the adaptor protein Dreadlocks (Dock). We demonstrate that Dock is localized to the synapse via an SH2-mediated protein interaction. Dock is not necessary for Pak localization, but is necessary to restrict Pak signaling to control GluR abundance. A second, genetically separable function of Pak kinase signaling controls muscle membrane specialization through the regulation of synaptic Discs-large (Dlg). In this pathway, Dock is dispensable. We present a model in which divergent Pak signaling is able to coordinate two different features of postsynaptic maturation, receptor abundance and muscle membrane specialization.

Introduction

Synapse development involves coordinated changes in synapse function and morphology. For example, at the vertebrate NMJ, synapse maturation involves expansion of the acetylcholine receptor (AChR) field in order to keep pace with a growing muscle and nerve terminal. At the same time, the postsynaptic muscle membrane becomes highly specialized including the formation of postsynaptic muscle membrane folds (Sanes and Lichtman, 1999). These muscle folds themselves are subdivided into specialized zones. AChRs localize to the tops of the folds adjacent to the presynaptic terminal while other cytoskeletal proteins and signaling molecules localize to the base of the muscle folds (Sanes and Lichtman, 1999). A large number of resident synaptic proteins have been identified, and their functions assessed genetically or biochemically. But, relatively little is know about how synaptic signaling pathways are organized to coordinately control different features of the synapse (Sheng and Pak, 1999; Allison et al., 2000; Husi et al., 2000; Walikonis et al., 2000).

Synapse maturation at the Drosophila NMJ shares many features with the maturation of the vertebrate NMJ. The nascent embryonic synapse grows tremendously over the course of four days of larval development. During this time the postsynaptic receptor field increases in size to keep pace with muscle growth and the elaboration of the presynaptic nerve terminal. At the same time, the postsynaptic muscle membrane develops into a highly convoluted series of folds termed the subsynaptic reticulum (SSR). Mechanistically, the development of the SSR requires the presence of Discs-large (Dlg), the Drosophila homologue of PSD-95 (Lahey et al., 1994). However, it remains unknown how developmental changes in glutamate receptor abundance are coordinated with the formation of the SSR.

Previous work at the Drosophila NMJ has supported a model in which Pix, a guanine nucleotide exchange factor, and Pak, a serine threonine kinase, are generally required for postsynaptic maturation. In the absence of Pix, many synaptic proteins are absent from the synapse including Pak (localized by Pix) and Dlg (Parnas et al., 2001). In the absence of these proteins, glutamate receptor levels are also decreased and the SSR do not form. Mutations that delete Pak cause a similar disruption of postsynaptic development. Based upon these data, the authors proposed a model that Pix recruits Pak to the synapse, and that Pak signaling is subsequently required for postsynaptic development. However, Pak signaling was not previously investigated since only the Pak null mutation was analyzed in any detail.

Here we demonstrate that Pak signaling diverges into two independent, genetically separable signaling pathways that are capable of coordinating glutamate receptor abundance with the formation of SSR at the Drosophila NMJ. One pathway regulates glutamate receptor abundance. Within this pathway, Pak activity is specified by a required interaction with the adaptor protein Dock (Nck homologue), which we demonstrate is a synaptic protein at the Drosophila NMJ. A second Pak-signaling pathway controls the synaptic abundance of Dlg and the elaboration of SSR. Pak activity within this signaling pathway is independent of Dock function and requires an intact kinase domain.

Results

Pak kinases are a family of serine threonine kinases that are defined by their binding to, and activation by, the Rho family small GTPases, Rac and Cdc42 (Daniels and Bokoch, 1999). Pak(s) can affect the actin cytoskeleton through the phosphorylation of proteins such as Myosin Light Chain Kinase (MLCK) and LIM Kinase (Manser et al., 1997; Li et al., 2001). Paks can also function as a Map4K within the MAP kinase cascade in vertebrates, Drosophila and yeast (Dan et al., 2001). Pak and related family members including the yeast Ste20 gene have a conserved domain structure. The N-terminal half of Pak includes a proline rich domain that, in Drosophila, binds the second SH3 domain of Dock (Hing et al., 1999). The N-terminal portion of Pak also includes an auto-inhibitory domain, a Cdc42/Rac interaction domain, a proline rich domain demonstrated to bind the Rho-type GEF Pix, and a domain recently implicated in the dimerization of two inactive Pak monomers (Parrini et al., 2002). The C-terminal region of Pak encompasses the kinase domain.

In our genetic analysis of Pak signaling we have taken advantage of previously characterized point mutations that disrupt the *Pak* gene (table 1). These mutations have been used to investigate Pak-mediated signaling at the growth cone (Hing et al., 1999). The *Pak*^{6} mutation induces a premature stop codon that truncates the Pak protein within the Cdc42/Rac interaction domain and eliminates the Pix interaction domain as well as the kinase domain (Hing et al., 1999). *Pak*^{6} is reported to be a severe loss-of-function mutation or a genetic null (Hing et al., 1999; Parnas et al., 2001). The *Pak*^{3} and *Pak*^{5} alleles are point mutations that specifically disrupt the kinase domain of Pak (Hing et al., 1999). The *Pak*^{4} allele is a mutation that disrupts an N-terminal proline-rich domain necessary for Pak binding to the second SH3 domain of the adaptor protein Dock (Hing et al., 1999). Importantly, the *Pak*^{4} mutation has been biochemically shown to block the Pak-Dock interaction (Hing et al., 1999).

We first analyzed GluRIIA abundance in Pak mutations at the mature third instar synapse. In this experiment, we analyzed each Pak mutation over a deficiency that uncovers the *Pak* locus. We also examined the heteroallelic combination *Pak*^{3}/*Pak*^{6}. The gross morphology of the *Pak* mutant synapses is normal, though there appears to be an increase in the variability of bouton size and number. It was previously reported that certain Pak allelic combinations caused the muscles to become thin and degenerate (Parnas et al., 2001). We have observed a similar effect in the *Pak*^{11}/*Pak*^{6} allelic combination. However, when these Pak mutations are placed over a deficiency chromosome that uncovers the *Pak* locus, the muscles appear grossly normal, suggesting that the muscle defects are due to second site mutations on the *Pak* chromosomes. Thus, in all of our experiments, we include an analysis of Pak (or Dock) mutations over deficiency chromosomes.

The Kinase and Dock Interaction Domains of *Pak* are Necessary Postsynaptically for Normal GluRIIA Abundance.

We have assessed the abundance of GluRIIA at the third instar NMJ using previously characterized antibodies (Petersen et al., 1997; Parnas et al., 2001). Here we demonstrate a significant decrease in GluRIIA abundance in all *Pak* mutant combinations compared to wild type and heterozygous controls (Figure 1 A, B). Interestingly, GluRIIA abundance is decreased similarly in the Pak null and Pak kinase domain mutations.

Quantitatively similar changes in GluRIIA abundance were also observed at the first instar NMJ (Supplemental Figure 1). The change in GluRIIA fluorescence intensity could reflect a change in GluRIIA abundance per receptor cluster or could reflect a selective elimination of clusters within the synapse. Therefore, we have quantified GluRIIA fluorescence intensity per cluster within wild type and *Pak* mutant synapses. We show a significant decrease in the fluorescence intensity within individual GluR clusters (Supplemental Figure 1D). In addition, we have quantified the density of GluRIIA puncta in wild type and *Pak* mutant synapses and demonstrate that there is no change in this parameter (Supplemental Figure 1E). These data indicate that signaling via the Pak kinase domain is necessary to specify GluRIIA abundance within the normal complement of GluRIIA clusters at the Drosophila NMJ.

Analysis of Pak kinase mutations suggests that Pak kinase activity is necessary for normal GluRIIA abundance. However, an alternate possibility is that Pak localization to the synapse requires an intact kinase domain. Therefore, we also determined the Pak proteins levels at the synapse in each of the *Pak* mutant combinations (Figure 1B). Synaptic Pak staining levels are severely decreased only in the null mutant background (*Pak*^{6}*/Df(3R)Win*^{11}). Pak staining at the synapse is wild type in heterozygous controls, (*Df(3R)Win*^{11}/+) and in every other mutant combination tested including two independent mutant combinations that specifically disrupt the Pak kinase domain (*Pak*^{3}*/Pak*^{6} and *Pak*^{3}*/Df(3R)Win*^{11}). Since kinase domain mutations impair GluRIIA levels without altering Pak levels at the synapse, this supports the conclusion that Pak kinase signaling is necessary to specify GluRIIA levels. As an additional control for these experiments, we demonstrate that there is less than a 10% change in anti-HRP immunoreactivity in any genetic background (Figure 1B).

In our analysis we have also examined a point mutation that disrupts the proline rich, Dock interaction domain of Pak ($Pak^{4}/Df(3R)Win^{11}$). We show that GluRIIA levels are decreased in $Pak^{4}/Df(3R)Win^{11}$, even though Pak protein is present at the synapse at wild type levels (Figure 1B). In combination with our analysis of mutations that affect the Pak kinase domain, these data suggest that both Pak kinase activity and a protein-protein interaction mediated by the proline-rich Dock interaction domain are necessary for normal GluRIIA abundance. In experiments described below, we provide evidence that a Pak-Dock interaction is indeed required to achieve normal GluRIIA abundance.

The co-localization of Pak with the postsynaptic glutamate receptors and the effects of the *Pak* mutations on GluRIIA abundance argue that Pak functions postsynaptically in muscle. However, Pak and Pix protein are found in the nerve as well as the muscle (Parnas et al., 2001). Therefore, we have attempted to rescue Pak activity selectively in muscle or nerve by expressing a Pak cDNA under UAS control. Antibody staining using anti-Pak demonstrated high levels of muscle overexpression and synaptic targeting of the transgenic Pak protein, whereas neuronally expressed Pak did not localize synaptically (data not shown). Expression of $UAS\text{-}Pak^{SH}$ in either nerve or muscle in a wild type background did not have any morphologic effects (data not shown). We then overexpressed $UAS\text{-}Pak^{SH}$ in muscle using a muscle-specific GAL4 driver (*G14-GAL4*). Muscle overexpression of $UAS\text{-}Pak^{SH}$ in the *Pak* mutant background (Pak^{3}/Pak^{6}) rescues GluRIIA levels toward wild type abundance (rescue of 43.82% ± 7.92%, $p<0.002$). Neuronal overexpression of $UAS\text{-}Pak^{SH}$ using a neuronal-specific GAL4 driver (*1407-*

GAL4) did not significantly rescue GluRIIA levels (rescue of 10.2% ± 6.41%, $p = 0.35$). Although we cannot rule out a function of Pak in additional tissues, these data demonstrate an essential function of Pak postsynaptically. These data also demonstrate that while Pak is necessary for normal GluRIIA abundance, Pak overexpression is not sufficient to increase GluRIIA levels. Consistent with this conclusion, we have overexpressed a myristolated Pak transgene which functions as an activated kinase in growth cones (Hing et al., 1999). Overexpression of this transgene in muscle does not alter GluRIIA abundance (data not shown). Together, these data argue that Pak is necessary postsynaptically for normal GluRIIA abundance.

An additional set of experiments provides evidence that Pak may function postsynaptically to control GluRIIA abundance. In most systems, Pak is activated by Rac and Cdc42 (Daniels and Bokoch, 1999). We find that muscle overexpression of either dominant-negative Cdc42 (UAS-Cdc42^{N17}) or dominant-negative Rac (UAS-Rac^{N17}) had no effect on synapse development or GluRIIA abundance as has been previously observed (Parnas et al., 2001). However, when UAS-Cdc42^{N17} and UAS-Rac^{N17} are co-expressed in muscle, we observe a significant decrease in GluRIIA abundance without alteration of gross synapse development (Figure 2 A, B). It is unclear why co-expression of the dominant-negative transgenes is necessary for the decrease in GluRIIA levels. However, since Pak can bind to both Rac and Cdc42, there may be some redundancy that is overcome by co-expression of these transgenes. Pak is also known to interact with Trio (a Rac GEF) in photoreceptor guidance (Newsome et al., 2000). We find no change in GluRIIA levels in Trio mutations (*trio*^{P3}; data not shown). Thus, while we do not directly demonstrate that Cdc42/Rac activate Pak, these data, in combination with our structure function analysis and biochemical evidence from other systems, supports a model in which Pak is activated postsynaptically to control GluR levels at the NMJ.

Finally, we have performed experiments to address whether Pak controls GluRIIA abundance transcriptionally. In other systems it has been shown that Pak can function as a Map4K and could, therefore, modulate GluRIIA transcription (Dan et al., 2001). However, it is well established that Pak can also function as a cytoskeletal regulator through the phosphorylation of Lim Kinase and Myosin Light Chain Kinase (Manser et al., 1997; Li et al., 2001). In this capacity Pak could function locally at the synapse to control GluRIIA levels. To distinguish between these alternatives, we performed real-time RT-PCR on cDNA samples derived from wild type, *Df(3R)Win*^{11}/+ and *Pak*^{6}/*Df(3R)Win*^{11}animals and calculated the 'fold induction' of GluRIIA transcript levels for the mutant genotypes compared to wild type. We find no evidence of altered GluRIIA levels based on this analysis (*Df(3R)Win*^{11}/+ has fold induction of 0.98 ± 0.2; *Pak*^{6}/*Df(3R)Win*^{11} has fold induction of 1.2 ± 0.2). Thus, we favor the hypothesis that Pak acts locally at the synapse to control GluRIIA stabilization or turnover.

Impaired GluRIIA Abundance Alters Postsynaptic Quantal Size but Does Not Impair Synaptic Homeostasis.

To confirm that changes in GluRIIA antibody staining intensity correspond to a functional absence of GluRIIA, we next assayed synaptic function in the *Pak* mutant background. Quantal size was determined as the average amplitude of the spontaneous miniature excitatory postsynaptic potentials (mEPSPs). Quantal size is similar in the wild type and two heterozygous genetic controls. However, quantal size was significantly reduced in *Pak*^{6}*/Df(3R)Win*^{11} animals, demonstrating that reduced GluRIIA staining correlates with a functional deficit that is consistent with less GluRIIA at the synapse (Figure 3A). There was no change in the average muscle input resistance or resting membrane potential in any genetic background. These data support the conclusion that Pak is necessary for the regulation of quantal size by controlling GluRIIA abundance at the synapse. Furthermore, the positive correlation between quantal size and the anti-GluRIIA staining levels supports the use of anti-GluRIIA as a reliable reporter of GluRIIA abundance.

We then tested whether Pak specifically controls GluRIIA levels versus those of other glutamate receptor subunits at the synapse. There are two additional known GluR subunits expressed at the Drosophila NMJ, although antibodies are readily available only for GluRIIA. In a previous study of the Drosophila Pix mutation, it was shown that while GluRIIA levels are decreased, overexpressed GluRIIB was normally localized and its levels were unchanged (Parnas et al., 2001). However, the abundance of an overexpressed protein can be misleading, particularly since it was not previously determined whether the changes in GluR levels was the consequence of altered receptor transcription.

In our analysis we first compared quantal size in *Pak*^{6}*/Df(3R)Win*^{11} and GluRIIA knockout animals. The synapse in the *GluRIIA*^{SP16} null mutant is morphologically wild type, and two remaining glutamate receptor subunits are responsible for synaptic conductances that achieve a quantal size that is roughly 50% of that observed in wild type (Petersen et al., 1997; DiAntonio et al., 1999). Consistent with some GluRIIA staining remaining in the *Pak*^{6}*/Df(3R)Win*^{11} animal, the *GluRIIA*^{SP16} null mutation reveals a greater reduction in quantal size compared to $Pak^{6}/Df(3R)Win^{11}$(Figure 3A). We then assayed quantal size in a $GluRIIA^{SP16};Pak^{3}/Pak^{6}$ double mutant. If Pak specifically controls GluRIIA, we would expect that quantal size in the double mutant would be identical to that observed in the GluRIIA knockout alone. In the $GluRIIA^{SP16};Pak^{3}/Pak^{6}$ double mutation we observe a small but statistically significant further reduction in quantal size compared to the GluRIIA null mutation alone (Figure 3A). Thus, Pak may affect the abundance of other GluR subunits. However, since the additional reduction in quantal size in the double mutation is so small it argues that the primary function of Pak signaling is to control the abundance of GluRIIA at the synapse. This argument is further supported by the observation that EPSP and mEPSP half-widths are decreased in the *Pak* mutant animals (Figure 3C), similar to what is observed in mutations that specifically delete GluRIIA (Petersen et al., 1997).

We next assayed the physiological consequence of altered GluRIIA abundance during evoked stimulation at the NMJ. Robust homeostatic signaling mechanisms have been demonstrated to increase presynaptic release in response to a decrease in postsynaptic quantal size at the Drosophila NMJ (Petersen et al., 1997; Davis et al., 1998; Paradis et al., 2001). In a previous study of Pix mutations, it was suggested that homeostatic signaling might be impaired by lack of Pix and Pak signaling (Parnas et al., 2001). To directly test whether synaptic homeostasis occurs in a *Pak* mutant background, we quantified presynaptic release (quantal content) calculated by dividing the average EPSP amplitude by the average quantal size (Davis et al., 1998; Paradis et al., 2001). Quantal content is not statistically increased in the $Pak^{6}Df(3R)Win^{11}$ animal, though there is a trend this direction (Figure 3B). This result might suggest that Pak is required for synaptic homeostasis. However, we observe a robust increase in presynaptic quantal content in the *GluRIIA*^{SP16}*;Pak*^{3}*/Pak*^{6} double mutant (Figure 3B). This result clearly demonstrates that Pak does not disrupt the putative retrograde signaling system that is thought to be required for synaptic homeostasis at the Drosophila NMJ.

At this point, our data support a model in which Pak is localized to the synapse via an interaction with Pix. Subsequent Pak activation by Rac/Cdc42 is necessary to control GluRIIA abundance at the NMJ. However, as shown earlier, a structure function analysis reveals that a point mutation in the proline rich Dock-interaction domain of Pak is also necessary for normal GluRIIA abundance. We therefore turned our attention to an analysis of Dock at the Drosophila NMJ.

Dock Localizes to the NMJ and Controls GluRIIA Abundance

Previous experiments suggest that Dock may be present at the Drosophila NMJ (Desai et al., 1999). However, the function of Dock during synapse formation is not understood, nor has the function of Dock during subsequent synapse development been assessed. We therefore tested whether the Dock protein is present at the larval NMJ, and whether Dock is required for regulation of GluRIIA abundance at the NMJ.

Antibody staining with a previously characterized Dock antibody demonstrates that Dock localizes to the NMJ throughout larval development (Figure 4 and data not shown). A previously characterized P-element insertion in *dock* is viable to the late larval stages and eliminates Dock immunoreactivity at the NMJ when placed over a deficiency chromosome that uncovers the *dock* locus (Figure 4). This is consistent with previous studies demonstrating that *dock*^{P1} is a strong loss-of-function or null allele (Garrity et al., 1996).

We next assayed GluRIIA abundance in two independent Dock mutations; *dock*^{P1} and *dock*^{4}. The *dock*^{4} mutation specifically disrupts the SH2 domain of Dock. We find that GluRIIA levels are significantly reduced in the *dock*^{P1} and *dock*^{4} mutant backgrounds compared to wild type and heterozygous controls (Figure 5A, B). As with Pak mutations, the gross morphology of the synapse is unaffected. Thus, Dock is necessary for normal GluRIIA abundance at the synapse. Interestingly, we find that GluRIIA staining is decreased to levels that are quantitatively similar to those observed in the *Pak* mutant background (compare Figure 5B with 1B). Together with the observation that GluRIIA abundance is decreased in the *Pak*^{4} mutation (a point mutation in the Pak-Dock interaction domain), these data strongly suggest that a Pak-Dock interaction is necessary to control GluRIIA levels.

Dock Localization Requires an Intact SH2-Domain and is Not Required for Pak Localization to the NMJ.

It has been suggested that Dock localizes Pak to the membrane of the Drosophila growth cone. This is based in part of the demonstration that myristolated (activated) Pak can bypass the requirement for Dock during axon pathfinding in the Drosophila visual system (Hing et al., 1999). At the Drosophila NMJ, however, data suggest that membrane associated Pix is necessary for the localization of Pak to the synapse (Parnas et al., 2001). We have therefore assayed Pak localization in the *dock* mutant background, and Dock localization in the *Pak* mutant background. We find that Pak is normally localized in synaptic puncta in the Dock mutant background (Figure 6B). We also find that Dock is normally localized in a Pak mutant background (Figure 6C). These data demonstrate that Pak and Dock are independently localized to the synapse. These data also support the previous conclusion that Pak is localized to the synapse via an interaction with membrane associated Pix (Parnas et al., 2001).

The question remains as to how Dock is localized to the synapse. Dock is an adaptor protein that is known to bind transmembrane receptors via a conserved SH2 domain (Schmucker et al., 2000; Song et al., 2003). Here we demonstrate that a mutation in the SH2 domain of Dock severely impairs the synaptic localization of Dock (Figure 6A). These data suggest that Dock may be localized to the synapse via a persistent interaction with a synaptic transmembrane protein.

Evidence that Signaling via Dock and Pak Converge to Control GluRIIA Levels

Despite the observation that Pak and Dock are localized to the synapse by independent mechanisms, several lines of evidence indicate that Pak and Dock function together to control GluRIIA abundance. We have shown that mutations that disrupt the ability of Pak to bind Dock (*Pak*^{4}) reduce GluRIIA abundance to levels that are quantitatively similar to that observed in Dock mutations alone (*Pak*^{4}, Figure 1). To further test whether Dock and Pak function together to control GluRIIA levels, we have quantified GluRIIA levels in double mutant combinations of *Pak* and *dock* (Figure 7). We observe that GluRIIA levels are significantly decreased in a transheterozygous combination of *dock*^{P1} and *Pak*^{6} as compared to wild-type animals, and animals that are heterozygous for either mutation alone (Figures 1B, 5D). Furthermore, one mutant copy of *dock* in a *Pak* mutant background does not enhance the reduction in GluRIIA levels seen in the *Pak* null mutant alone, and one mutant copy of *Pak* in the *dock* null mutant background creates only a small further change in GluRIIA levels (Figure 7). While the absence of a strong dominant interaction supports the idea that *dock* and *Pak* interact genetically, a better test would be to examine GluRIIA abundance in the double mutant background. Unfortunately, we were unable to attain viable homozygous double mutations. Since *dock* and *Pak* have functions in other tissues during embryonic and larval development, we suspect that the lethality of the double mutant is due to pleiotropic effects of the double mutants. Given than Pak and Dock are localized independently at the synapse and are known to physically and genetically interact, we propose that Dock functions to localize activated Pak signaling to control GluRIIA abundance at the synapse.

Pak Signaling Controls Synaptic Dlg and Postsynaptic Muscle Development Independently of Dock.

It was previously shown that Pix and Pak null mutations cause a decrease in Dlg abundance at the NMJ (Parnas et al., 2001). In every case where Dlg levels were decreased, there was a parallel reduction in the elaboration of the postsynaptic muscle membrane folds, termed the subsynaptic reticulum (SSR). Because Dlg mutations impair SSR development (Lahey et al., 1994), it was hypothesized that the decrease in Dlg observed in Pix and Pak mutations causes impaired development of the postsynaptic SSR.

However, previously published data demonstrate that not all *Pak* mutations cause the same decrease in synaptic Dlg levels (Parnas et al., 2001). Specifically, Dlg levels were shown to be normal in the *Pak*^{4} mutation and there was no change the elaboration of the SSR. The reason for this discrepancy comparing the *Pak* null mutation and the *Pak*^{4} mutation was not previously explored (Parnas et al., 2001). Here we demonstrate that Pak signaling, and an intact Pak kinase domain are necessary for normal Dlg levels, but that Dock (and the Pak-Dock interaction) are not necessary for normal Dlg levels.

We first demonstrate that Dlg levels are severely decreased in the Pak kinase domain mutations (Figure 8 A,B). Thus, the kinase domain is necessary for normal Dlg levels. We then confirmed previously published data demonstrating the *Pak*^{4} mutation, which disrupts binding to Dock, causes only a slight change in Dlg levels (no change in Dlg was previously reported by Parnas et al., 2001). We further demonstrate that Dlg levels are unchanged compared to heterozygous controls in two independent Dock mutations (Figure 8B) including the presumed null allele (*dock*^{P1}*/Df(2L)ast*^{2}). Note that Dlg levels are slightly decreased when comparing the heterozygous control [*Df(2L)ast*^{2}*/+*] to wild type. The appropriate comparisons, however, are between *dock*^{4}*/Df(2L)ast*^{2} and *Df(2L)ast*^{2}*/+* which controls for the genetic background of the *Df* chromosome. Also not that Dlg levels in the *dock* null, *dock*^{P1}*/Df(2L)ast*^{2} are not statistically different from wild type. Thus, it appears that Pak signaling diverges downstream of Pix. One branch of the Pak signaling pathway interacts with Dock and is restricted to control GluRIIA levels, while a genetically separable Pak signaling pathway specifies synaptic Dlg levels and governs postsynaptic muscle development. Finally, the minor change in Dlg levels seen in the *Pak*^{4} could indicate that a second, unknown, SH3 domain containing protein is involved in Pak signaling to control Dlg levels.

Discussion

Here we have defined a postsynaptic signaling network that can coordinate the regulation of glutamate receptor abundance at the active zone with the developmental elaboration of the postsynaptic muscle membrane specialization termed the subsynaptic reticulum (Figure 9). This signaling network is centered on the Pak kinase. In our model Pak is localized to the postsynaptic membrane via an interaction with Pix as suggested previously (Parnas et al., 2001). Pak is likely activated by Rac and/or Cdc42 in muscle (Figure 2). Upon activation, Pak signaling appears to diverge into two genetically separable pathways. One branch of Pak signaling converges with Dock-mediated signaling to specify the abundance of GluRIIA (Figures 1, 4, 5, 7). Dock itself is necessary for normal GluRIIA abundance and is recruited to the postsynaptic membrane via an independent SH2 mediated interaction with an as yet unidentified synaptic protein, perhaps a receptor tyrosine kinase (Figure 5, 6). The second branch of Pak signaling controls the synaptic levels of Dlg, which subsequently specify the development of the postsynaptic muscle membrane folds (Figure 8). This pathway requires the Pak kinase activity, but is independent of synaptic Dock. Since Pak-dependent regulation of GluRIIA abundance alters synaptic function (Figure 3), this signaling system can independently specify and possibly coordinate structural and functional synapse development at the Drosophila NMJ.

This represents a simple, linear model for the coordinate regulation of structural and functional synapse development. There are, however, indications that this signaling system includes additional complexity. There is a small reduction in Dlg levels in the *Pak*^{4} mutation, though the change in GluRIIA levels are more severe. This could indicate that Pak-dependent regulation of Dlg includes an additional, as yet unidentified, SH3-domain containing protein. Dock and its vertebrate homologue Nck are know to interact with a variety of signaling molecules, and Dock could be localized to the synapse via interactions other than a receptor tyrosine kinase or transmembrane protein. Finally, the changes in GluRIIA and Dlg have been quantified for the Pix mutation, and are observed to be consistently more severe than the changes documented in our study (Parnas et al., 2001). This could represent differences in the methods of visualization and quantification. Alternatively, Pix may have additional outputs, independent of Pak, that function in parallel to control Dlg and GluRIIA levels.

Mechanisms of Neurotransmitter Receptor Regulation

There are interesting parallels and obvious differences between our model of synapse development at the Drosophila NMJ compared to synapse formation at the vertebrate NMJ. At the vertebrate NMJ, the signaling system that controls the initial clustering of AChRs, and the subsequent expansion of these clusters during synapse development, requires the activation of a receptor tyrosine kinase (MuSK) and the effector protein Rapsyn. In addition to controlling receptor clustering and abundance, MuSK and Rapsyn are also required for general postsynaptic differentiation (Sanes and Lichtman, 1999). Our data demonstrating that the Dock SH2 domain is necessary for GluR abundance implicates an as yet unidentified receptor tyrosine kinase at the Drosophila NMJ. However, there is no clear MuSK homologue in Drosophila. Furthermore, although synapse development in Drosophila is compromised, it proceeds in the absence of Pak or Dock, whereas synapse development at the vertebrate NMJ is blocked in MuSK and Rapsyn knockout animals. Indeed our electrophysiological data demonstrate that glutamate receptors clusters must persist in Pak mutant animals, since quantal events and evoked synaptic transmission persist despite a severe decrease in the levels of GluRIIA. Thus, in Drosophila, it appears that Pak-Dock signaling is necessary for the developmental maturation of the postsynaptic receptor field as opposed to initial synapse assembly.

At central synapses in *C. elegans*, glutamate receptor abundance is regulated by ubiquitin-mediated signaling (Burbea et al., 2002). At these synapses, GluR-1 is ubiquinated *in vivo* and receptor abundance can be bi-directionally modulated by manipulation of the ubiqutin signaling system (Burbea et al., 2002). In Drosophila, however, pharmacological manipulation of the ubiquitin-proteosome system does not alter GluR abundance at the synapse (Speese et al., 2003). Furthermore, a C-terminal sequence of GluR-1 that is ubiquinated in *C. elegans* is conserved from worm to vertebrate AMPA receptors, but is not conserved in Drosophila GluRIIA. Thus, signaling via Pak and Dock may represent an alternative or additional mechanism to control glutamate receptor abundance at the synapse.

The means by which Pak signaling affects GluRIIA abundance is not clear. We demonstrate that receptor transcription is not altered in the Pak mutant background. GluRIIA abundance requires the convergence of Dock and Pak signaling, as well as the presence of Pix, and all of these proteins are localized to the postsynaptic membrane. Thus, it seems likely that Pak functions locally, at the synapse to control receptor abundance.

One means by which Pak could influence the abundance of receptors at postsynaptic membrane is through modulation of the synaptic cytoskeleton. Consistent with this hypothesis, Pak is known to signal to the actin cytoskeleton through the phosphorylation of Myosin Light Chain Kinase (MLCK) and LIM Kinase (Manser et al., 1997; Li et al., 2001). There is increasing evidence for a role of actin in the stabilization and maintenance of neurotransmitter receptors in other systems (Lisman and Zhabotinsky, 2001). In this context, Dock may be required to restrict Pak-mediated regulation of the actin cytoskeleton to the postsynaptic density and glutamate receptor clusters.

Regulation of receptor abundance during development and plasticity

Regulated changes in the stoichiometry of transmitter receptor subunits is a well-established phenomenon in both the central and peripheral nervous systems (Wu et al., 1996; Sanes and Lichtman, 2001). Although developmental changes in receptor subunit composition have not been documented at the Drosophila NMJ, we hypothesize that convergent signaling, acting through Dock and Pak, could define a signaling system important for such phenomena. In support of such a possibility, our genetic analysis indicates that the regulation of GluRIIA is quite specific since changes in GluRIIA abundance can account for the majority of the decrease in postsynaptic quantal size observed in the Pak mutant background. In GluRIIA null mutations, quantal size is reduced by approximately 50% (DiAntonio et al., 1999). In the *GluRIIA*^{SP16}*;Pak*^{6}*/Df(3R)Win*^{11} double mutants, there is only a slight further reduction in quantal size beyond that observed in the *GluRIIA* null mutation alone (Figure 3A). This suggests that the primary effect of Pak signaling is to regulate GluRIIA with only a slight additional effect on other GluRII subunits. This possibility is further supported by the previous demonstration that over-expressed GluRIIB is normally localized in the Pix mutation which lacks synaptic Pak (Parnas et al., 2001).

The regulation of GluR subunit composition is also an essential mechanism underlying homeostatic quantal scaling at vertebrate central synapses. The molecular mechanisms underlying quantal scaling of AMPA-type receptors are largely unknown. However, the regulated trafficking of NMDA receptors has been proposed as a mechanism to account for the scaling of the NMDA receptor current (Mu et al., 2003). In Drosophila, homeostatic changes to postsynaptic quantal size have been observed in response to altered muscle innervation (Davis et al., 1998). It is therefore interesting to speculate that Pak and Dock signaling may be involved in the mechanisms of quantal scaling.

Figures and Tables

Table 2-1. Mutant alleles of *dock* and *Pak*

Alleles	Molecular Lesion	References
dock^{P1}	P element insertion in first intron	Garrity et al., 1996
dock^{4}	C320Y, disruption of SH2 domain	Newsome et al., 2000
Pak^{3}	G569D, disruption of kinase domain	Hing et al., 1999
Pak^{4}	P9L, disruption of dock interaction domain	Hing et al., 1999
Pak^{5}	D553N, disruption of kinase domain	Hing et al., 1999
Pak^{6}	R113Stop, truncation in CRIB domain	Hing et al., 1999

Figure 2-1. Decreased GluRIIA Abundance at the Third Instar NMJ in *Pak* Mutant Animals

(A) Representative NMJ from wild type and *Pak* mutant animals are shown that are co-stained with anti-GluRIIA and anti-HRP. At the *Pak* mutant NMJ synaptic morphology is grossly normal, but GluRIIA abundance is substantially decreased. (B) Quantification of the fluorescence intensity of anti-GluRIIA, anti-HRP and anti-PAK staining at the NMJ of wild type, control and *Pak* mutant animals. Data are expressed as % wild type fluorescence intensity. The genotypes corresponding to each bar are shown below the graph. There is a statistically significant decrease GluRIIA fluorescence intensity in the *Pak* mutant combinations compared to wild type and control NMJ. $Pak^{3}/Df(3R)Win^{11}$ =57% ± 2.3%, n = 17; $Pak^{4}/Df(3R)Win^{11}$=72% ± 4.4%, n = 17; $Pak^{6}/Df(3R)Win^{11}$ =56% ± 3.8%, n = 18; and Pak^{3}/Pak^{6} =72% ± 2.2%, n = 6. The average anti-HRP fluorescence varies less than 10% across all genotypes. Anti-Pak fluorescence is significantly decreased only in the $Pak^{6}/Df(3R)Win^{11}$ combination compared to wild type (23.7 ± 4.7%). In all graphs statistical significance is indicated as follows (* $p < 0.05$, ** $p < 0.00005$).

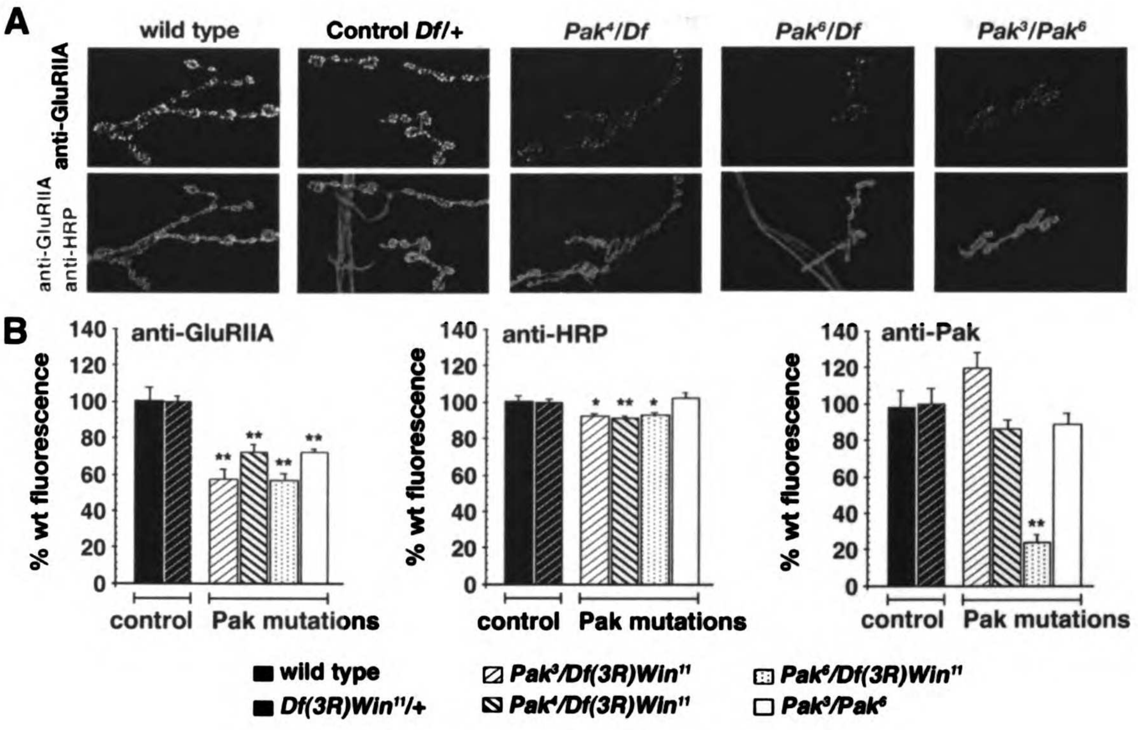
A
wild type
Control Df/+
Pak4/Df
Pak6/Df
Pak3/Pak6
anti-GluRIIA
anti-GluRIIA
anti-HRP
B
anti-GluRIIA
anti-HRP
anti-Pak
% wt fluorescence
0
20
40
60
80
100
120
140
*
**
control
Pak mutations
wild type
Df(3R)Win11/+
Pak3/Df(3R)Win11
Pak4/Df(3R)Win11
Pak6/Df(3R)Win11
Pak3/Pak6

Figure 2-2. Simultaneous Disruption of Cdc42 and Rac in Muscle Leads to Decreased GluRIIA Levels.

(A) Wild type (left) and transgenic larvae (right) that simultaneously overexpress dominant-negative Rac and dominant-negative Cdc42 (MHC-Gal4/UAS-Rac^{n17}; UAS-Cdc42^{N17}/+) are shown stained with anti-HRP and anti-GluRIIA. (B) GluRIIA levels are significantly decreased only in MHC-Gal4/UAS-Rac^{n17}; UAS-Cdc42^{N17}/+, when both dominant-negative constructs are postsynaptically expressed (73.6% ± 3.3%, n = 17). Significance is denoted as follows (* $p < 0.0001$).

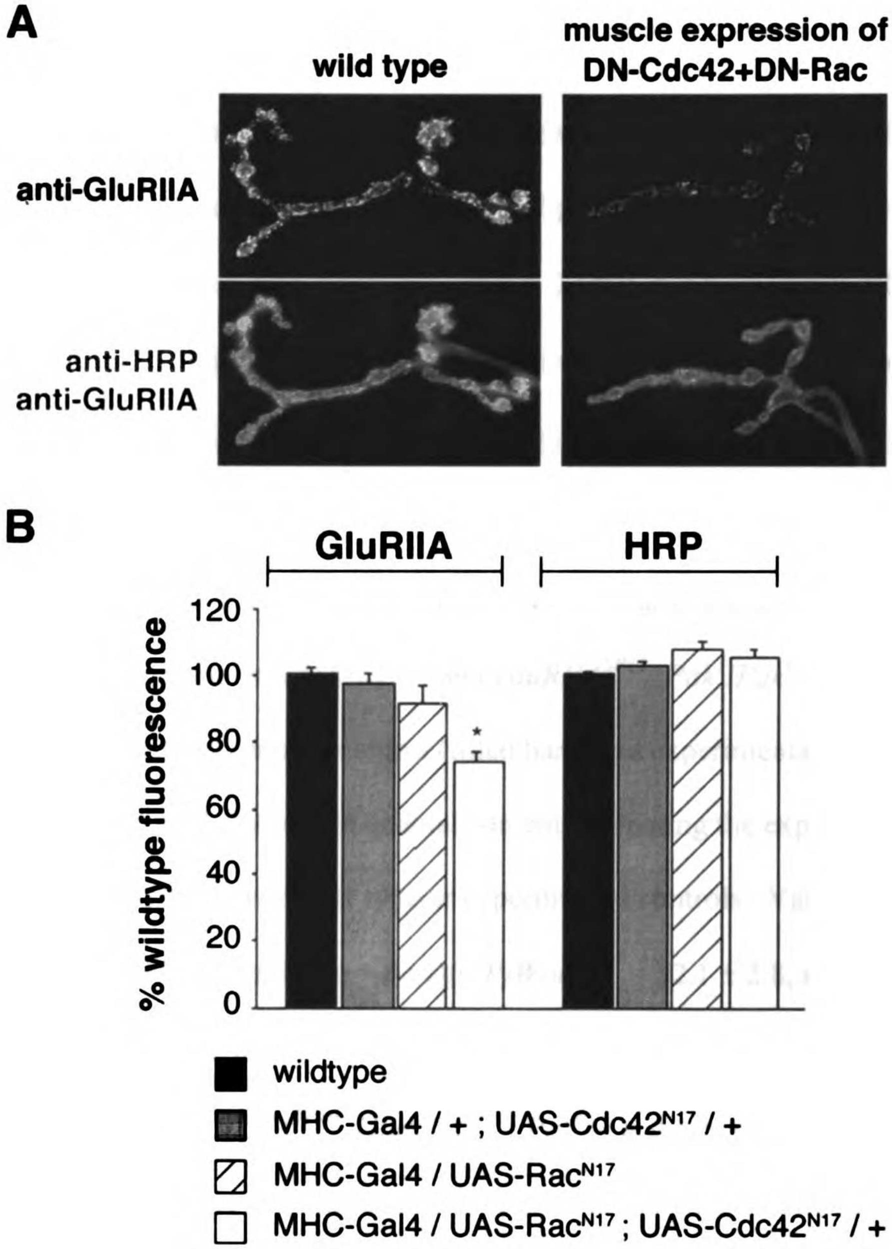
A
wild type
muscle expression of DN-Cdc42+DN-Rac
anti-GluRIIA
anti-HRP
anti-GluRIIA
B
GluRIIA
HRP
% wildtype fluorescence
120
100
80
60
40
20
0
*
wildtype
MHC-Gal4 / + ; UAS-Cdc42^{N17} / +
MHC-Gal4 / UAS-Rac^{N17}
MHC-Gal4 / UAS-Rac^{N17} ; UAS-Cdc42^{N17} / +

Figure 2-3. Decreased Quantal Size and Normal Homeostatic Compensation at *Pak* Mutant NMJ

(A) Quantification of quantal size in control (filled bar) and experimental genotypes (open bars). Wild type and heterozygous controls ($Df(3R)Win^{11}/+$ and $Pak^{6}/+; GluRIIA^{SP16}/+$) have quantal sizes equal to 1.1mV ± 0.1mV, n = 6 ; 0.98mV ± 0.7mV, n = 6 and 0.96mV ± 0.83mV, n = 5 respectively. Experimental genotypes all showed significant decreases in quantal size: $Pak^{6}/Df(3R)Win^{11}$=0.73mV ± .07mV, n = 6; $GluRIIA^{SP16}$ = 0.51mV ± 0.01mV, n = 18; $GluRIIA^{SP16}; Pak^{6}/+$ = 0.46mV ± 0.02mV, n = 5; $GluRIIA^{SP16}; Pak^{3}/Pak^{6}$ = 0.4mV ± 0.01, n = 7. There is also a small, yet statistically significant, difference between $GluRIIA^{SP16}$ and $GluRIIA^{SP16}; Pak^{3}/Pak^{6}$ (B) Quantification of quantal content in control (filled bars) and experimental genotypes (open bars). There is no difference in quantal content comparing the experimental genotype $Pak^{6}/Df(3R)Win^{11}$ with wild type or experimental controls. Values are as follows: wild type = 34.5mV ± 1.5, n = 6 ; $Df(3R)Win^{11}/+$ = 32.1 ± 2.8, n = 6; $Pak^{6}/+; GluRIIA^{SP16}/+$ = 39.3 ± 5.2, n = 5; $Pak^{6}/Df(3R)Win^{11}$ = 40.7 ± 3.7, n = 6. The experimental genotypes $GluRIIA^{SP16}$, $GluRIIA^{SP16}; Pak^{6}/+$ and $GluRIIA^{SP16}; Pak^{3}/Pak^{6}$ all showed significant increases in quantal content compared to wild type and genetic controls indicating that homeostatic compensation has occurred. Values are as follows: $GluRIIA^{SP16}$ = 58 ± 3.7mV, n = 15; $GluRIIA^{SP16}; Pak^{6}/+$ = 48.8 ± 5.2mV, n = 5 and $GluRIIA^{SP16}; Pak^{3}/Pak^{6}$ = 63.6 ± 8.7, n = 6). (C) Representative traces of evoked potentials (left; each trace represents the average of 10 individual traces) and spontaneous miniature potentials (right) from control ($Df(3R)Win^{11}/+$) and *Pak* mutant NMJ ($Pak^{6}/Df(3R)Win^{11}$). The traces show the reduction in quantal size in Pak mutant animals and the wild type EPSP amplitude indicative of effective synaptic homeostasis. Scale bar for evoked release is 10mV, 50ms and for spontaneous traces is 1mV, 250ms. Significance is denoted as follows (* $p < 0.05$, ** $p < 0.002$, *** $p < 0.00002$).

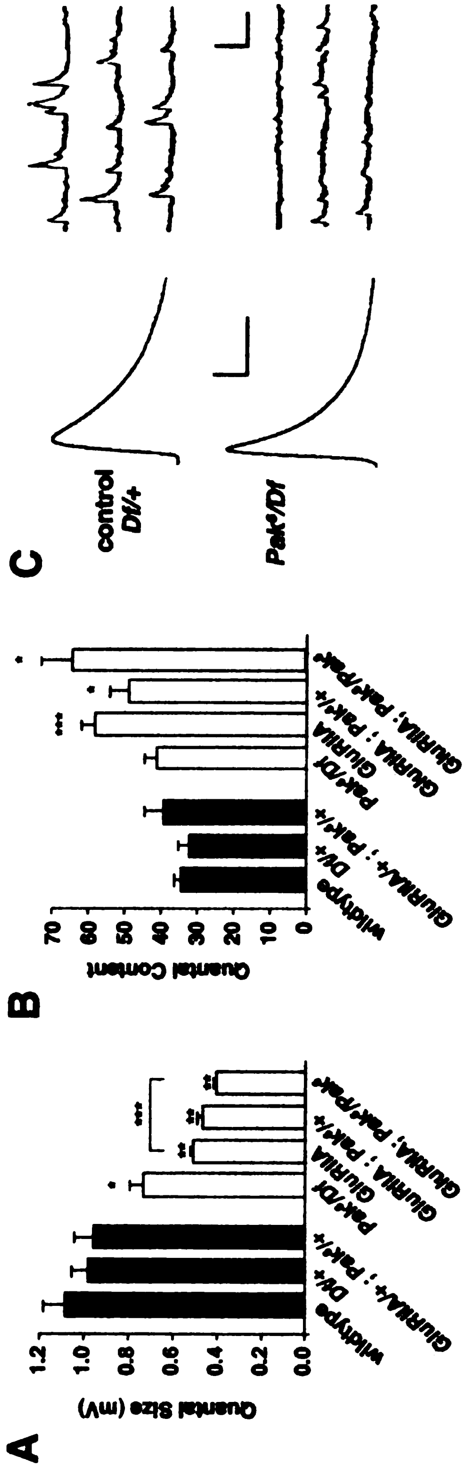
A
Quantal Size (mV)
1.2
1.0
0.8
0.6
0.4
0.2
0.0
wildtype
Df/+
Pak6/+
GluRIIA/+ ; Pak6/+
Pak6/Df
GluRIIA
GluRIIA ; Pak6/+
GluRIIA; Pak6/Pak6
*
**
***
B
Quantal Content
70
60
50
40
30
20
10
0
*
C
control
Df/+
Pak6/Df

Figure 2-4. Synaptic Localization of Dock

A wild type (left) and a *dock* mutant NMJ (right; $dock^{P1}/Df(2L)ast^{2}$) are shown stained with anti-HRP and anti-Dock. Anti-dock immunoreactivity is localized to the NMJ in wild type. In *dock* null animals, anti-Dock staining is completely absent from the NMJ (top right). The images shown are calibrated identically.

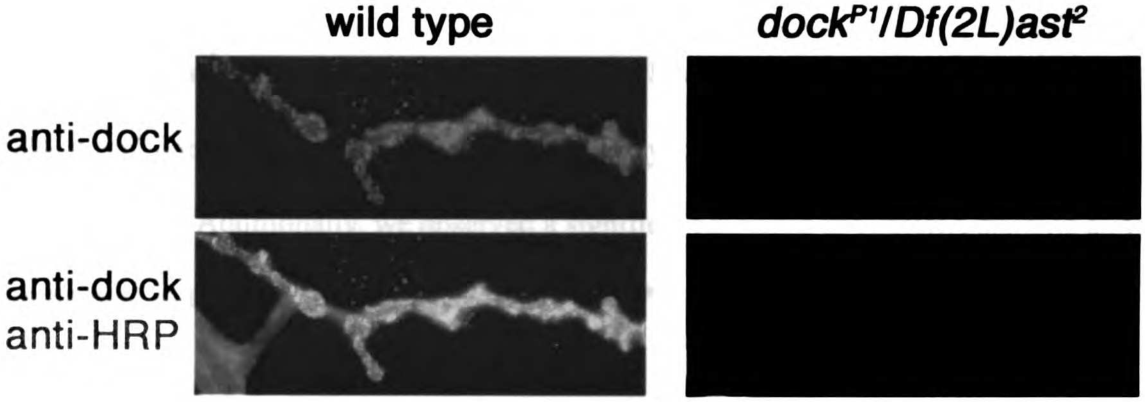
wild type
dock^P1/Df(2L)ast^2
anti-dock
anti-dock
anti-HRP

Figure 2-5. Synaptic Localization of GluRIIA is Decreased in *dock* Mutants

(A) Representative images of a wild type (left) and a *dock* null NMJ ($dock^{P1}/Df(2L)ast^2$) stained with anti-GluRIIA, anti-Pak and anti-HRP. GluRIIA staining is reduced in the *dock* mutant animals without a corresponding decrease in Pak levels at the synapse. (B) Quantification of the fluorescence intensity of anti-GluRIIA, anti-HRP and anti-PAK staining. There is a significant decrease in the intensity of GluRIIA staining in $dock^{P1}/Df(2L)ast^2$ null animals (61.2% ± 3.6%, n = 8) and $dock4/Df(2L)ast^2$ (64.3% ± 4.8%, n = 6) compared to wild type and the heterozygous controls $dock^{P1}/+$, $dock^4/+$ and $Df(2L)ast^2/+$. Additionally, we observed a significant increase in GluRIIA staining and Pak staining in the $dock^{P1}/+$ animals (* $p < 0.05$, ** $p < 0.0002$).

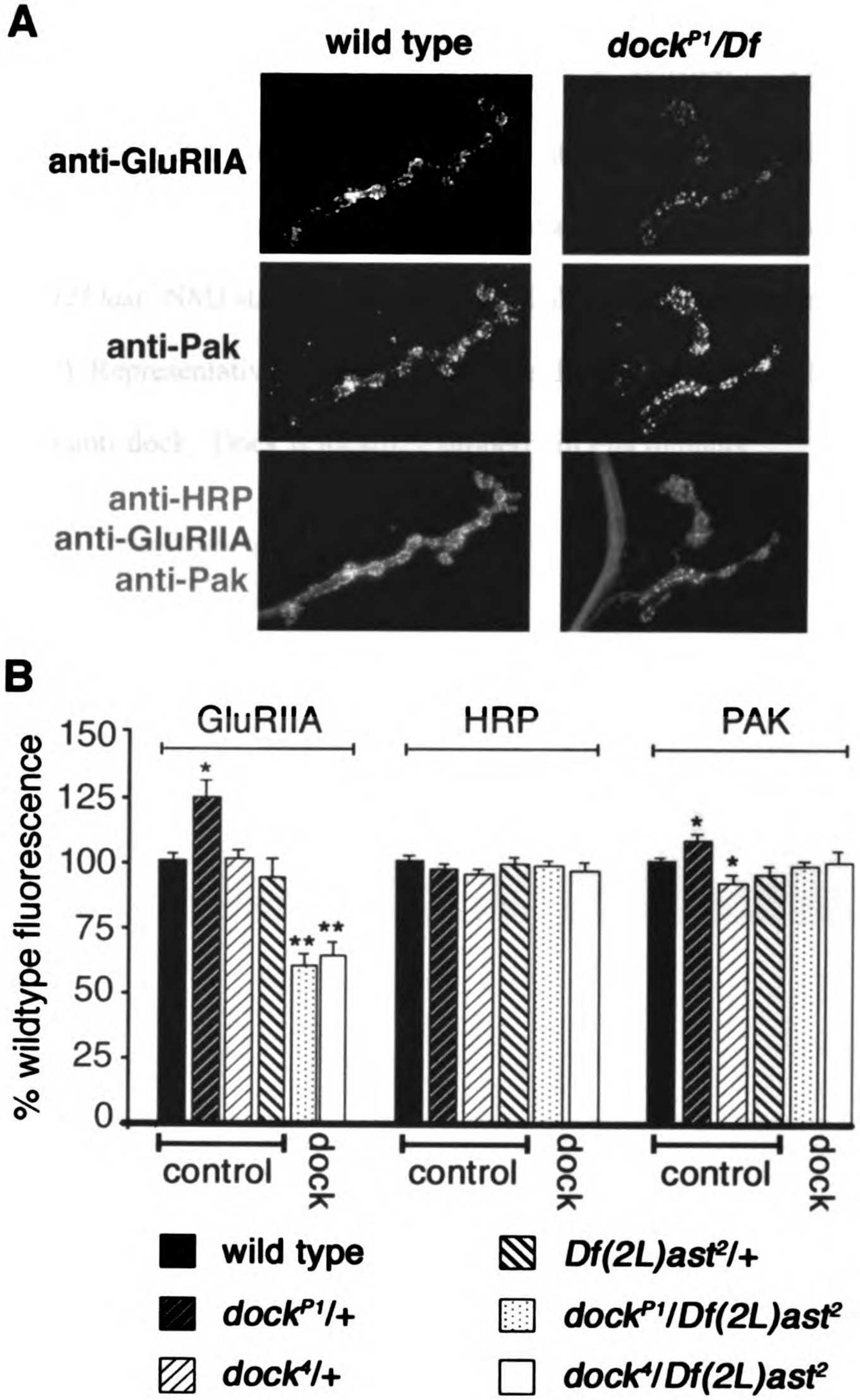
A
wild type
dockP1/Df
anti-GluRIIA
anti-Pak
anti-HRP
anti-GluRIIA
anti-Pak
B
GluRIIA
HRP
PAK
% wildtype fluorescence
150
125
100
75
50
25
0
*
*
**
**
*
*
control
dock
control
dock
control
dock
wild type
dockP1/+
dock4/+
Df(2L)ast2/+
dockP1/Df(2L)ast2
dock4/Df(2L)ast2

Figure 2-6. Dock and Pak are Synaptically Localized Independently of Each Other

(A) Representative images of a wild type (left) and a *dock*^{4}/*Df(2L)ast*^{2} NMJ stained with anti-dock and anti-HRP. Dock protein, with a point mutation in the SH2 domain, is no longer highly localized at the synapse. (B) Representative images of wild type (left) and a *dock*^{P1}/*Df(2L)ast*^{2} NMJ stained with anti-Pak. Pak is localized properly in *dock* null mutants. (C) Representative images of wild type (left) and *Pak*^{4}/*Df(3R)Win*^{11} NMJ stained with anti-dock. Dock is localized properly in *Pak* mutants.

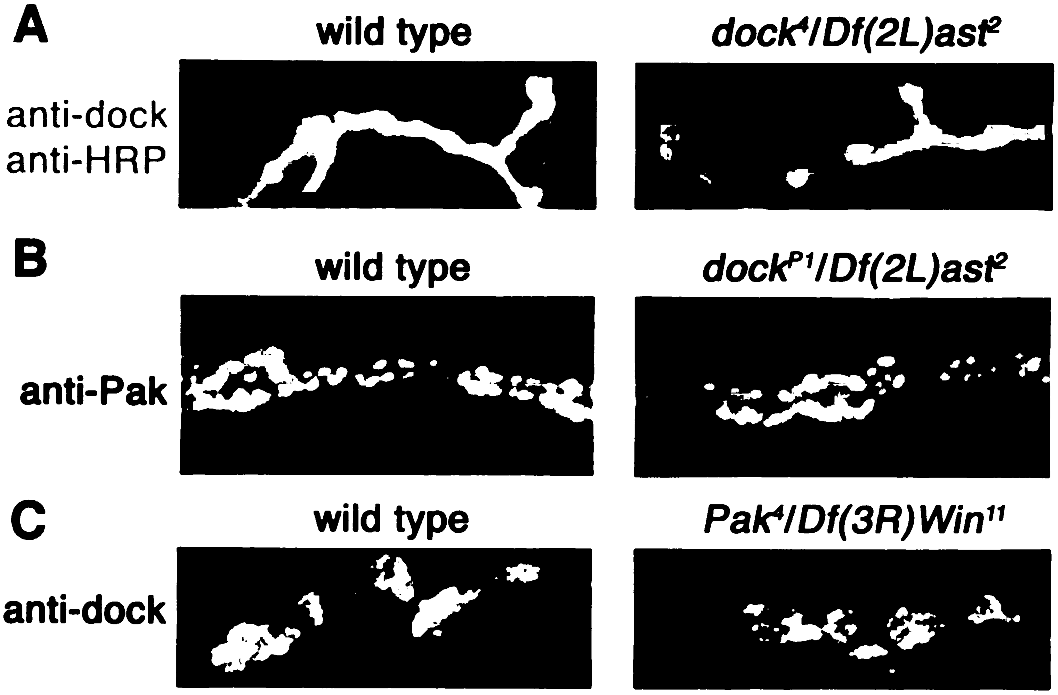
A
wild type
dock^4/Df(2L)ast^2
anti-dock
anti-HRP
B
wild type
dock^{P1}/Df(2L)ast^2
anti-Pak
C
wild type
Pak^4/Df(3R)Win^{11}
anti-dock

Figure 2-7. Dock and Pak Interact Genetically to Regulate Synaptic GluRIIA Levels

Quantification of anti-GluRIIA and anti-Pak fluorescent intensities in *Pak* and *dock* double mutant combinations. As compared to wild type, the $dock^{P1}$/+; Pak^{6}/+ trans-heterozygous animals show a decrease in GluRIIA staining at the synapse (72% ± 2.2%, n = 6). A further reduction in GluRIIA staining is seen in a *dock* null animal with one copy of a Pak mutant gene, $dock^{P1}$/*Df(2L)ast*^{2}; Pak^{6}/+ (49% ± 3.0%, n = 6), and in the *Pak* mutant animal with one mutant copy of *dock*, $dock^{P1}$/+; Pak^{6}/*Df(3L)Win*^{11} (57% ± 2.4%, n = 6). For ease of comparison, bars representing the single mutants, $dock^{P1}$/*Df(2L)ast*^{2} and Pak^{6}/*Df(3L)Win*^{11}, are included from Figures 2 and 5. As an additional control, Pak^{6}/+ animals are shown which have a reduction in GluRIIA levels (89% ± 2.2%, n=7). Levels of significance are as follows (* $p < 0.05$, ** $p < 0.0005$, *** $p < 0.000005$).

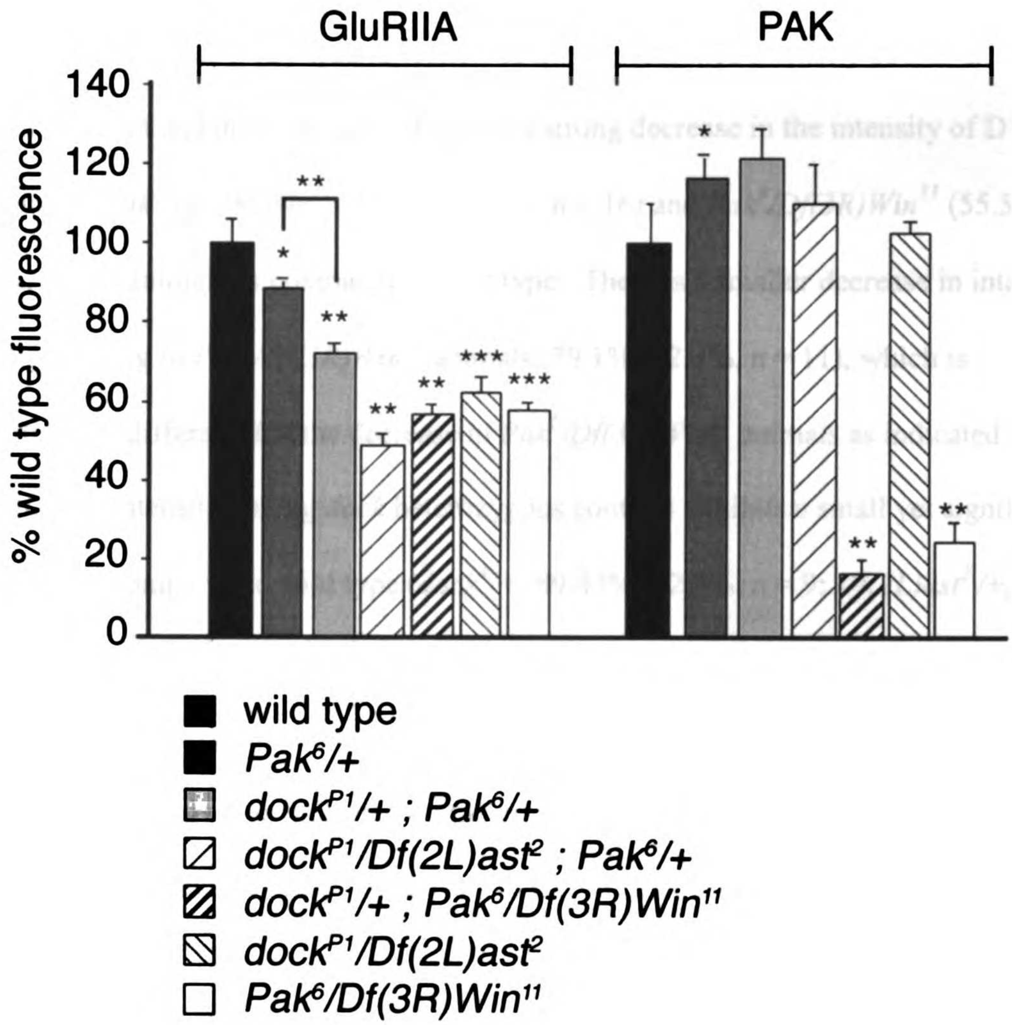
GluRIIA
PAK
% wild type fluorescence
140
120
100
80
60
40
20
0
*
**
**
**
**
***
***
*
**
**
wild type
Pak⁶/+
dockᴾ¹/+ ; Pak⁶/+
dockᴾ¹/Df(2L)ast² ; Pak⁶/+
dockᴾ¹/+ ; Pak⁶/Df(3R)Win¹¹
dockᴾ¹/Df(2L)ast²
Pak⁶/Df(3R)Win¹¹

Figure 2-8. Synaptic Localization of Dlg is Decreased in *dock* and *Pak* Mutants

Representative images of a wild type (left), *Pak*^{4}/*Df(3R)Win*^{11} (center) and *Pak*^{3}/*Df(3R)Win*^{11} (center) NMJs stained with anti-Dlg. Dlg staining is severely reduced only in the Pak kinase domain point mutation (*Pak*^{3}), and not the dock interaction domain point mutation (*Pak*^{4}). (B) Quantification of the fluorescence intensity of anti-Dlg staining in *Pak* and *dock* mutants. There is a strong decrease in the intensity of Dlg staining in *Pak*^{3}/*Df(3R)Win*^{11} (50.5% ± 2.0%, n = 16) and *Pak*^{5}/*Df(3R)Win*^{11} (55.5% ± 2.9%, n = 6) animals as compared to wild type. There is a smaller decrease in intensity of Dlg staining in *Pak*^{4}/*Df(3R)Win*^{11} animals (79.1% ± 2.4%, n = 11), which is significantly different that the decrease in *Pak*^{5}/*Df(3R)Win*^{11} animals as indicated on the graph. Dlg intensity among *dock* heterozygous controls exhibits a small yet significant decrease as compared to wild type (*dock*^{4}/+, 89.43% ± 2.5%, n = 9; *Df(2L)ast*^{2}/+, 86% ± 2.7%, n = 8). *dock*^{4}/*Df(2L)ast*^{2} NMJs also exhibit a small yet significant decrease in Dlg staining as compared to wild type (80.8% ± 3.0%, n = 10) NMJs. As compared to heterozygous controls as indicated on the graph, there is no significant decrease in Dlg staining in *dock* mutant synapses. Levels of significance are as follows (* $p < 0.005$, ** $p < 0.0000001$).

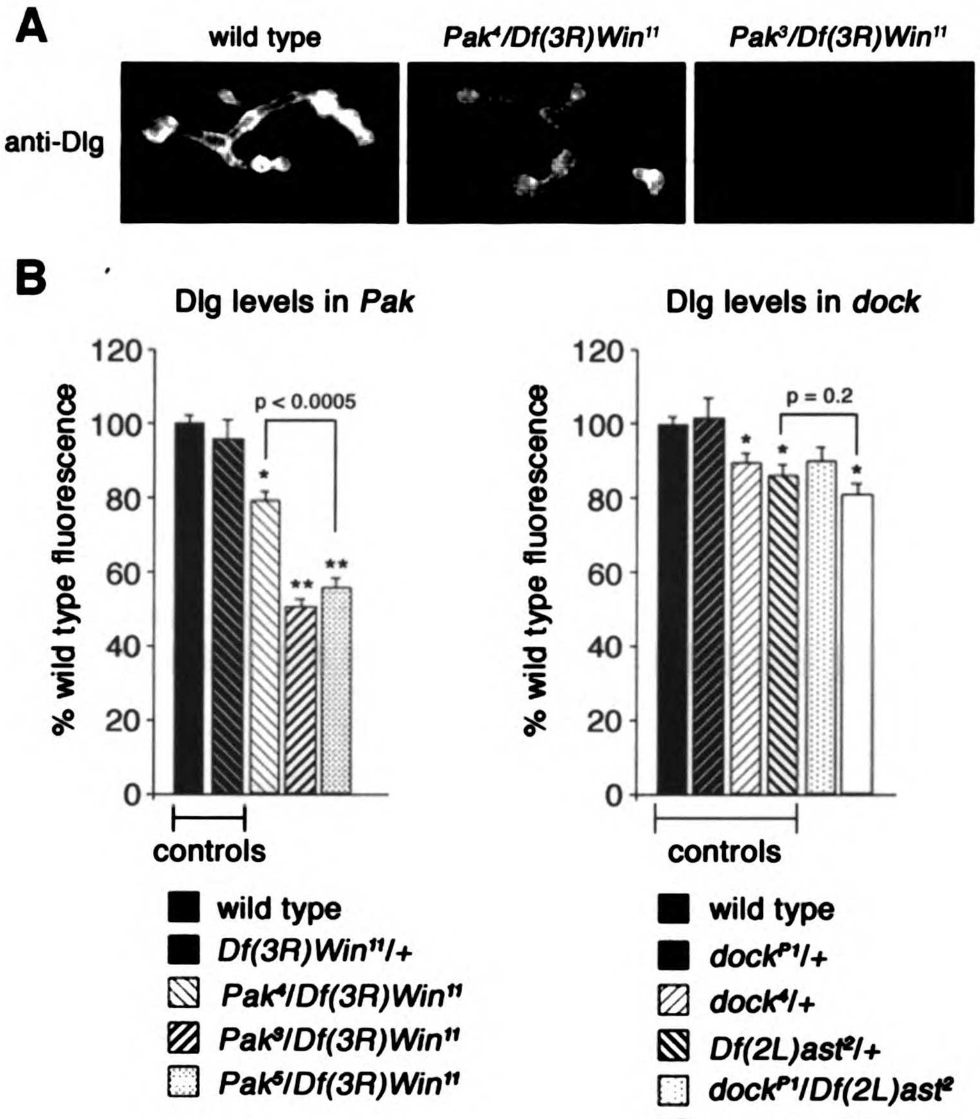
A
wild type
$Pak^4/Df(3R)Win^{11}$
$Pak^3/Df(3R)Win^{11}$
anti-Dlg
B
Dlg levels in *Pak*
% wild type fluorescence
120
100
80
60
40
20
0
p < 0.0005
*
**
**
controls
wild type
$Df(3R)Win^{11}/+$
$Pak^4/Df(3R)Win^{11}$
$Pak^3/Df(3R)Win^{11}$
$Pak^5/Df(3R)Win^{11}$
Dlg levels in *dock*
% wild type fluorescence
120
100
80
60
40
20
0
p = 0.2
*
*
*
controls
wild type
$dock^{P1}/+$
$dock^4/+$
$Df(2L)ast^2/+$
$dock^{P1}/Df(2L)ast^2$
$dock^4/Df(2L)ast^2$

Figure 2-9. The Postsynaptic Pix-Pak-Dock Signaling System

Pix localizes Pak to the synaptic membrane. Upon activation Pak signaling diverges. In one branch, Pak binds to Dock. Dock itself is recruited to the synapse via an essential SH2 mediated interaction with an unknown synaptic protein. Dock-Pak binding is required for normal GluR abundance. Pak signaling also diverges to control Dlg levels and thereby regulate the formation of the postsynaptic muscle membrane folds.

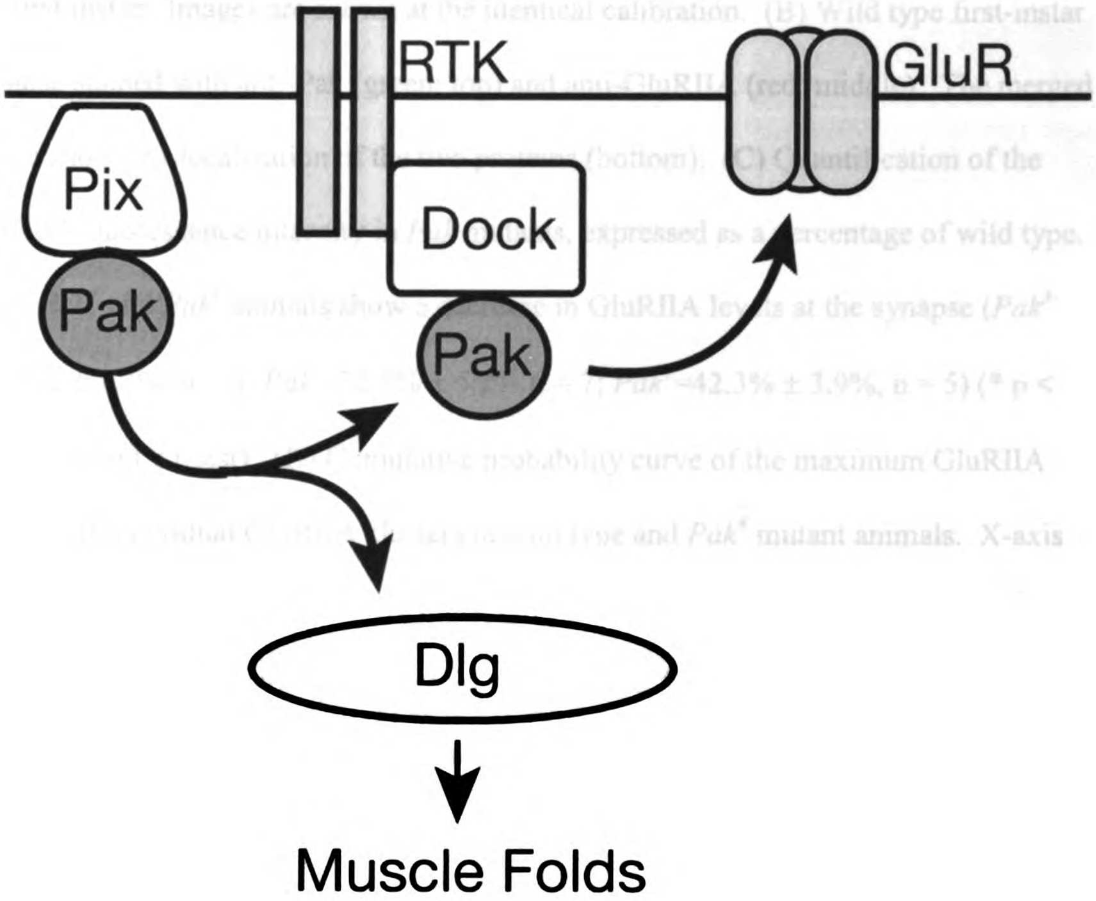
RTK
GluR
Pix
Dock
Pak
Pak
Dlg
Muscle Folds

Supplemental Figure 2-1. Decreased GluRIIA Abundance at the Newly Formed NMJ in *Pak* Mutant Animals

(A) NMJ from first instar wild type, Pak^{6} and Pak^{3} larvae are shown that are stained with anti-Dlg (green; top row) and anti-GluRIIA (red; middle row). Merged images are shown in the bottom row. GluRIIA abundance at the NMJ is decreased in the all *Pak* mutants in the first instar. Images are shown at the identical calibration. (B) Wild type first-instar synapse stained with anti-Pak (green; top) and anti-GluRIIA (red; middle). The merged image shows co-localization of the two proteins (bottom). (C) Quantification of the GluRIIA fluorescence intensity in *Pak* mutants, expressed as a percentage of wild type. Pak^{3}, Pak^{4} and Pak^{6} animals show a decrease in GluRIIA levels at the synapse (Pak^{3} =72.5% ± 1.3%, n = 3; *Pak* =72.7% ± 5.2% n = 7; Pak^{6}=42.3% ± 3.9%, n = 5) (* $p < 0.002$, student's t-test). (D) Cumulative probability curve of the maximum GluRIIA staining of individual GluRIIA clusters in wild type and Pak^{4} mutant animals. X-axis values are in arbitrary fluorescence units. (E) Average GluRIIA receptor cluster density per synapse area was calculated for wild type (4.8 ± 0.5) and Pak^{6}/Df (4.5 ± 0.4, n=11). There is no change in this parameter comparing these genotypes.

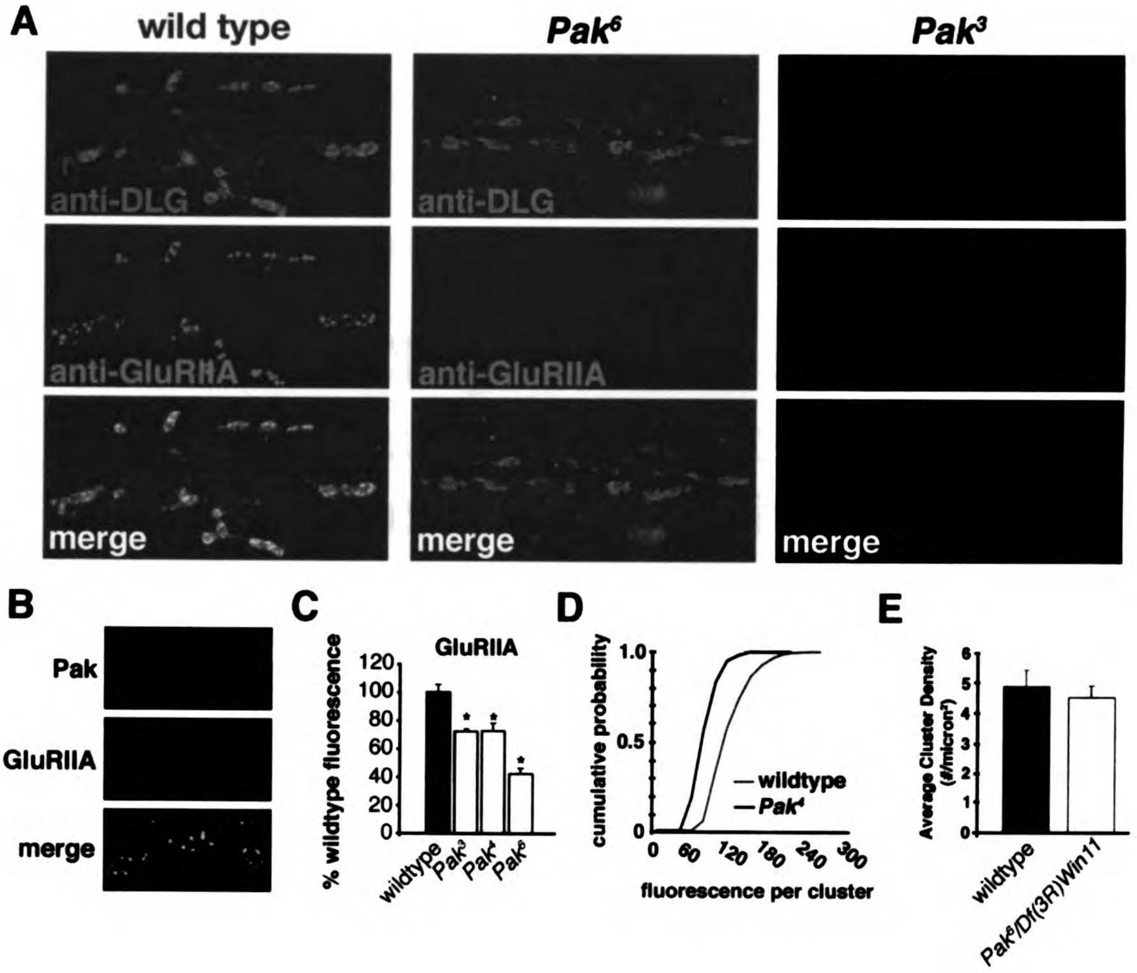
A
wild type
Pak6
Pak3
anti-DLG
anti-DLG
anti-GluRIIA
anti-GluRIIA
merge
merge
merge
B
Pak
GluRIIA
merge
C
GluRIIA
% wildtype fluorescence
0
20
40
60
80
100
120
*
*
*
wildtype
Pak3
Pak4
Pak6
D
cumulative probability
0
0.5
1.0
0
60
120
180
240
300
fluorescence per cluster
— wildtype
— Pak4
E
Average Cluster Density (#/micron²)
0
1
2
3
4
5
6
wildtype
Pak6/Df(3R)Win11

Chapter Three:

Imaging GluRIIA receptors using α-bungarotoxin binding site tagged receptors

Summary

Glutamate receptor trafficking is highly regulated in neurons. Proper trafficking is necessary for basal excitatory synaptic transmission, as well as some forms of synaptic plasticity. It is thus of great importance to understand glutamate receptor trafficking *in vivo*. Here we create an α-bungarotoxin (αBT) binding-site-tagged glutamate receptor subunit for expression at a mature Drosophila neuromuscular junction. These engineered subunits traffic properly to the postsynaptic density and co-localize with endogenous glutamate receptor subunits. In addition, receptors containing the modified subunits are functional. By imaging the tagged glutamate receptor subunit over time, by binding with a fluorescently conjugated αBT, we can visualize the internalization and insertion of glutamate receptors into the membrane. Here we show that after inserting into the plasma membrane, glutamate receptors at the mature NMJ are largely immobile. This sort of approach is very flexible and can be used to study the trafficking of a variety of membrane proteins.

Introduction

Postsynaptic ionotropic glutamate receptors mediate fast excitatory neurotransmission at a variety of synapses. Both the levels of glutamate receptors and the subunit composition of these receptors are modulated throughout development and are known to play a critical role in synaptic plasticity (Malinow and Malenka, 2002; Bredt and Nicoll, 2003). Much of what is known about glutamate receptor trafficking comes from studies of cultured vertebrate neurons.

During development of the Drosophila larval neuromuscular junction (NMJ), an established glutamatergic model synapse, the embryonic synapse grows tremendously over the course of four days of larval development. During this time the postsynaptic glutamate receptor clusters increase both in size and number to keep pace with muscle growth and the elaboration of the presynaptic nerve terminal. The regulated trafficking of glutamate receptors is thus an essential part of functional synaptic development and synaptic maintenance at the NMJ. There exist five subunits (GluRIIA, GluRIIB, GluRIII, GluRIID and GluRIIE) of the ionotropic glutamate receptor at the Drosophila NMJ (Qin et al., 2005; Featherstone et al., 2005). Synaptic GluRIIA levels are regulated throughout larval development by a number of signaling pathways including the p21-activated kinase pathway (Albin and Davis, 2004).

Numerous studies of glutamate receptor trafficking, both in vertebrates and in Drosophila, have used fluorescent fusion proteins of receptor subunits (for example Shi et al., 2001; Rasse et al., 2005). Studies examining trafficking of the Drosophila GluRIIA subunit at the NMJ used a GFP-tagged receptor to visualize postsynaptic GluRIIA clusters (Rasse et al., 2005). While the fluorescently tagged receptor has been useful in describing GluRIIA cluster formation, the GFP tagged receptor subunit does not allow one to distinguish between surface receptors and intracellular pools. In order to accurately quantify surface receptor trafficking, we needed to engineer a differently type of glutamate receptor.

For 30 years work at the vertebrate NMJ, another established model for studying receptor trafficking, used fluorescently conjugated α-bungarotoxin (αBT) to visualize endogenous nicotinic acetylcholine receptors (AChR) (Ravdin and Axelrod, 1977; Rich and Lichtman, 1989). αBT is a highly toxic component of *Bungarus multicinctus* snake venom, binds directly to the AChR and is a potent antagonist of this receptor. A small 13 amino acid binding site on the AChR has been shown to bind to αBT with high affinity (Katchalski-Katzir et al. 2003). In addition to the tight specific binding to the AChR, αBT can be conjugated to a number of different fluorophores to facilitate biological labeling. Not all toxins can tolerate the conjugation of a fluorophore and still retain their binding properties. Thus, αBT is an ideal toxin to study postsynaptic receptors at the NMJ. Consequently a relatively huge amount is known about AChR trafficking during development.

Such high affinity fluorescently tagged ligands are not readily available for use in studying glutmate trafficking. Similar to recent work looking at AMPA glutamate receptor trafficking (Sekine-Aizawa and Huganir, 2004), we engineered a Drosophila GluRIIA receptor subunit that contained the 13 amino acid binding site from the AChR in an extracellular domain. These αBT tagged GluRIIA subunits were expressed in the animal and we demonstrate that these tagged receptors both cluster normally in the postsynaptic density with other receptor subunits and form functional glutamate receptors. By using fluorescently conjugated αBT, which does not cross the plasma membrane, we were able to specifically visualize just surface GluRIIA subunits. We also show that once inserted into the membrane at a mature synapse, these glutamate receptor subunits exhibit very little internalization or insertion. Given its small size, using the αBT site as a tag for surface protein expression is a powerful tool that can be transferred to a variety of membrane proteins.

Results

GluRIIA$^{\alpha BT}$ subunits are targeted properly to postsynaptic receptor clusters at the NMJ.

To analyze surface trafficking of the GluRIIA subunit in an *in vivo* system, we engineered a modified GluRIIA$^{\alpha BT}$ subunit that contained an extracellular 13 amino acid αBT binding site (Figure 1 A). This subunit was expressed in a *GluRIIA*^{SP16} null animal from a transgene containing the GluRIIA promoter (Petersen et al., 1997). Labeling of the NMJ with an alexa fluor 488-conjugated αBT showed normal clustering of the GluRIIA$^{\alpha BT}$ subunits with virtually no background αBT binding in a wild type animal (Figure 1 B). The GluRIIA$^{\alpha BT}$ clusters oppose sites of nc82 staining, an established presynaptic active zone marker (Wagh et al., 2006) (Figure 1 C). In addition, the GluRIIA$^{\alpha BT}$ clusters colocalized with GluRIII subunits (Figure 1 D), a required subunit for glutamate receptors surface expression at the NMJ (Marrus et al., 2004), thus demonstrating the GluRIIA$^{\alpha BT}$ receptors can form a complex with the other GluR subunits.

Functional analysis of GluRIIA$^{\alpha BT}$ subunits.

We next assessed the synaptic function of GluRIIA$^{\alpha BT}$ containing receptors at the third instar NMJ to test if the modified GluRIIA subunit could rescue functionality at a *GluRIIA*^{SP16} null synapse. Quantal size was determined as the average amplitude of the spontaneous miniature excitatory postsynaptic potentials (mEPSPs). Quantal size was significantly reduced in *GluRIIA*^{SP16} animals, demonstrating that absence of the GluRIIA subunit leads to a functional deficit consistent with previous studies. GluRIIA null animals expressing the GluRIIA$^{\alpha BT}$ subunit had significantly larger quantal size, demonstrating a strong partial rescue of GluRIIA$^{\alpha BT}$ subunit in a *GluRIIA*^{SP16} animal (Figure 2 A). We next assayed the physiological consequence of GluRIIA$^{\alpha BT}$ subunit expression during evoked stimulation at the NMJ. Animals expressing the GluRIIA$^{\alpha BT}$ subunit, despite having a quantal size slightly smaller than wild type, had wild-type sized EPSPs (Figure 2B). Representative mEPSP and EPSP traces for wild type, *GluRIIA*^{SP16} and GluRIIA$^{\alpha BT}$ genomic rescue animals are show in Figure 2 D – F.

Robust homeostatic signaling mechanisms have been demonstrated to increase presynaptic release in response to a decrease in postsynaptic quantal size at the Drosophila NMJ (Petersen et al., 1997; Davis et al., 1998; Paradis et al., 2001), as demonstrated by the almost wild type size EPSP in *GluRIIA*^{SP16} (Figure 2 B). To directly measure synaptic homeostasis, we quantified presynaptic release (quantal content) calculated by dividing the average EPSP amplitude by the average quantal size (Davis et al., 1998; Paradis et al., 2001). Quantal content is statistically increased in the GluRIIA$^{\alpha BT}$ genomic rescue animal, allowing for the normal sized EPSP (Figure 2 C). These results clearly demonstrate that the expression of GluRIIA$^{\alpha BT}$ does not disrupt the activation of the retrograde signaling system that is thought to be required for synaptic homeostasis at the Drosophila NMJ.

αBT binding does not disrupt GluRIIA$^{\alpha BT}$ function.

αBT is known to be a potent inhibitor of the AChR at the vertebrate NMJ. To test the effect of αBT binding on GluRIIA$^{\alpha BT}$ function, we measured quantal sizes in

GluRIIA$^{\alpha BT}$ genomic rescue animals after incubation in αBT-alexa fluor-488. Compared to GluRIIA$^{\alpha BT}$ genomic rescue animals that were preincubated in saline alone, the αBT incubated animals did not show any change in average quantal size. The average quantal size in GluRIIA$^{\alpha BT}$ genomic rescue animals with incubation in saline alone was 0.55 ± 0.04; n = 8. The average quantal size after incubation in αBT was 0.60 ± 0.04; n = 9. Thus, αBT binding to the Drosophila NMJ does not have an effect on glutamate receptor conductance or muscle depolarization.

GluRIIA$^{\alpha BT}$ levels are decreased compared to wild type GluRIIA levels.

Given the incomplete rescue of quantal size in GluRIIA$^{\alpha BT}$ genomic rescue animals (Figure 2 A), we hypothesized that the GluRIIA$^{\alpha BT}$ subunit may not be trafficked to the synapse in wild type levels. In fact, the range of quantal sizes for a wild type animal (0.95 – 1.2mV) was smaller than the range for the GluRIIA$^{\alpha BT}$ genomic rescue animals (0.5mV – 0.9mV). To evaluate levels of GluRIIA$^{\alpha BT}$, we performed immunofluorescent stainings of the NMJ using an anti-GluRIIA antibody. Similar to the electrophysiological quantal size results, the amount of anti-GluRIIA staining in GluRIIA$^{\alpha BT}$ genomic rescue animals was decreased compared to wild type animals (Figure 3). No change in control staining for HRP (a presynaptic membrane marker) was found (Figure 3). The GluRIIA$^{\alpha BT}$ subunits, while functional and properly localized, do not seem to be synaptically localized at wild type levels, despite being driven by the endogenous promoter (see Discussion).

GluRIIA$^{\alpha BT}$ subunits at a mature NMJ are relatively stable.

To visualize the internalization and insertion of GluRIIA$^{\alpha BT}$ subunits in the GluRIIA$^{\alpha BT}$ genomic rescue animals, dissected larval preps were incubated with αBT-alexa fluor-488 (applied 1st) to label the majority of surface receptors subunits. After washing and incubation, for either 30 minutes or 3 hours, preps were incubated in αBT-alexa fluor-594 (applied 2st) to bind any remaining unlabeled subunits or newly inserted subunits. After fixation and subsequent imaging, levels of fluorescence were quantified. Both fluorescently conjugated αBTs, as well as a control fluorescently conjugated anti-HRP antibody, showed no significant change when comparing labeling with a 30 minute incubation or a 3 hour incubation (Figure 4). In addition, no internalized pool of fluorescent GluRIIA$^{\alpha BT}$ was found. Thus, we hypothesize during this timescale, no significant internalization or insertion of receptor subunits occurs. Alternatively, internalization and subsequent degeneration of the receptors might occur too rapidly for the experimental design to accurately measure.

The GluRIIA$^{\alpha BT}$ subunit can be a powerful tool to examine the internalization and insertion of glutamate receptors in various mutant backgrounds that might have defects in receptor trafficking. We attempted to use this tool in a number of mutants known to have a deficit in GluRIIA levels at the synapse. Baseline variability in GluRIIA$^{\alpha BT}$ subunit expression was too variable in these mutant backgrounds to measure receptor dynamics as was done in the genomic rescue animals. With various modifications to the protocol, however, the GluRIIA$^{\alpha BT}$ subunit might still be an effective tool to look at receptor dynamics in mutant backgrounds (see Discussion).

Discussion

Here we have engineered a GluRIIA$^{\alpha BT}$ subunit containing the αBT binding site from the vertebrate acetylcholine receptor. We have shown that glutamate receptors containing this subunit are capable of trafficking and inserting postsynaptically at the Drosophila NMJ. These modified subunits co-localize with antibody stainings for the obligate subunit GluRIII, and oppose stainings for the pre-synaptic active zone marker nc82. When expressed as a genomic rescue construct in a *GluRIIA*^{SP16} null animal, the GluRIIA$^{\alpha BT}$ subunits form functional receptors which partially rescue the quantal size deficit in *GluRIIA*^{SP16} animals to almost 70% of wild type levels.

Over a 3 hour period, no internalization or insertion of GluRIIA$^{\alpha BT}$ subunits from the mature third-instar synapse was seen. While this supports data from the Sigrist lab, where a photoactivatable GFP-tagged GluRIIA receptor also exhibited little trafficking into or out of the mature synapse, it may be worthwhile to repeat the experiments both on a longer and shorter timescale. Recent work from the Huganir lab (Sekine-Aizawa and Huganir, 2004) looked at membrane insertion of AMPA receptors containing an αBT binding site tag. Neuronal AMPA insertion was seen in as little as 5 minutes.

Unfortunately quantification of internalization and insertion of GluRIIA$^{\alpha BT}$ subunits in various mutant background was not possible. The mutants were selected because they exhibited a decrease in GluRIIA levels at the synapse. In these backgrounds, the levels of GluRIIA$^{\alpha BT}$ subunits were decreased compared to the GluRIIA$^{\alpha BT}$ genomic rescue, but the levels were too variable to perform a proper analysis. A number of modifications to the protocol can be made to facilitate the success

of these experiments. Perhaps expressing the GluRIIA$^{\alpha BT}$ subunit under a more general muscle promoter might eliminate the variability in expression levels. Alternatively, cloning a larger section of upstream genomic DNA might more fully recapitulate the endogenous promoter function. Another tactic might be to perform live imaging on individual synapses thus eliminating the probably of animal variability in GluRIIA$^{\alpha BT}$ subunit expression. A two-photon microscope should be used to limit the amount of bleaching of the fluorescently conjugated αBT. Attempts at live imaging on the Zeiss Axiovert were difficult due to fast bleaching (data not shown).

Despite the difficulties in using the GluRIIA$^{\alpha BT}$ subunit, the tagging of proteins with an αBT binding site still remains a powerful technique that can be used to study the trafficking of a variety of membrane proteins.

Figures

Figure 3-1. GluRIIA$^{\alpha BT}$ subunits are properly localized at the NMJ.

(A) Amino acid sequence of the a-bungarotoxin binding site tag which is placed in the extracellular N-terminal region of the GluRIIA receptor (B) Representative NMJ from wild type and GluRIIA$^{\alpha BT}$ genomic rescue animals are shown that are bound by αBT-alexa fluor-488 (green) and co-stained with anti-HRP (red). (C) Synaptic bouton from GluRIIA$^{\alpha BT}$ genomic rescue animals bound by αBT-alexa fluor-488 (green) and co-stained with anti-nc82 (red). (D) Synaptic bouton from GluRIIA$^{\alpha BT}$ genomic rescue animals bound by αBT-alexa fluor-488 (green) and co-stained with anti-GluRIII (red).

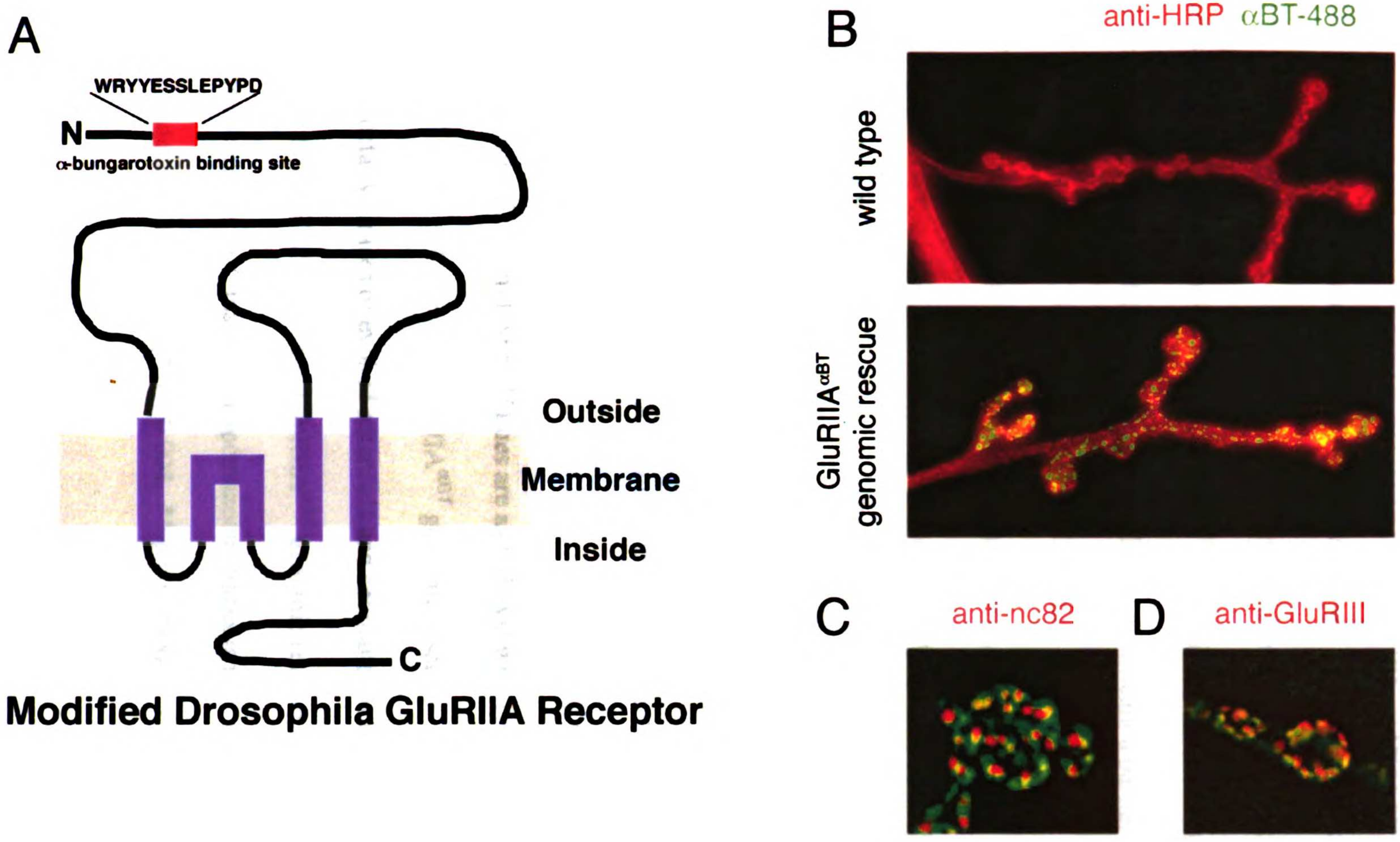
A
WRYYESSLEPYPD
N
α-bungarotoxin binding site
Outside
Membrane
Inside
C
Modified Drosophila GluRIIA Receptor
B
anti-HRP αBT-488
wild type
GluRIIA^αBT genomic rescue
C
anti-nc82
D
anti-GluRIII

Figure 3-2. Receptors containing the GluRIIA$^{\alpha BT}$ subunits are functional.

(A) Quantification of quantal size in control (open bar), *GluRIIA*^{SP16} (grey bar) and GluRIIA$^{\alpha BT}$ genomic rescue animals (filled bars). Wild type controls have a quantal size equal to 1.1mV ± 0.04mV, n = 11. *GluRIIA*^{SP16} animals have a significant decrease in quantal size (0.28mV ± 0.01mV, n = 9). GluRIIA$^{\alpha BT}$ genomic rescue animals have a quantal size approaching wild type levels, thus exhibiting significant a partial rescue (0.73mV ± 0.4mV; n = 11). (B) Quantification of EPSP size in control (open bar), *GluRIIA*^{SP16} (grey bar) and GluRIIA$^{\alpha BT}$ genomic rescue animals (filled bars). Wild type controls have an average EPSP size equal to 33.4mV ± 1.9mV, n = 11. *GluRIIA*^{SP16} animals have a slight but significant decrease in EPSP size (26.1mV ± 0.9mV, n = 9). GluRIIA$^{\alpha BT}$ genomic rescue animals have an EPSP not statistically different than wild type (37.3mV ± 1.9mV; n = 11). (C) Quantification of quantal content in control (open bar), *GluRIIA*^{SP16} (grey bar) and GluRIIA$^{\alpha BT}$ genomic rescue animals (filled bars). There is are significant increases in quantal content comparing the *GluRIIA*^{SP16} and GluRIIA$^{\alpha BT}$ genomic rescue animals to wild type. Values are as follows: wild type = 31.5 ± 1.6, n = 11 ; *GluRIIA*^{SP16} = 94.9 ± 4.4, n = 9; GluRIIA$^{\alpha BT}$ genomic rescue = 53.3 ± 4.1, n = 11.

(D – F) Representative traces of evoked potentials and spontaneous miniature potentials (insets) for wild type, *GluRIIA*^{SP16} and GluRIIA$^{\alpha BT}$ genomic rescues respectively. Scale bar for evoked release is mV, ms and for spontaneous traces is mV, ms.

Significance is denoted as follows (* $p < 0.004$, ** $p < 0.00002$). Error bars represent ± SEM.

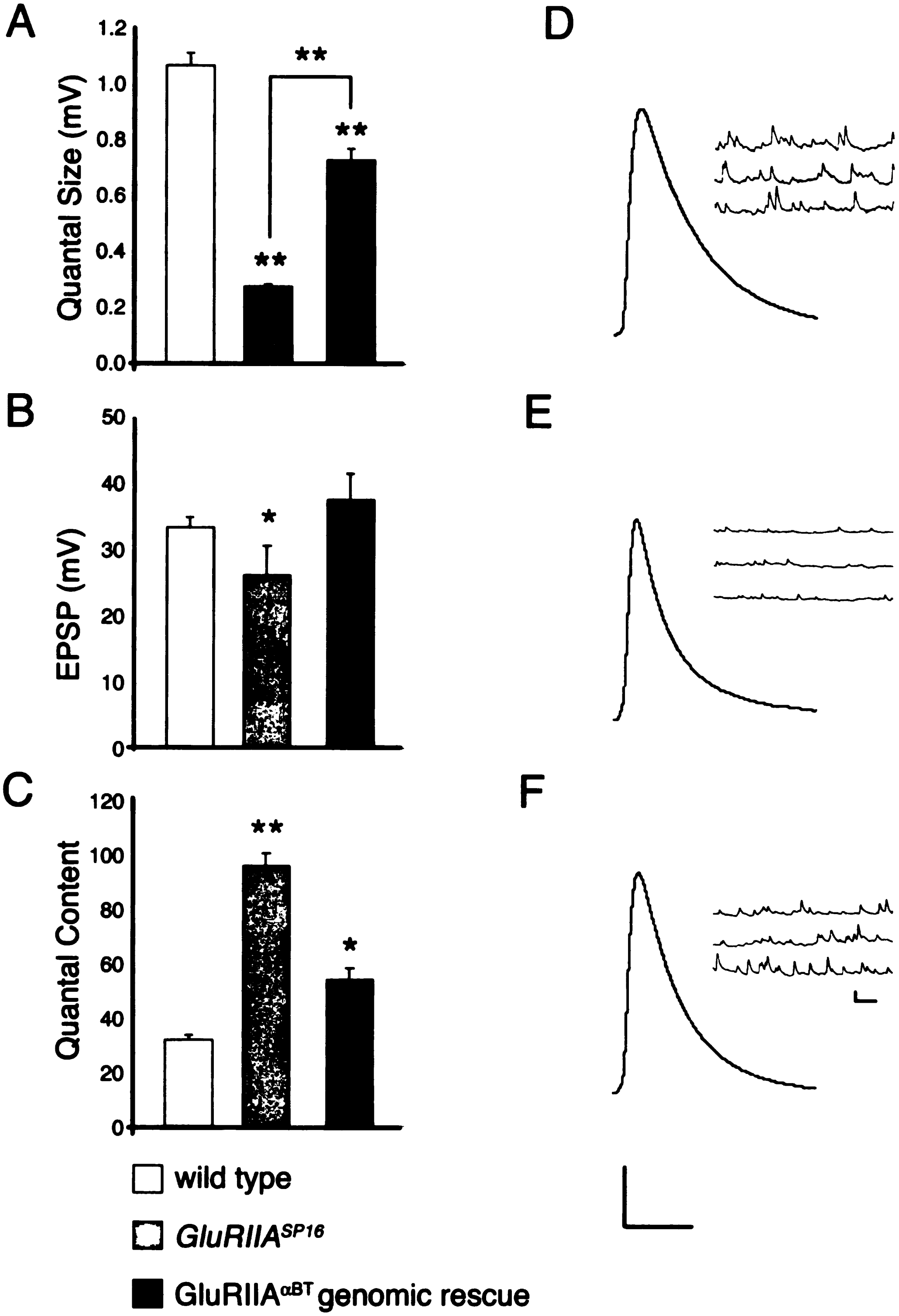
A
1.2
1.0
0.8
0.6
0.4
0.2
0.0
Quantal Size (mV)
**
**
**
B
50
40
30
20
10
0
EPSP (mV)
*
C
120
100
80
60
40
20
0
Quantal Content
**
*
D
E
F
☐ wild type
▨ *GluRIIA^SP16*
■ GluRIIA^αBT genomic rescue

Figure 3-3. Expression of GluRIIA$^{\alpha BT}$ subunits at the NMJ.

Representative images of NMJs staining with anti-HRP (left column) and anti-GluRIIA (right column). Genotypes are: wild type (top row), *GluRIIA*^{SP16} (middle row) and GluRIIA$^{\alpha BT}$ genomic rescues (bottow row). Note that while the GluRIIA$^{\alpha BT}$ subunits do traffic to the synapse properly, they are likely reduced in number compared to a wild type animal.

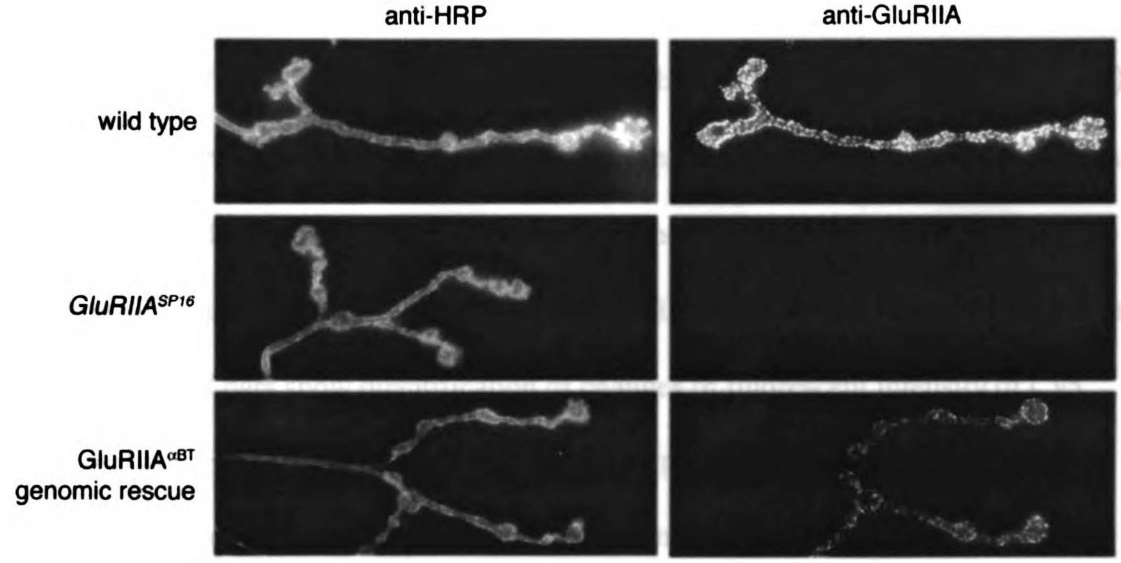
anti-HRP
anti-GluRIIA
wild type
GluRIIA^{SP16}
GluRIIA$^{\alpha BT}$
genomic rescue

Figure 3-4. No significant insertion or internalization of GluRIIA$^{\alpha BT}$ subunits is detected.

First set of bars show quantification of changes in fluorescent intensity of αBT-alexa fluor-488 applied before a 30 minute (open bar) or 3 hour (filled bar) incubation in saline showed no significant difference (30 minute = 100 ± 13, n = 6; 3 hour = 98 ± 2.5, n = 6). Middle set of bars show quantification of changes in fluorescent intensity of αBT-alexa fluor-594 applied after a 30 minute (open bar) or 3 hour (filled bar) incubation in saline also showed no significant difference (30 minute = 100 ± 22, n = 6; 3 hour = 74 ± 9.7, n = 6). Final set of bars show quantification of changes in fluorescent intensity of Cy5 conjugated anti-HRP applied after fixation of preps previously incubated for 30 minute (open bar) or 3 hour (filled bar) saline also showed no significant difference (30 minute = 100 ± 9.5, n = 6; 3 hour = 90 ± 9.7, n = 6).

Error bars represent ± SEM.

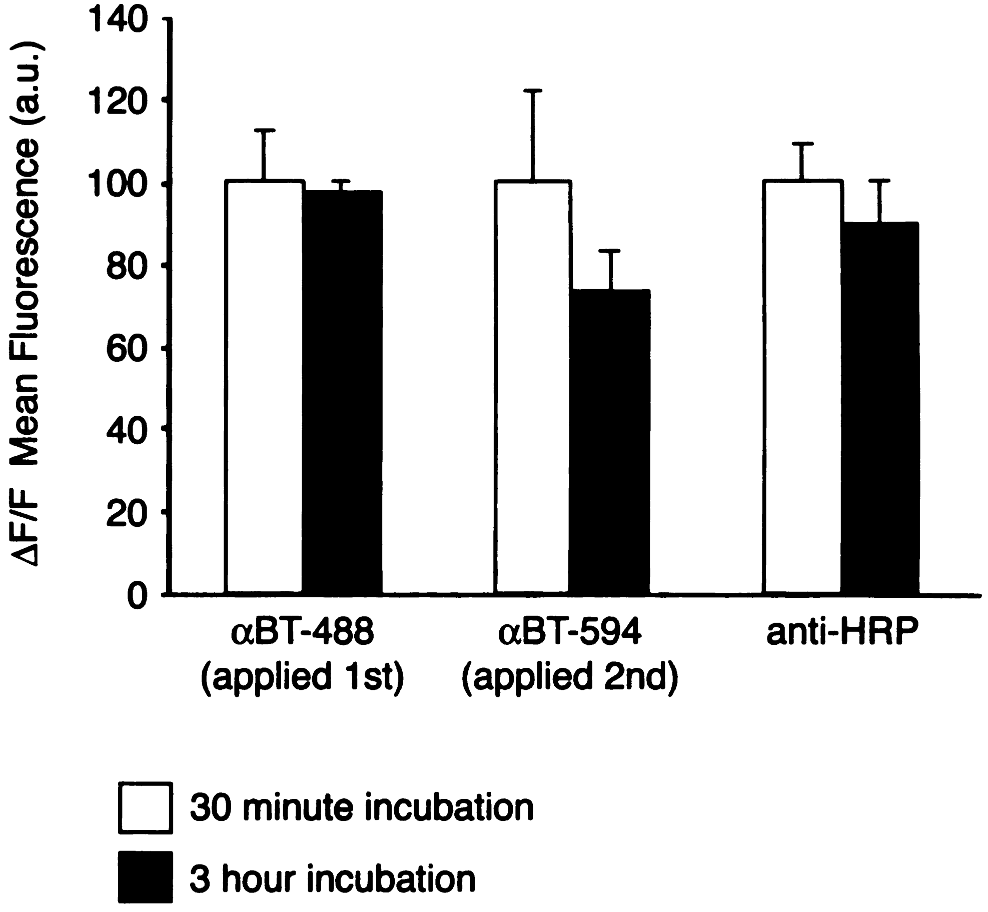

ΔF/F Mean Fluorescence (a.u.)
0
20
40
60
80
100
120
140
αBT-488 (applied 1st)
αBT-594 (applied 2nd)
anti-HRP
30 minute incubation
3 hour incubation

Chapter Four:

Calculus identifies a novel secreted inhibitor of synaptic homeostasis at the Drosophila NMJ

Summary

Homeostatic mechanisms exist at the Drosophila neuromuscular junction (NMJ) such that proper synaptic strength is maintained despite impaired muscle excitability. The mechanisms that underlie synaptic homeostasis are not known. Here we identify *Calculus* (*calc*), as a secreted inhibitor of synaptic homeostasis. Overexpression of Calc protein leads to a complete block of homeostasis induced by two different experimental manipulations. Overexpression of *calc* leads to developmental abnormalities of ventral nerve cord condensation, but does not alter baseline synaptic function or synaptic morphology at the NMJ. Data demonstrate that synaptic development can occur normally in the absence of synaptic homeostasis. Thus, homeostasis is a form of plasticity, independent of neuromuscular development, which may be invoked to ensure normal muscle depolarization in the face of developmental or disease related abnormalities.

Introduction

A fundamental feature of the nervous system is its ability to adapt to changing activity levels and a changing environment, while still maintaining stability. Our hypothesis is that homeostatic mechanisms exist to compensate for perturbations that alter excitability such that an appropriate excitation level is maintained (Davis and Bezprozvanny, 2001; Turrigiano, 1999; Turrigiano and Nelson, 2004; Davis, 2006). One type of homeostasis, synaptic homeostasis, occurs through changes in synaptic efficacy and has been documented in preparations ranging from the vertebrate CNS to the invertebrate PNS.

Synaptic homeostasis experiments generally involve examining synaptic function before and after a perturbation that changes excitation of the postsynaptic cell. In cultured cortical neurons, a homeostatic process known as 'synaptic scaling' compensates for a chronic activity blockade by increasing synaptic strength via an increase in miniature excitatory postsynaptic current (mEPSC) amplitudes (Turrigiano et al., 1998). A similar sort of synaptic scaling is also seen *in vivo* in rat visual cortex where monocular deprivation results in an increase in mEPSC size (Desai et al., 2002). At the Drosophila neuromuscular junction (NMJ), decreases in muscle innervation and neurotransmitter release, resulting from altered levels of a cell-adhesion molecule, lead to a compensatory upregulation of miniature excitatory postsynaptic potential (mEPSP) amplitude (Davis and Goodman, 1998a).

In addition to the regulation of postsynaptic receptor function, synaptic homeostasis can modulate synaptic efficacy via the regulation of presynaptic neurotransmitter release. Both vertebrate and invertebrate NMJs demonstrate synaptic homeostasis when muscle excitability is perturbed. The strength of a neuromuscular synapse must be precisely maintained to depolarize the muscle to contraction. If the strength is too high, the muscle will undergo tetanus. If the strength is too low, a muscle will fail to contract. Early evidence supporting the existence of synaptic homeostasis at the NMJ came from studies of the human disease, myasthenia gravis. Myasthenia gravis is an autoimmune disease where nicotinic acetylcholine receptors (AChR) are progressively lost from the NMJ (Richman and Agius, 2003). In response to the decrease in postsynaptic receptor function, a compensatory increase in presynaptic transmitter release occurs (Cull-Candy et al., 1980). Experimental perturbations leading to a decrease in AChR sensitivity at the rat NMJ also result in compensatory increases in transmitter release (Plomp et al, 1992; Sandrock et al., 1997).

At the Drosophila NMJ, three distinct experimental perturbations have been demonstrated to result in synaptic homeostasis via the regulation of presynaptic neurotransmitter release. Two such manipulations at the Drosophila NMJ involve creating an impairment of postsynaptic glutamate receptor sensitivity. Either mutations in the GluRIIA subunit of the glutamate receptor (Petersen et al., 1997), or overexpression of the activated catalytic subunit of protein kinase A (PKA) (Davis et al., 1998), lead to a reduction of mEPSP size via a decrease in the current through the postsynaptic glutamate receptors. A third manipulation, independent of glutamate receptor function, utilizes postsynaptic overexpression of the Kir2.1 potassium channel to impair muscle depolarization (Paradis et al., 2001). All three perturbations result in a compensatory increase in presynaptic transmitter release such that proper muscle depolarization is restored.

Here we describe a novel secreted protein that can block homeostasis at the Drosophila NMJ. The *calculus* (*calc*) gene was identified in a gain-of-function P-element screen using the EP collection (see below). Only a single line was found to inhibit homeostasis when expressed at the Drosophila NMJ. Overexpression of Calc protein completely blocks homeostasis, yet appears to have no effect on normal NMJ function or NMJ synaptic morphology. Calc is the first example of a molecule that can systemically inhibit synaptic homeostasis.

Results

Gain-of-function screen for an inhibitor of homeostasis.

Homeostasis at the Drosophila larval NMJ involves a retrograde signal from the muscle resulting in upregulation of presynaptic neurotransmitter release. Little else, however, is known about the underlying mechanisms of synaptic homeostasis. In addition, no one to date has described the existence of an inhibitor of synaptic homeostasis. To determine if an inhibitor of synaptic homeostasis can exist, we performed a gain-of-function screen where each of the 2300 EP lines (Rorth, 1996) were postsynaptically expressed at the NMJ in the PKA background. The EP collection is a set of Drosophila fly lines, each of which contains a transposable element (EP element) inserted randomly into the genome. The EP element binds the yeast transcription factor Gal4 and can thereby drive transcription of a nearby gene 3' to the insertion site. Expression of these random genes can be spatially and temporally restricted by using the EP collection in combination with fly lines that express the Gal4 transcription factor in a defined pattern (Brand and Perrimon, 1993). To determine if synaptic homeostasis could be perturbed at the Drosophila NMJ, each of the 2300 independent EP lines were expressed in a muscle with impaired excitability (G. Davis, unpublished results).

The PKA background consists of overexpression of the catalytic subunit of PKA specifically in muscle. Overexpression of PKA leads to a decrease in the average amplitude of mEPSPs (quantal size) by modulation of the sensitivity to glutamate of GluRIIA subunit-containing postsynaptic receptors. The presynaptic motoneurons compensate for the decrease in quantal size by increasing presynaptic transmitter release (Davis et al., 1998). Despite the fact that these animals are compensating perfectly for

the decrease in muscle excitability, they are still somewhat less viable compared to controls. We reasoned that since a homeostatic animal is sub-viable, an animal in which homeostasis is blocked would exhibit an even greater enhancement of lethality. Each EP line that enhanced lethality in the PKA background was retested in a secondary screen that examined synaptic morphology. After eliminating any lines where expression led to defective NMJ structure, we were left with just a single candidate inhibitor of homeostasis. This EP line is positioned to drive the expression of a gene corresponding to a predicted gene we call *calculus (calc).*

Since *calc* was identified based on the overexpression phenotype of increased in lethality in the PKA background, we next examined the survivability of animals overexpressing Calc in a different homeostatic background. Animals overexpressing the Kir2.1 potassium channel in muscle exhibit a decrease in muscle excitability, which is homeostatically compensated for by an increase in neurotransmitter release (Paradis et al., 2001; see below). Overexpression of Calc protein in Kir2.1 expressing muscle leads to an enhancement of lethality. *Kir2.1* expression alone leads to a moderate 30% lethality of animals, when compared to non-*Kir2.1* expressing sibling controls. Overexpression of both *Kir2.1* and *calc* leads to 86% lethality, a clear enhancement.

Calc encodes a novel secreted protein.

The P-element insertion Calc^{EP} lies upstream of the *calc* gene. Gene predictions indicate that two splice forms of the gene, Calc-A and Calc-B, exist (Figure 1A). Both transcripts of *calc* contain signal sequences and the resulting protein is likely cleaved between the 24th and 25th residue (SignalIP 3.0; Bendtsen et al, 2004). Calc-A, corresponding to the

longer transcript, encodes a novel protein with homologues in another Drosophila species, D. pseudoobscura, as well as in a number of distantly related arthropods such as mosquito and honeybee. Alignments indicate that Calc-A contains a number of conserved cysteine residues (data not shown). The Calc-B isoform is not conserved. While there exist no known vertebrate homologues of *calc*, an analogous signaling pathway in vertebrates may exist. Small, secreted peptides often evolutionarily diverge much faster than the receptors they bind to do. When the signaling pathway *calc* interacts with is identified, the pathway components may very likely have vertebrate homologues.

Protein sequence analysis indicated that Calc is a secreted protein. To test this directly, we used Schneider S2 cells to examine if the Calc protein can be secreted. Calc protein tagged with a V5 epitope was expressed in S2 cells. Using an anti-V5 antibody, the tagged Calc-A (Figure 1B) and Calc-B (data not shown) proteins were detected in the S2 cell lysate, as well as in purified media, indicating that that Calc can be secreted. In contrast, the non-secreted control protein Enabled was detected only in cell lysates.

Calc expression pattern.

We next examined the expression of *calc* in Drosophila embryos. Using *in situ* hybridization techniques, *calc* is specifically expressed in the salivary glands, the proventriculus, oenocytes and in a subset of cells in the ventral nerve cord on either side of the midline (Figure 2A, B). Oenocyte staining was also still visible in the third-instar preparation (data not shown). In addition, after cloning the genomic region upstream of the *calc* gene, we created a *calc-Gal4* transgenic fly. We used *calc-Gal4* line to drive a

nuclearly localized *lacZ* gene (UAS-nls.lacZ) in *calc*-expressing tissues in. β-galactosidase expression was additionally found in third-instar fat bodies (data not shown).

Early Calc overexpression affects the anatomical structure of the VNC.

To fully characterize the gain-of-function phenotypes associated with overexpression of Calc, we used the Calc^{EP} line to ectopically express Calc in a variety of tissues. When driving Calc with an early neuronal driver (*C155-Gal4*), the larval brain underwent a dramatic change in morphology. In the Calc-expressing brains, the ventral nerve cord (VNC) is much longer than in wild-type animals (Figure 3A and B). The elongated VNC does not seem to be due to an increase in neuronal proliferation. Examination of Calc-expressing brains with a variety of neuronal cell-type markers such as anti-5HT (seratonergic neurons, Figure 3A and B), anti-eve (subset of motoneurons and interneurons, data not shown), and anti-CAP (subset of peptidergic neurons, data not shown) did not show an obvious change in number of these various cell types. Alternatively, the increase in length of Calc-expressing brains could be due to a failure of VNC condensation during embryogenesis. Condensation leads to a coordinated decrease in size and an increase in cellular density without a large change in cell number (Olofsson and Page, 2005). VNC condensation begins at embryonic stage 15. Late stage 16 embryos which expressing Calc neuronally, as compared to wild-type embryos, already exhibit a condensation phenotype consistent with the third-instar findings (data not shown).

The elongated VNC phenotype found in animals expressing Calc was not limited to neuronally expressed Calc protein. Consistent with our findings that Calc is a secreted protein, early muscle overexpression of *calc* (*24B-Gal4* or *G14-Gal4*) also lead to an elongated VNC (data not shown). Expressing *calc* in muscles using a driver that does not express strongly until the 1st instar larval stage (*MHC-Gal4*), after VNC condensation is complete, does not result in altered VNC gross morphology. Thus *calc* expression in the embryo can alter nerve condensation. This phenotype is unlikely due to an enhancement of neuronal proliferation, though all cell types, including glia, have yet to be analyzed.

Calc expression in wild-type animals has no effect on function.

To characterize the functional consequences of *calc* overexpression, we first examined *calc* overexpression in a wild-type background. We compared Calc protein overexpression in muscle (*MHC-Gal4*), fat body (*TF060-Gal4*) and neurons (*C155-Gal4*). Calc expression did not change the average muscle input resistance, resting membrane potential or normal innervation pattern (see below) in any of these genetic backgrounds. Quantal size was determined as the average amplitude of the spontaneous mEPSPs. EPSP amplitude was calculated as the amount of depolarization of the muscle membrane in response to evoked motoneurons stimulation. Both quantal size and EPSP size were not significantly affected by *calc* overexpression (Figure 4A and B). Quantal size was slightly smaller in animals where Calc was neuronally or muscularly overexpressed, but this was not significantly different than the two controls. In addition, we also calculated presynaptic release (quantal content), calculated by dividing the average EPSP amplitude by the average quantal size (Davis et al., 1998; Paradis et al., 2001). Again, Calc overexpression had no significant effect on presynaptic release. Also, despite the grossly abnormal length of the VNC in neuronally expressing Calc animals, the function of the NMJ was normal.

Overexpression of Calc blocks homeostasis.

To confirm that *calc* encodes a specific inhibitor of synaptic homeostasis, Calc protein was overexpressed in two independent homeostatic backgrounds, Kir2.1-expressing muscles and *GluRIIA*^{SP16} mutants. Expression of the human Kir2.1 inwardly rectifying potassium channel in muscle impairs muscle depolarization without altering postsynaptic glutamate receptor function. In Kir2.1-expressing muscle there is a persistent outward potassium current which decreases muscle input resistance and leads to a hyperpolarized resting potential. The impairment of muscle input resistance in Kir2.1-expressing muscles leads to a decrease in quantal size (Figure 5A and Paradis et al., 2001). The additional expression of *calc* in Kir2.1-expressing animals leads to no further decrease in quantal size (Figure 5A).

In Kir2.1-expressing animals, a homeostatic increase in presynaptic neurotransmitter release occurs that compensates for the decrease in quantal size. In fact, the compensation results in precisely wild-type levels of peak EPSP amplitude, despite a decrease in resting membrane potential. The muscle appears to monitor absolute membrane depolarization and make changes in presynaptic neurotransmitter release to maintain the appropriate synaptic efficacy (Paradis et al., 2001). To directly test if *calc* expression can inhibit synaptic homeostasis, we next assayed the physiological consequence of Calc protein expression on evoked stimulation. Again, due to robust synaptic homeostasis, Kir2.1-expressing muscles precisely reach wild-type potentials upon stimulation (Figure 5B and Paradis et al., 2001). Expression of *calc* in Kir2.1-expressing animals blocks homeostasis such that wild-type levels of depolarization are no longer met (Figure 5B). The gain-of-function block of homeostasis can be reproduced by expressing a corresponding *calc* cDNA (isoform Calc-B, data not shown).

The homeostatic Kir2.1 background used for the above experiment limited our analysis to an overexpression of *calc* in muscle cells. To further examine the ability of *calc* to act as an inhibitor of homeostasis we used the GluRIIA null mutant background (*GluRIIA*^{SP16}). The synapse in the *GluRIIA*^{SP16} mutant is morphologically wild-type, and the remaining glutamate receptor subunits are responsible for synaptic conductances that achieve a quantal size that is roughly 50% of that observed in wild type. The motoneuron that innervates these compromised muscles homeostatically compensates for the decrease in quantal size with increased neurotransmitter release (Petersen et al., 1997; DiAntonio et al., 1999).

We next tested whether overexpression of Calc by the fat bodies, a tissue that normally expresses Calc, can block homeostasis in a *GluRIIA*^{SP16} background. There was no change in the average muscle input resistance or resting membrane potential in any genetic background. As expected, quantal size in the *GluRIIA*^{SP16} background, both with and without Calc overexpression, is about half the size of wild-type (Figure 6A). To directly test whether synaptic homeostasis was blocked, we quantified presynaptic release (quantal content) calculated by dividing the average EPSP amplitude by the average quantal size (Davis et al., 1998; Paradis et al., 2001). Quantal content is dramatically increased in the *GluRIIA*^{SP16} background, indicating a robust homeostasis. If we now overexpress Calc in the fat bodies (*TF060-Gal4*), the increase in quantal content is blocked (Figure 6B). Thus, Calc overexpression in the fat bodies can completely block homeostasis. In addition, experiments overexpressing Calc in either neurons (*C155-Gal4*) or muscle (*MHC-Gal4*), in a *GluRIIA*^{SP16} background, also led to a complete block of homeostasis (G. Davis, personal communication). Given that Calc is a secreted protein, it appears that Calc can block homeostasis non-cell autonomously. It may be sufficient to just secrete Calc into the hemolymph, which has access to the NMJ.

Overexpression of *calc* in *GluRIIA*^{SP16} mutant animals blocks homeostasis such that quantal content does not compensate for impaired muscle excitability. In fact, quantal content remains at wild-type levels (Figure 6B). Homeostasis may be blocked in these animals, but normal development and normal levels of neurotransmitter release can occur in the absence of GluRIIA subunits.

Calc blocks homeostasis without altering NMJ structure.

We previously found that Calc protein expression can block homeostasis in a *GluRIIA*^{SP16} mutant background when expressed by either muscle, neuron or fat body specific drivers. Here we examine the structure of the NMJ where homeostasis is blocked. Individual boutons (varicosities in the nerve terminal) were counted in a control animals (*MHC-Gal4*), in animals with normal homeostatic compensation (*Calc*^{EP}, *GluRIIA*^{SP16}) and in animals where Calc expression leads to a block of homeostasis (*Calc*^{EP}, *GluRIIA*^{SP16}; *MHC-Gal4*). In these three genotypes, bouton number is not significantly different from wild-type (Figure 7A and B). In addition, we examined a number of synaptic markers in these Calc-expressing NMJs. All markers that we examined, including the presynaptic active zone marker nc82, the NCAM-like pre and postsynaptic protein FasII, the glutamate receptor subunit GluRIII, and the predominantly postsynaptically localized protein Dlg all appeared normal both in level and localization pattern (Figure 7C). Calc expression at the NMJ does not appear to alter NMJ structure, despite the ability of the Calc protein to block homeostasis.

Discussion

Here we have identified a novel secreted inhibitor of homeostasis at the Drosophila NMJ. The *calc* gene was identified in a gain-of-function genetic screen for homeostatic molecules. In addition to the screen background, Calc overexpression can completely block homeostasis in two additional homeostatic backgrounds (*Kir2.1*-expression and *GluRIIA*^{SP16}) (Figure 5 and 6). The block of homeostasis was achieved without affecting the morphology of the NMJ synapse (Figure 7). Overexpression of Calc in an otherwise wild-type animal also had no functional effects (Figure 4). Thus, Calc is a specific inhibitor of homeostasis.

calc expression studies identified *calc* as being predominantly expressed in non-neuronal tissues such as the fat body, the salivary gland, the proventriculus and oenocytes (Figure 2). It may seem as if the wide variety of cell types which express Calc have rather diverse functions. In addition to their main function, however, the salivary glands and and proventriculus both play a role in the immune response. These organs can release the anti-fungal peptide drosomycin (Ferrandon et al., 1998) or the anti-microbial peptides attacin/diptericin (Tzou et al., 2000) respectively. The fat bodies are well-studied organ that, in larvae, can secrete at least 7 different anti-microbial peptides directly into the hemolymph (Tzou et al., 2002). The exact function of larval oenocytes is unknown, though they are thought to be specialized secretory cells (Gould et al., 2001). It is also known that anti-microbial peptides in invertebrates tend to be cysteine-rich (Dimarcq et al., 1998). Given the expression pattern of *calc* in a number of immune-related tissues, as well as the highly conserved cysteine rich structure of the protein (Figure 1B), we speculate that Calc may also act as a novel anti-microbial type protein.

Although *calc* is also expressed in a small number of VNC neurons, this is not necessarily surprising, nor is it contradictory, to the possible immune related function of Calc. Given the relative isolation of the drosophila CNS and the other tissues due to the blood-brain barrier (Schwabe et al., 2005), it is possible that the CNS has adapted traditional immune signaling molecules to serve a different function. Components of the NF-kappaB signaling cascade, which regulates the innate immune response in both vertebrates and invertebrates, are found both in the vertebrate CNS and at the Drosophila NMJ (Mattson, 2005; Cantera et al., 1999; E. Heckscher, personal communication). NF-kappaB in vertebrates can regulate synaptic plasticity and plays a role in learning and memory (Meffert et al., 2003; Kaltschmidt et al., 2006; O'Riordan et al., 2006). At the Drosophila NMJ, the NF-kappaB signaling pathway is required for normal NMJ structure and function (Cantera et al., 1999; E. Heckscher, personal communication). In vertebrates, the classic immune system signaling molecule TNF-α is also found in the CNS (Stellwagen and Malenka, 2006). TNF-α has been recently described as a mediator of synaptic homeostasis in vertebrate cultures (Stellwagen and Malenka, 2006).

All of the proteins identified as playing a role in synaptic homeostasis, such as TNF-α, are positive regulators. *calc* is the first example of an inhibitor of synaptic homeostasis. The means by which *calc* blocks synaptic homeostasis are not clear. Given that Calc is a secreted protein, the site of action of Calc is unknown. Calc protein could be inhibiting any of the three phases of homeostasis at the NMJ. First, *calc* could be blocking the molecular mechanisms that monitor muscle cell excitability. Alternatively, Calc could be blocking the retrograde signaling cascade that signals from the muscle to the neuron to regulate presynaptic neurotransmitter release. Finally, Calc could be interfering with the presynaptic mechanisms that result in increased neurotransmitter release. However, since *calc* overexpression does not alter baseline neurotransmitter release, Calc protein is not affecting some aspect of the release machinery directly but might alter the signaling that would upregulation of release. Future experiments will focus on identification of which part of the homeostatic signaling cascade *calc* is interfering with. In addition, to fully understand the role of endogenous Calc protein, loss-of-function screens to identify mutations in *calc* are being performed. Given that *calc* is an inhibitor of synaptic homeostasis, a loss-of-function mutation in *calc* might not necessarily have any phenotype at the NMJ in a wild-type animal.

It is interesting to speculate on why the nervous system would need a general inhibitor of synaptic homeostasis. Given that blocking homeostatic compensation (at least in the fly) leads to an increase in lethality, the existence of such an inhibitor seems dangerous. One can, however, imagine a situation arising where neuronal or muscular cellular excitability is only temporarily impaired. Under conditions of temporary acute stress, such as sleep and eating disturbances or a disease state, learning and memory is impaired (Shors, 2004). Given that the changes in cellular firing patterns and cellular excitability underlying nervous system impairment are only temporary, one would not want the nervous system to drastically change presynaptic neurotransmitter release or postsynaptic receptor levels. Such changes, once the temporary stressor is eliminated, would lead to inappropriate synaptic efficacy and might be more detrimental to nervous system function than the original stressor.

One of the most interesting points to come out of this study, is that homeostasis works independently of development at the Drosophila NMJ. Over four days of larval growth, larval muscles increase tremendously in size and a corresponding increase in synaptic efficacy is required to assure appropriate muscle contraction. To achieve this, the motoneuron increases both in size and strength. It has been hypothesized that this coordination between transmitter release efficacy and the size of the muscle is an example of homeostasis. However, given that overexpression of *calc* throughout larval development does not disrupt motoneuron growth or function, it seems that synaptic homeostasis is not required for this developmental coordination. While we have not ruled out the existence of other independent homeostatic signaling mechanisms that function during development, we hypothesize that the developmental increase in muscle size and motoneurons transmitter release efficacy are independent, but temporally coordinated, developmental events. We suggest that homeostasis does not regulate fundamental NMJ development, but rather constrains the variability associated with a robust but, ultimately, imperfect developmental program.

Figures

Figure 4-1. Secreted Calc protein structure and gene sequence.

(A) The Calc protein structure. The open reading frame of the transcript is marked by the red boxes. The arrow on the EP element indicates direction of Gal4-induced transcription. (B) Western blot of total cell lysate and purified medium from Schneider cells transfected with pMT-Calc-V5/His after induction of expression. The migration of the Calc-V5 band fits well with the predicted size of the secreted protein.

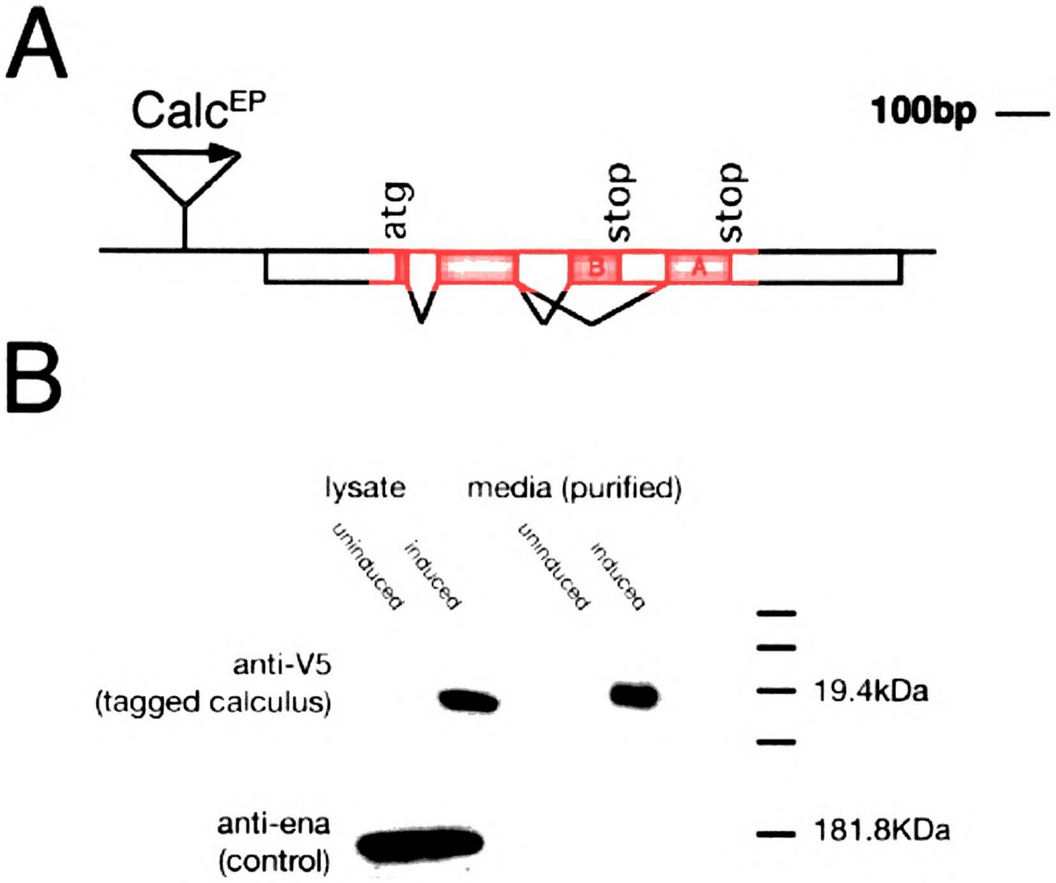
A
Calc^{EP}
100bp
atg
stop
stop
B
A
B
lysate
media (purified)
uninduced
induced
uninduced
induced
anti-V5
(tagged calculus)
anti-ena
(control)
19.4kDa
181.8KDa

Figure 4-2. Calc expression pattern.

In situ analysis found *calc* transcript to be specifically expressed in (A) the salivary glands (black arrow), proventriculus (white arrow) and oenocytes (arrowheads). Using the *Calc-Gal4* construct to drive lacZ, (B) *calc* expression was also seen in a few clusters of CNS cells on either side of the midline.

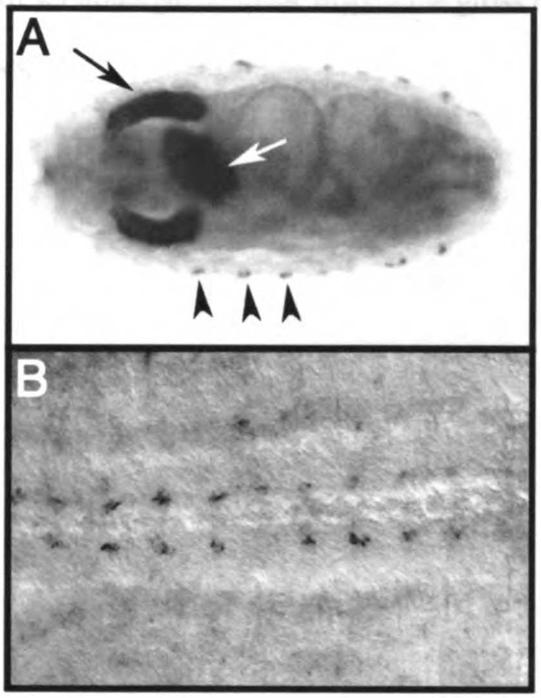
A
B

Figure 4-3. Early Calc overexpression leads to an elongated CNS.

Anti-serotonin (red) staining in third-instar larval brains from (A) wild-type and (B) calc-overexpressing (*C155-Gal4/+; Calc*^{EP} /+) animals. Note there appears to be no net change in the number of seratonergic neurons, dispite the gross morphological changes in the *calc*-expressing CNS.

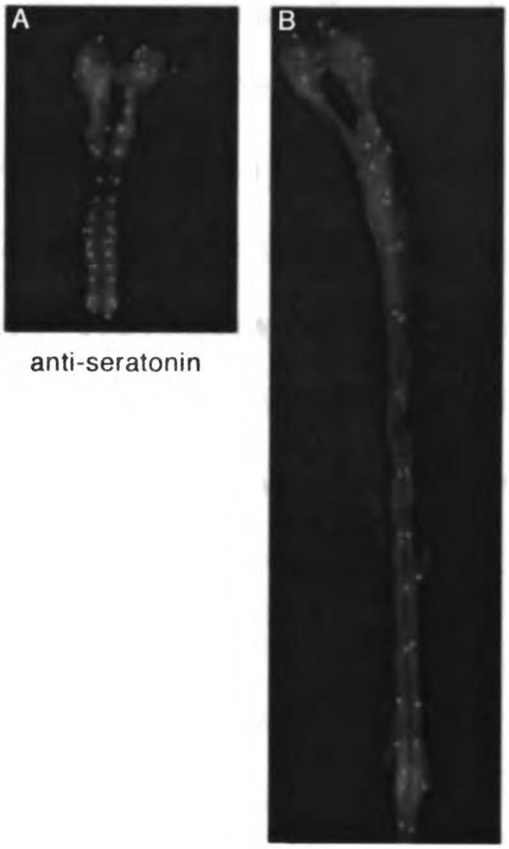

anti-seratonin

Figure 4-4. Calc overexpression in neuron, fat body or muscle has no functional affect.

Quantification of (A) quantal size, (B) EPSP size and (C) quantal content in control genotypes compared to animals overexpressing Calc in muscle, fat body or neuron. Quantal size values are as follows: *w* = 1.0mV ± 0.1, n = 9; *yw* = 1.1mV ± 0.06, n = 18; *Calc*^{EP}*/+; MHC-Gal4/+* = 0.8mV ± 0.04, n = 8; *Calc*^{EP}*/+; TF060-Gal4/+* = 1.2mV ± 0.08, n = 8; *C155-Gal4/+; Calc*^{EP}*/+* = 0.8mV ± 0.04, n = 7. EPSP values are as follows: *w* = 40mV ± 3.9, n = 7; *yw* = 37mV ± 1.0, n = 17; *Calc*^{EP}*/+; MHC-Gal4/+* = 39mV ± 1.2, n = 8; *Calc*^{EP}*/+; TF060-Gal4/+* = 35mV ± 2.0, n = 8; *C155-Gal4/+; Calc*^{EP}*/+* = 38mV ± 1.5, n = 7. Quantal content values are as follows: *w* = 39.2 ± 3.9, n = 7; *yw* = 33.8 ± 1.5, n = 17; *Calc*^{EP}*/+; MHC-Gal4/+* = 47± 2.4, n = 8; *Calc*^{EP}*/+; TF060-Gal4/+* = 30.7 ± 1.6, n = 8; *C155-Gal4/+; Calc*^{EP}*/+* = 46.6 ± 3.0, n = 7. There is no significant difference between the Calc-overexpressing genotypes and the two control genotypes in any parameter tested.

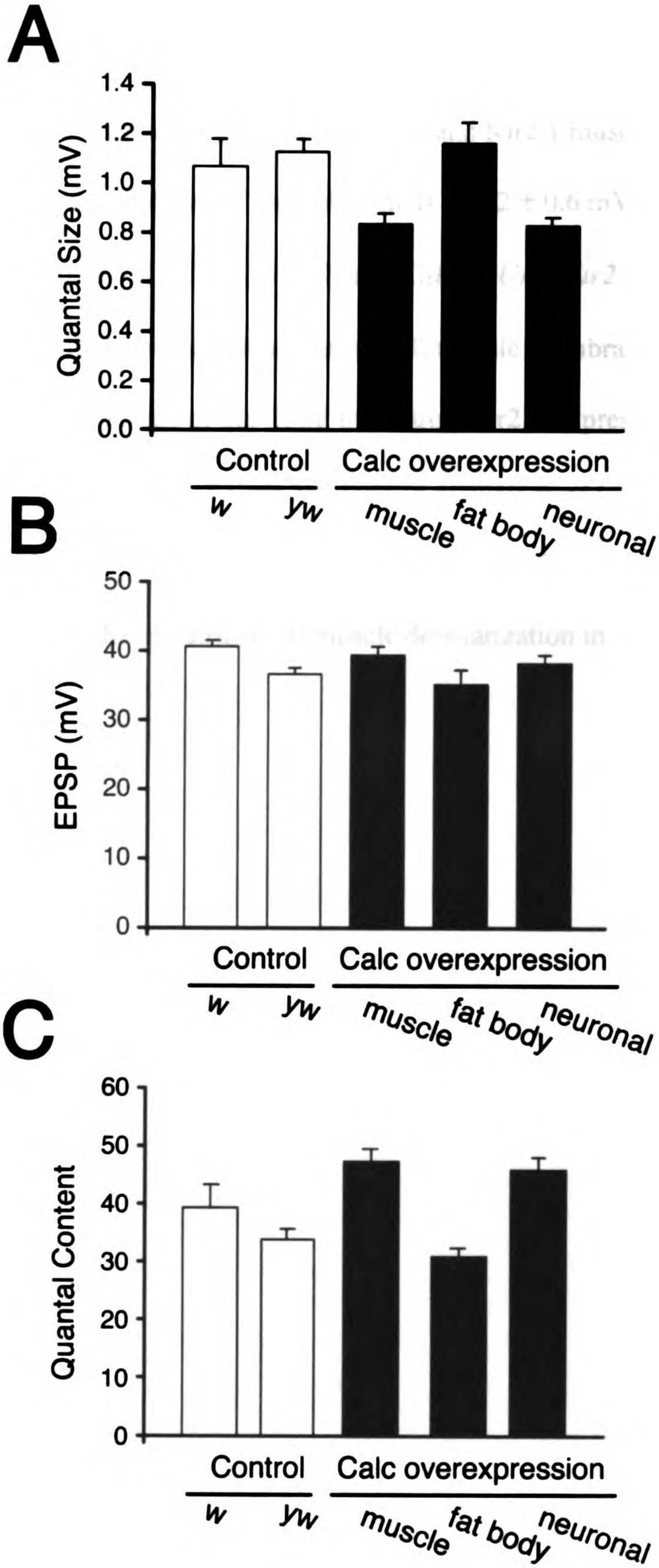
A
Quantal Size (mV)
1.4
1.2
1.0
0.8
0.6
0.4
0.2
0.0
Control
Calc overexpression
w
yw
muscle
fat body
neuronal
B
EPSP (mV)
50
40
30
20
10
0
Control
Calc overexpression
w
yw
muscle
fat body
neuronal
C
Quantal Content
60
50
40
30
20
10
0
Control
Calc overexpression
w
yw
muscle
fat body
neuronal

Figure 4-5. Calc-expression in Kir2.1 animals impairs postsynaptic depolarizations. (A) Quantification of the average amplitude of the spontaneous mEPSPs (quantal size) in control, Kir2.1 muscle expressing animals and Calc- and Kir2.1 muscle co-expressing animals. The average quantal size of control animals = 2.2 ± 0.6 mV, n = 8; *UAS-Kir2.1/MHC-Gal4* = 0.45 ± 0.11 mV, n = 12; and *Calc*^{EP}*; UAS-Kir2.1/MHC-Gal4* = 0.49 ± 0.12 mV, n = 12. (B) Quantification of the overall muscle membrane voltage that is achieved by the peak amplitude of the EPSP in control, Kir2.1-expressing and Calc/Kir2.1-expressing animals. Values are: control animals = -27 ± 1.9 mV, n = 8; *UAS-Kir2.1/MHC-Gal4* = -32 ± 3 mV, n = 12; and *Calc*^{EP}*; UAS-Kir2.1/MHC-Gal4* = -54 ± 4.4 mV, n = 12. Note the impairment of muscle depolarization in the Calc-expressing animals.

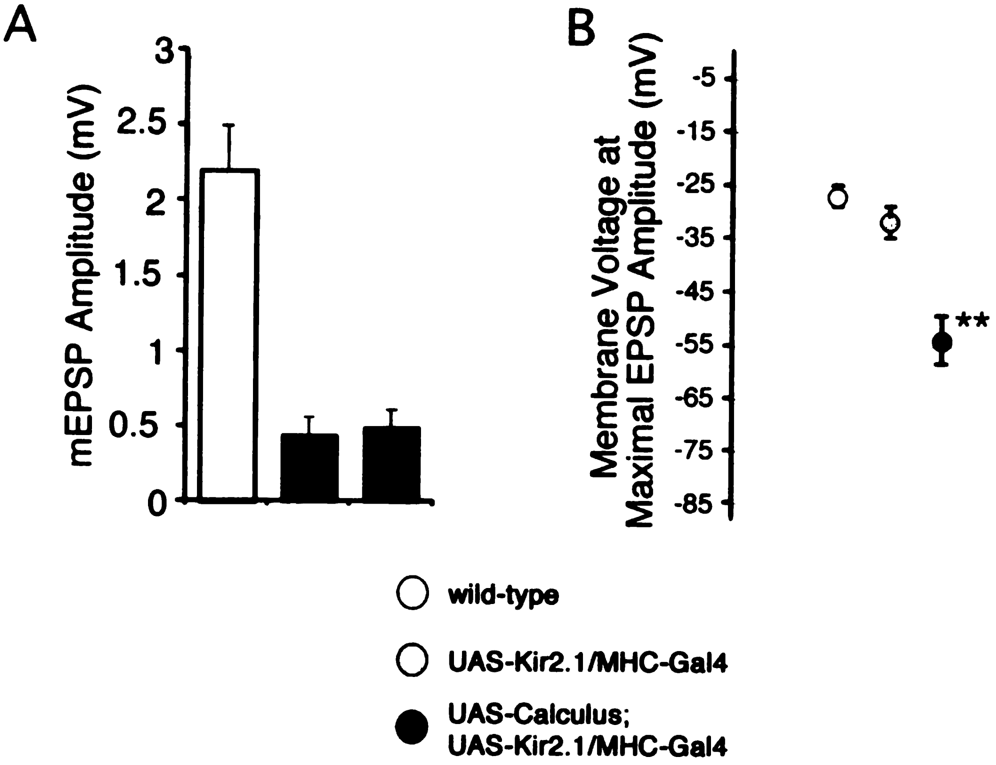
A
mEPSP Amplitude (mV)
0
0.5
1
1.5
2
2.5
3
B
Membrane Voltage at Maximal EPSP Amplitude (mV)
-5
-15
-25
-35
-45
-55
-65
-75
-85
**
○ wild-type
○ UAS-Kir2.1/MHC-Gal4
● UAS-Calculus; UAS-Kir2.1/MHC-Gal4

Figure 4-6. Calc overexpression in fat bodies completely blocks *GluRIIA*^{SP16} induced homeostasis.

Quantification of (A) quantal size and (B) quantal content in wild-type, GluRIIA null homeostatic animals and GluRIIA null animals expressing Calc in the fat body. Quantal size values are as follows: wild type = 1.1mV ± 0.06, n = 11; *GluRIIA*^{SP16} = 0.47 ± 0.03, n = 10; *Calc*^{EP}, *GluRIIA*^{SP16}; *TF060-Gal4* = 0.5mV ± 0.04, n = 8. Quantal content values are as follows: wild type = 34 ± 1.8, n = 11; *GluRIIA*^{SP16} = 79 ± 3.4, n = 10; *Calc*^{EP}, *GluRIIA*^{SP16}; *TF060-Gal4* = 41 ± 4.7, n = 8. Significance is denoted as follows (* $p < 0.1$).

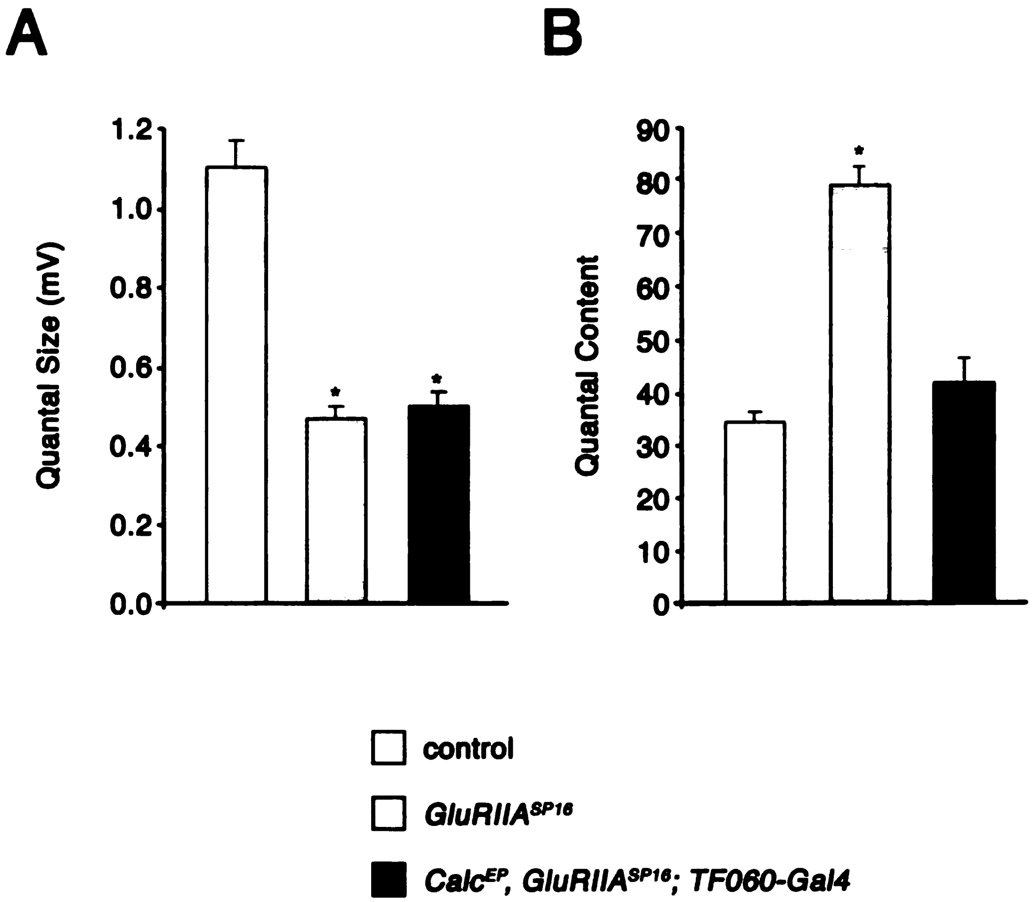
A
B
Quantal Size (mV)
1.2
1.0
0.8
0.6
0.4
0.2
0.0
*
*
Quantal Content
90
80
70
60
50
40
30
20
10
0
*
☐ control
☐ *GluRIIA^{SP16}*
■ *Calc^{EP}, GluRIIA^{SP16}; TF060-Gal4*

Figure 4-7. Calc overexpression has no morphological effect.

(A) Quantification of bouton number at the segment A2 muscle 6/7 synapse in control, GluRIIA null, and GluRIIA null animals overexpressing Calc in muscle. Values are as follows: control (*MHC-Gal4)* = 99 ± 6.7, n = 8; $Calc^{EP}$, $GluRIIA^{SP16}$ = 103 ± 3.7, n = 7; $Calc^{EP}$, $GluRIIA^{SP16}$; *MHC-Gal4* = 113 ± 5, n = 7. There is no significant different between bouton number in any of these genotypes. (B) Representative immunofluorescent images used for bouton counts. Synapses were stained with anti-nc82 (green). (C) Immunofluorescent images of single boutons in wild-type (left column) and GluRIIA null animals overexpressing Calc in muscle (right column). Boutons were stained with (top row) anti-nc82 (green) and anti-Dlg (red), and (bottom row) anti-FasII (green) and anti-GluRIII (red). All markers appear normal.

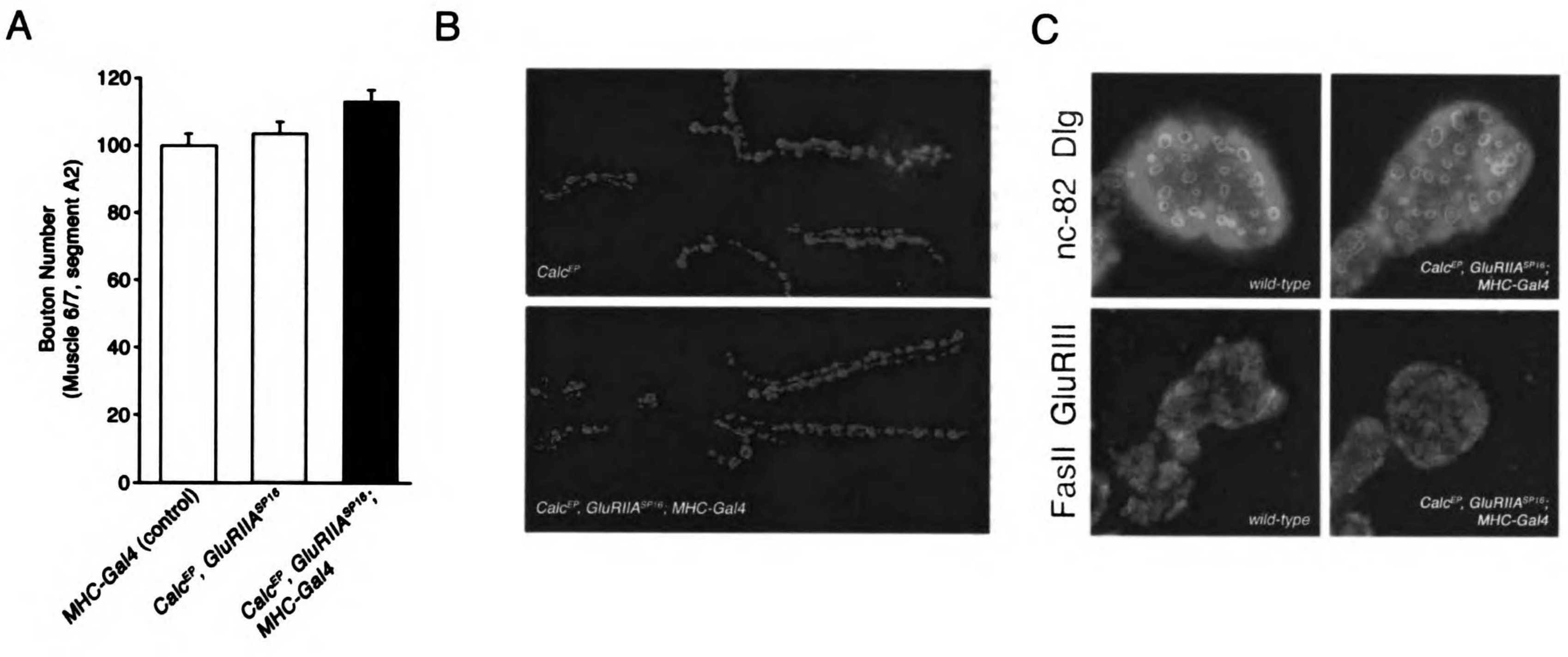
A
Bouton Number
(Muscle 6/7, segment A2)
0
20
40
60
80
100
120
MHC-Gal4 (control)
Calc^EP, GluRIIA^SP16
Calc^EP, GluRIIA^SP16; MHC-Gal4
B
Calc^EP
Calc^EP, GluRIIA^SP16; MHC-Gal4
C
nc-82 Dlg
FasII GluRIII
wild-type
Calc^EP, GluRIIA^SP16; MHC-Gal4
wild-type
Calc^EP, GluRIIA^SP16; MHC-Gal4

Chapter Five:
General Conclusions

The nervous system has an amazing capacity for change. Plasticity in the form of long-term potentiation or long-term depression, modifications to synapse morphology, and changes to the excitability of cells are all part of normal daily nervous system function. Yet despite the large capacity for plasticity, the nervous system is able to function properly within a physiological range of activity. It is clear that mechanisms exist by which the nervous system regulates synaptic efficacy such that proper synaptic function is maintained. The nervous system uses various forms of synaptic homeostasis to modify the efficacy of synaptic transmission. Understanding these mechanisms which regulate synaptic efficacy is necessary to understand how the nervous system functions.

The Drosophila NMJ has become a powerful system in which to study the mechanisms that regulate synaptic efficacy. We have only begun to scratch the surface of what molecules and signaling pathways, on both sides of the synapse, exist to regulate efficacy. In order to have a complete model of how the NMJ regulates synaptic efficacy, one needs to understand not just the signaling pathways that exist in the muscle to regulate and measure postsynaptic receptor function. One also needs to understand the signaling pathways in the neuron that regulate presynaptic neurotransmitter release.

Postsynaptic Sensor of Excitability

The two types of homeostatic paradigms discussed in Chapter 1, synaptic scaling and synaptic homeostasis via retrograde signaling, both require a postsynaptic sensor of excitability. It has been hypothesized that calcium signaling may play a role in sensing cellular excitability (Davis, 2006; Goldberg and Yuste, 2005). Calcium plays a crucial role in the excitation properties of neurons and is essential for the induction of various types of plasticity. In fact, recent studies have implicated the Calcium/calmodulin-dependent protein kinsase II (CaMKII) in synaptic homeostasis (Haghighi et al., 2003). CaMKII is highly concentrated at the NMJ and plays a role in NMJ function and development (Koh et al., 1999; Kazama et al., 2003). Haghighi et al. found that inhibiting CaMKII activity postsynaptically in muscle triggers a retrograde signal to motoneurons, leading to an increase in neurotransmitter release. Furthermore, in a GluRIIA mutant homeostatic background, overexpression of a constitutively active CaMKII leads to a partial block of the compensatory increase in neurotransmitter release. While CaMKII does appear to play a role in regulating synaptic efficacy at the Drosophila NMJ, it remains to be determined if CaMKII is acting as a monitor of muscle cell excitability or as a mediator of the retrograde signal. It would be interesting to examine if a constitutively active CaMKII can also block synaptic scaling. If CaMKII does effect synaptic scaling, CaMKII is likely acting more in the capacity of a general monitor of cellular excitability as opposed to a mediator of the retrograde signal involved in synaptic homeostasis.

Synaptic Scaling and the Regulation of Postsynaptic Receptors

Much research has been focused on identifying molecules that can modulate the abundance of postsynaptic neurotransmitter receptors (for example Bredt & Nicoll, 2003; Morishita et al., 2005). The molecular mechanisms identified could easily be co-opted by homeostatic mechanisms to regulate the increase in postsynaptic receptor quantal size during synaptic scaling. Recent work has identified one possible mechanism of synaptic scaling of NMDA receptors in cultured cortical neurons (Mu et al., 2003). Activity blockade leads to an increase in the abundance of the C2' splice form of the NMDA receptor NR1 subunit. An increase in activity leads to accumulation of the C2 variant. The C2/C2' splice event is thus activity dependant. The switch to the C2' splice form increases the rate of NMDA receptor trafficking to the membrane, by enhancing the exit of nascent receptors from the endoplasmic reticulum (ER). The C2 splice form retards ER exit. Thus, a chronic activity blockade of cortical neurons will lead to a net increase of NMDA receptor density such that synaptic efficacy is increased. It remains to be determined if a similar type of mRNA splice form regulation can regulate synaptic scaling at other synapses.

Synaptic Homeostasis and the Regulation of Presynaptic Neurotransmitter Release

While the majority of experiments demonstrating that a decrease in postsynaptic excitability can lead to an increase in presynaptic neurotransmitter release have been performed at vertebrate and Drosophila NMJs, there is some data supporting the idea that a presynaptic expression of synaptic homeostasis can occur at central neurons as well. Chronic activity blockades in hippocampal cultures lead to an increase in the size of presynaptic active zones and in the number of docked vesicles (Murthy et al., 2001). In a separate set of experiments, a block of postsynaptic AMPA receptors, also in hippocampal cultures, lead to an increase in the frequency of spontaneous vesicle release from the presynaptic neuron (Thiagarajan et al., 2005). The increase in presynaptic activity was largely due to accelerated vesicular turnover and partially due to an increase in the presynaptic vesicle pool.

There are still many unanswered questions regarding the mechanisms that underlie changes in synaptic efficacy. The hypothesis that calcium, in conjunction with CaMKII, could monitor muscle cell excitability needs to be followed up. There exist a number of sources for calcium in the Drosophila muscle including voltage gated calcium channels (Eberl et al., 1998) and ryanodine receptors (Sullivan et al., 2000). Genetic tools to study and/or alter calcium influx through these various channels should be examined in the context of homeostasis.

To address the regulation of postsynaptic receptors during synaptic scaling, mutations known to effect glutamate receptor abundance at the Drosophila NMJ, including p21-activated kinase (Pak, Chapter 2), should be placed in the FasII synaptic scaling background at the Drosophila NMJ. It is important to examine if Pak signaling is required for the increase in postsynaptic glutamate receptor function seen in response to a decrease in presynaptic innervation. In addition, it will be interesting to examine the postsynaptic subunit composition of the glutamate receptors in the FasII synaptic scaling background. While not thought to be alternatively spliced, a change in the subunit composition could account for a change in glutamate receptor sensitivity.

Finally, to dissect the retrograde signaling cascade involved in the increase in presynaptic neurotransmitter release in response to decreases in muscle excitability, a number of experimental avenues should be pursued. Localization of the site of action of the synaptic homeostasis inhibitor *calculus* (Chapter 4) must be determined. Calc is a secreted protein and identification of the receptor Calc binds to may reveal the signaling mechanisms that regulate synaptic homeostasis.

Experimental Procedures

Chapter Two: Coordinating Structural and Functional Synapse Development: Postsynaptic Pak Kinase Independently Specifies GluR Abundance and Postsynaptic Morphology

Fly Stocks

Flies were maintained at 25°C on normal food. The Pak mutants (*Pak*^{3}, *Pak*^{4}, *Pak*^{6}, *Pak*^{11}) and UAS-myristilated-Pak were a gift from Larry Zipursky (University of California, Los Angeles) and Huey Hing (University of Illinois at Urbana-Champaign). *dock*^{4} and *trio*^{P3} lines were a gift of Barry Dickson (IMP, Vienna). *Df(3R)Win*^{11}, *Df(2L)ast*^{2}, *dock*^{P1} and the Rac and Cdc42 dominant negative lines, UAS-Rac^{N17} and UAS-Cdc42^{N17}, were obtained from the Bloomington Stock Center. Wild type flies were *w*^{1118} for first-instar experiments and *yw* for third-instar experiments.

UAS-Pak^{SH} was constructed by performing site-directed mutagenesis (M504A and T566A) of a *Pak* cDNA (generous gift of Huey Hing), ligating into *pUAST*, and then transforming into the fly using standard germline transformation techniques. Mutations made were consistent with the creation of an ATP analogue-sensitive Pak allele without perturbation of wild type function (Weiss et al., 2000). As such, expression of UAS-Pak^{SH} can be used to rescue Pak expression in the *Pak* mutant background and restore Pak activity. In addition, this Pak mutation may also enable future experiments to specifically inhibit Pak kinase activity through the application of membrane permeable, inhibitory ATP analogues as done previously for *cla4* in yeast (Weiss et al., 2000).

Immunohistochemistry and Imaging

Wandering third instar larva were dissected in HL3 saline and fixed in Bouin's fixative (Sigma) for 2 minutes. For comparison of fluorescence intensities, mutant larval fillets were always stained in the same reaction tube with wild type controls, and fluorescence intensities were normalized to these wild type controls. Genotypes being directly compared were imaged identically. All images presented for comparison in this manuscript are calibrated identically.

The rabbit anti-Dock antibody (1:500) was a generous gift from Jack Dixon (University of Michigan). The rabbit anti-Pak antibody (1:500) was a gift from Larry Zipursky. The rabbit anti-Dlg antibody was a gift of Vivian Budnik (University of Massachusetts). mAb anti-GluRIIA (8B4D2, 1:10) and mAb-Dlg (1:50) were from the Developmental Studies Hybridoma Bank. TRITC conjugated anti-HRP (1:500) and secondary antibodies (1:200), FITC labeled anti-mouse and Cy5 labeled anti-rabbit, were provided by Jackson Immunoresearch Laboratories.

Images were digitally captured using a cooled CCD camera (Quantix Camera with Kodak 1401E chip) mounted on a Zeiss Axiovert 200 equipped with Nomarski and epifluorescent illumination. Images were acquired and analyzed using Slidebook software (Intelligent Imaging Innovations). Individual synapses were optically sectioned at 0.2μm (18–25 sections per synapse) using a piezo-electric driven z-drive controlling the position of a Zeiss 100x oil immersion objective. The intensity of the immunostaining was quantified as follows: A 2D projection of the maximum fluorescence at the NMJ (Muscle 4 in third-instar) was created from a series of 0.2μm synaptic sections. The average fluorescence was calculated over the entire synaptic area. For GluRIIA levels, we defined the synaptic area as delimited by HRP immunoreactivity and then averaging the GluRIIA staining intensity within this synaptic area. Anti-HRP staining recognizes presynaptic epitopes that are virtually unaffected in the Pak mutant background (Figure 1B). Axonal staining was eliminated from the analysis. The synaptic area defined by anti-HRP encompasses the vast majority of GluRIIA staining (Figure 1, merged images). Rare GluRIIA clusters that lay outside anti-HRP immunostaining were included manually. This technique was also used to quantify Pak immuno-reactivity in each mutant background. For analysis of Dlg levels, we quantified the average maximum fluorescence from the synapse delimited by Dlg. Dlg staining is present throughout the muscle membrane folds.

Electrophysiology

Wandering third instar larvae were selected after having left the food. Larvae were dissected in HL3 saline in 0.5mM Ca^{2+}. Whole muscle recordings were made from muscle 6, abdominal segment A3, of female larvae as previously described (Davis et al., 1996). Only recordings with a resting potential of at least –60mV and input resistances of at least 7 MΩ were included in our analysis. Quantal content was calculated by dividing the maximal EPSP amplitude by the average amplitude of the spontaneous miniature release events (mEPSP). Measurements of maximal EPSP and input resistance were done by hand using the cursor option in Clampfit (Axon Instruments). Measurements of spontaneous miniature release events were semiautomated using

MiniAnalysis software (Synaptosoft). For each recording 100-300 mEPSP events were averaged to determine the average mEPSP amplitude.

RNA Extraction and cDNA Preparation

Total RNA was extracted from 10 wandering third instar larvae, with CNS removed, per genotype using Trizol (Invitrogen) according to the manufacturer's instructions. For preparation of cDNA for real-time PCR analysis, 1 μl of total RNA was transcribed using an iScript cDNA Synthesis Kit (Bio-Rad).

Primer Design

Primers were designed using PrimerQuest (Integrated DNA Technologies). Each primer was designed to produce an approximately 100-bp amplicon. Primer sequences are as follows: GluRIIA forward (GACCATTTCCGAGGATGATGTGGA), GluRIIA reverse (CATCATTGGTTCGTTCACCGTTGG), RpL32 forward (CCACCAGTCGGATCGATATGCTAA) and RpL32 reverse (TTGGGCATCAGATACTGTCCCTTG).

Real-time reverse-transcription PCR (RT-PCR)

Real-time RT-PCR assays were performed using an iCycler (Bio-Rad) with SYBR-green fluorescence. Real-time PCR amplification was performed after an initial denaturation of 8 min at 95°C, followed by 50 cycles of 20 s denaturation at 95°, 30 s annealing at 60°C and 30 s extension at 72°C. Fluorescent detection was carried out at the annealing stage. The reaction was done in 50 μl using iQ SYBR Green Supermix (Bio-Rad) with 500 nM primer concentration and 1ng-1μg of cDNA. The threshold cycle was determined by the user and placed above baseline activity within the exponential increase phase. To look for changes in transcript levels in samples derived from control and experimental larvae, we compared the threshold cycles (C_t) for our genes of interest (GluRIIA) with a control housekeeping gene (RpL32) to determine ΔC_t. The difference between ΔC_t values for a wild type and mutant genotype ($\Delta\Delta C_t$) represents the degree of induction or inhibition of GluRIIA transcript. The relative value of this fold difference of induction can be determined using the equation 'fold induction' = $2^{-\Delta\Delta Ct}$. Data reported were analyzed as fold induction between mutant and wild type animals. Gene expression was measured in triplicate or duplicate for each genotype and repeated at multiple template concentrations.

Chapter Three: Imaging GluRIIA receptors using α-bungarotoxin binding site tagged receptors

Molecular biology and genetics

Flies were maintained at 25°C on normal food. Wild type flies for all experiments were *yw*.

To make an α-bungarotoxin binding site tagged GluRIIA receptor, the complementary DNA fragments encoding the 13-aa binding site (underlined) with flanking GluRIIA receptor DNA were synthesized with the following sequences (Operon): TTTATAATCATCATCGGGTTTCTGGAGGGGATTATAGCCCTTGGTGGCTGGCGCTACTACGAGAGCAGCCTGGAGCCCTACCCCGATGACGAT (sense) and CGTCATCGGGGTAGGGCTCCAGGCTGCTCTCGTAGTAGCGCCAGCCACCAAGGGCTATAATCCCCTCCAGAAACCCGATGATGATTATAAATGCA (antisense). The two fragments were annealed to each other and subcloned into the GluRIIA clone by replacing the endogenous sequence between the N-terminal *NsiI* and *PvuI* sites. The tagged GluRIIA clone with endogenous promoter sequence (generous gift of Aaron DiAntonio) was cloned into pCasper4 and then transformed into the fly using standard germline transformation techniques. The a-bungarotoxin binding site sequence chosen corresponds to a high affinity binding site as described by Katchalski-Katzir et al. 2003.

Immunohistochemistry

For GluRIIA antibody staining, wandering third instar larva were dissected in HL3 saline and fixed in Bouin's fixative (Sigma) for 2 minutes. For comparison of fluorescence intensities, mutant larval fillets were always stained in the same reaction tube with wild type controls, and fluorescence intensities were normalized to these wild type controls. Genotypes being directly compared were imaged identically. All images presented for comparison in this manuscript are calibrated identically.

mAb anti-GluRIIA (8B4D2, 1:10) was from the Developmental Studies Hybridoma Bank. FITC conjugated anti-HRP (1:500) and secondary TRITC labeled anti-mouse antibodies (1:200), were provided by Jackson Immunoresearch Laboratories.

α-bungarotoxin binding

Wandering third instar larvae were selected after having left the food. Larvae were minimally dissected in HL3-FCS saline containing 2% heat inactivated fetal calf serum (Gibco BRL-Life Technologies) and 0.5mM Ca^{2+} (Ball et al., 2003) such that only the head and tail were pinned down. Live preps were incubated with Alexa Fluor -488 conjugated α-bungarotoxin (5μg/ml) for 10 minutes (Molecular Probes), washed, and after set period of time, incubated with Alexa Fluor -594 conjugated α-bungarotoxin (5μg/ml) for 10 minutes. After washing, preps were then fixed with 4% paraformaldehyde for 8 minutes for imaging. Preps were subsequently incubated with rabbit anti-GluRIII (1:5000, gift of A. DiAntonio), mouse anti-nc82 (1:50, gift of E. Buchner) or Cy5 conjugated anti-HRP (1:500) from Jackson Immunoresearch Laboratories. Secondary antibodies (1:200) were provided by Jackson Immunoresearch Laboratories.

Imaging

Images were digitally captured using a cooled CCD camera (Quantix Camera with Kodak 1401E chip) mounted on a Zeiss Axiovert 200 equipped with Nomarski and epifluorescent illumination. Images were acquired and analyzed using Slidebook software (Intelligent Imaging Innovations). Individual synapses were optically sectioned at 0.2µm (18–25 sections per synapse) using a piezo-electric driven z-drive controlling the position of a Zeiss 100x oil immersion objective. For images in this document, a 2D projection of the maximum fluorescence at the NMJ (Muscle 4 in third-instar) was created from a series of 0.2µm synaptic sections.

Electrophysiology

Wandering third instar larvae were selected after having left the food. Larvae were dissected in HL3 saline in 0.5mM Ca^{2+}. Whole muscle recordings were made from muscle 6, abdominal segment A3, of female larvae as previously described (Davis et al., 1996). Only recordings with a resting potential of at least –60mV and input resistances of at least 6 MΩ were included in our analysis. Quantal content was calculated by dividing the maximal EPSP amplitude by the average amplitude of the spontaneous miniature release events (mEPSP). Measurements of maximal EPSP and input resistance were done by hand using the cursor option in Clampfit (Axon Instruments). Measurements of spontaneous miniature release events were semiautomated using MiniAnalysis software (Synaptosoft). For each recording 100-300 mEPSP events were averaged to determine the average mEPSP amplitude.

To examine the effect of α-bungarotoxin binding on the modified GluRIIA$^{\alpha BT}$ subunits, GluRIIA$^{\alpha BT}$ genomic rescue animals were incubated in plain saline, or saline containing Alexa Fluor-488 conjugated α-bungarotoxin (5μg/ml) for 10 minutes. Electrophysiology was performed as above.

Chapter Four: Calculus identifies a novel secreted inhibitor of synaptic homeostasis at the Drosophila NMJ

Molecular biology and genetics

Flies were maintained at 25°C on normal food. *Calc*^{EP} was a gift of Pernille Rorth. *UAS-nls.lacZ* and *TF060-Gal4 (Lsp2-Gal4)* were obtained from the Bloomington Stock Center. Wild type flies for all experiments were *yw* unless otherwise noted.

To make *calc* promoter Gal4 line, the sequence upstream of *calc* to the 3' end of the neighboring gene (CG15673), was cloned into pGATB. The *calc-Gal4* construct was then transformed into the fly using standard germline transformation techniques.

To determine the lethality associated with *calc* expression in the Kir2.1 background, the following crosses were set up:

MHC-Gal4, UAS-Kir2.1/TM6b, Tub-Gal80 x yw

MHC-Gal4, UAS-Kir2.1/TM6b, Tub-Gal80 x Calc^{EP}

To determine the percent lethality, we compared the number of progeny that contained the experimental *Kir2.1* chromosome to the number of progeny that contained the *TM6b* balancer chromosome. A 50/50 ratio of experimental to balancer chromosome containing progeny would result in a 0% lethality rate.

Immunohistochemistry

For antibody stainings, wandering third instar larva were dissected in HL3 saline and fixed for 8 minutes in 4% paraformaldehyde fixitive. For comparison of fluorescence intensities, larval fillets were always stained in the same reaction tube with wild type controls, and fluorescence intensities were normalized to these wild type controls.

Genotypes being directly compared were imaged identically. All images presented for comparison in this manuscript are calibrated identically.

mAb anti-GluRIII (1:5000) was a generous gift of A. DiAntonio. Rabbit anti-CAP (1:250) was a gift of Jae Park. Mouse anti-nc82 (1:50) was a gift of E. Buchner. Rabbit anti-5HT (1:500, Sigma), rabbit anti-GFP (1:500, Molecular Probes) and rabbit anti-dlg (1:10,000) were also used. mAb-FasII (1:10) and mAb-evenskipped (1:50) were from the Developmental Studies Hybridoma Bank. Cy5 conjugated anti-HRP (1:500) and secondary FITC and TRITC labeled antibodies (1:200) were provided by Jackson Immunoresearch Laboratories.

In situ hybridization

Whole-mount embryonic and larval body-wall preparation in situ hybridizations were performed using single-stranded digoxigenin-labeled RNA probes and AP immunochemistry essentially as described in O'Neill and Bier, 1994 .

For preparing antisense RNA probes, full length cDNA clone of the Calc-B spliceform was in vitro transcribed using T3 RNA polymerase. Control probes for the antisense strand gave no specific signal.

Histochemical detection of β-galactosidase activity

Dissected larvae were fixed in 1% glutaraldehyde in phosphate-buffered saline (PBS) pH 7.5 for 5 minutes. After X-gal staining, preps were rinsed with PBS-Triton, equilibrated in PBS:glycerol (1:1), and mounted on slides for viewing.

Imaging

NMJ images were digitally captured using a cooled CCD camera (Quantix Camera with Kodak 1401E chip) mounted on a Zeiss Axiovert 200 equipped with Nomarski and epifluorescent illumination. Images were acquired and analyzed using Slidebook software (Intelligent Imaging Innovations). Individual synapses were optically sectioned at 0.2μm (18–25 sections per synapse) using a piezo-electric driven z-drive controlling the position of a Zeiss 100x oil immersion objective. For images in this document, a 2D projection of the maximum fluorescence at the NMJ was created from a series of 0.2μm synaptic sections.

Electrophysiology

Wandering third instar larvae were selected after having left the food. Larvae were dissected in HL3 saline in 0.5mM Ca^{2+}. Whole muscle recordings were made from muscle 6, abdominal segment A3, of female larvae as previously described (Davis et al., 1996). Only recordings with a resting potential of at least –60mV and input resistances of at least 6 MΩ were included in our analysis. Quantal content was calculated by dividing the maximal EPSP amplitude by the average amplitude of the spontaneous miniature release events (mEPSP). Measurements of maximal EPSP and input resistance were done by hand using the cursor option in Clampfit (Axon Instruments). Measurements of spontaneous miniature release events were semiautomated using MiniAnalysis software (Synaptosoft). For each recording 100-300 mEPSP events were averaged to determine the average mEPSP amplitude.

Cell Culture and Western blot

cDNA encoding the *calc* gene was cloned into pMT/V5-His (Invitrogen) using *Xho* and *Kpn* restriction sites and following primers (underlined sequence corresponds to *calc* gene:

Forward 5' AGTCTAGGTACCGACATGTCGCCGAGAA 3'

Reverse 5' GTGACCTCGAGCAATCAGGACGCAG 3'

Schneider S2 cells were cultured and transformed with the pMT-Calc-V5/His construct using standard protocols as outlined by the Drosophila Expression System Manual (DES Manual 25-0190C, Invitrogen). V5-and His-tagged Calc protein was purified using Ni-NTA Agarose beads (Qiagen). For Western blots, samples were run on a 15% polyacrylamide gel. Proteins were transferred to PVDF membranes (Amersham) by electroblotting; membranes were incubated with anti-V5 (1:5000, Invitrogen) or anti-enabled (1:500, Developmental Studies Hybridoma Bank overnight at 4°C and with secondary antibody (1:1000) for 1 hour at room temperature. Visualization of protein was done using ECL Western Blotting Analysis System as specificed by the manufacturer (Amersham).

References

Albin SD, Davis GW (2004) Coordinating structural and functional synapse development: postsynaptic p21-activated kinase independently specifies glutamate receptor abundance and postsynaptic morphology. J Neurosci 24:6871-6879.

Allison DW, Chervin AS, Gelfand VI, Craig AM (2000) Postsynaptic scaffolds of excitatory and inhibitory synapses in hippocampal neurons: maintenance of core components independent of actin filaments and microtubules. J Neurosci 20:4545-4554.

Ball R, Xing B, Bonner P, Shearer J, Cooper RL (2003) Long-term in vitro maintenance of neuromuscular junction activity of Drosophila larvae. Comp Biochem Physiol A Mol Integr Physiol 134:247-255.

Bendtsen JD, Nielsen H, von Heijne G, Brunak S (2004) Improved prediction of signal peptides: SignalP 3.0. J Mol Biol 340:783-795.

Borghese L, Fletcher G, Mathieu J, Atzberger A, Eades WC, Cagan RL, Rorth P (2006) Systematic analysis of the transcriptional switch inducing migration of border cells. Dev Cell 10:497-508.

Brand AH, Perrimon N (1993) Targeted gene expression as a means of altering cell fates and generating dominant phenotypes. Development 118:401-415.

Bredt DS, Nicoll RA (2003) AMPA receptor trafficking at excitatory synapses. Neuron 40:361-379.

Budnik V, Koh YH, Guan B, Hartmann B, Hough C, Woods D, Gorczyca M (1996) Regulation of synapse structure and function by the Drosophila tumor suppressor gene dlg. Neuron 17:627-640.

Burbea M, Dreier L, Dittman JS, Grunwald ME, Kaplan JM (2002) Ubiquitin and AP180 regulate the abundance of GLR-1 glutamate receptors at postsynaptic elements in C. elegans. Neuron 35:107-120.

Cantera R, Kozlova T, Barillas-Mury C, Kafatos FC (1999) Muscle structure and innervation are affected by loss of Dorsal in the fruit fly, Drosophila melanogaster. Mol Cell Neurosci 13:131-141.

Cull-Candy SG, Miledi R, Trautmann A, Uchitel OD (1980) On the release of transmitter at normal, myasthenia gravis and myasthenic syndrome affected human end-plates. J Physiol 299:621-638.

Dalva MB, Takasu MA, Lin MZ, Shamah SM, Hu L, Gale NW, Greenberg ME (2000) EphB receptors interact with NMDA receptors and regulate excitatory synapse formation. Cell 103:945-956.

Dan I, Watanabe NM, Kusumi A (2001) The Ste20 group kinases as regulators of MAP

kinase cascades. Trends Cell Biol 11:220-230.

Daniels RH, Bokoch GM (1999) p21-activated protein kinase: a crucial component of morphological signaling? Trends Biochem Sci 24:350-355.

Davis GW (2006) Homeostatic Control of Neural Activity: From Phenomenology to Molecular Design. Annu Rev Neurosci.

Davis GW, Goodman CS (1998a) Genetic analysis of synaptic development and plasticity: homeostatic regulation of synaptic efficacy. Curr Opin Neurobiol 8:149-156.

Davis GW, Goodman CS (1998b) Synapse-specific control of synaptic efficacy at the terminals of a single neuron. Nature 392:82-86.

Davis GW, Bezprozvanny I (2001) Maintaining the stability of neural function: a homeostatic hypothesis. Annu Rev Physiol 63:847-869.

Davis GW, Schuster CM, Goodman CS (1996) Genetic dissection of structural and functional components of synaptic plasticity. III. CREB is necessary for presynaptic functional plasticity. Neuron 17:669-679.

Davis GW, DiAntonio A, Petersen SA, Goodman CS (1998) Postsynaptic PKA controls quantal size and reveals a retrograde signal that regulates presynaptic transmitter release in Drosophila. Neuron 20:305-315.

Desai CJ, Garrity PA, Keshishian H, Zipursky SL, Zinn K (1999) The Drosophila SH2-SH3 adapter protein Dock is expressed in embryonic axons and facilitates synapse formation by the RP3 motoneuron. Development 126:1527-1535.

Desai NS, Cudmore RH, Nelson SB, Turrigiano GG (2002) Critical periods for experience-dependent synaptic scaling in visual cortex. Nat Neurosci 5:783-789.

Destexhe A, Marder E (2004) Plasticity in single neuron and circuit computations. Nature 431:789-795.

DiAntonio A, Petersen SA, Heckmann M, Goodman CS (1999) Glutamate receptor expression regulates quantal size and quantal content at the Drosophila neuromuscular junction. J Neurosci 19:3023-3032.

Dickson BJ (2002) Molecular mechanisms of axon guidance. Science 298:1959-1964.

Dimarcq JL, Bulet P, Hetru C, Hoffmann J (1998) Cysteine-rich antimicrobial peptides in invertebrates. Biopolymers 47:465-477.

Eberl DF, Ren D, Feng G, Lorenz LJ, Van Vactor D, Hall LM (1998) Genetic and developmental characterization of Dmca1D, a calcium channel alpha1 subunit gene in Drosophila melanogaster. Genetics 148:1159-1169.

El-Husseini AE, Schnell E, Chetkovich DM, Nicoll RA, Bredt DS (2000) PSD-95 involvement in maturation of excitatory synapses. Science 290:1364-1368.

Fan X, Labrador JP, Hing H, Bashaw GJ (2003) Slit stimulation recruits Dock and Pak to the roundabout receptor and increases Rac activity to regulate axon repulsion at the CNS midline. Neuron 40:113-127.

Fannon AM, Colman DR (1996) A model for central synaptic junctional complex formation based on the differential adhesive specificities of the cadherins. Neuron 17:423-434.

Featherstone DE, Rushton E, Rohrbough J, Liebl F, Karr J, Sheng Q, Rodesch CK, Broadie K (2005) An essential Drosophila glutamate receptor subunit that functions in both central neuropil and neuromuscular junction. J Neurosci 25:3199-3208.

Ferrandon D, Jung AC, Criqui M, Lemaitre B, Uttenweiler-Joseph S, Michaut L, Reichhart J, Hoffmann JA (1998) A drosomycin-GFP reporter transgene reveals a local immune response in Drosophila that is not dependent on the Toll pathway. Embo J 17:1217-1227.

Fuchs S, Kasher R, Balass M, Scherf T, Harel M, Fridkin M, Sussman JL, Katchalski-Katzir E (2003) The binding site of acetylcholine receptor: from synthetic peptides to solution and crystal structure. Ann N Y Acad Sci 998:93-100.

Garrity PA, Rao Y, Salecker I, McGlade J, Pawson T, Zipursky SL (1996) Drosophila photoreceptor axon guidance and targeting requires the dreadlocks SH2/SH3 adapter protein. Cell 85:639-650.

Goda Y, Davis GW (2003) Mechanisms of synapse assembly and disassembly. Neuron 40:243-264.

Goldberg JH, Yuste R (2005) Space matters: local and global dendritic Ca2+ compartmentalization in cortical interneurons. Trends Neurosci 28:158-167.

Golowasch J, Abbott LF, Marder E (1999) Activity-dependent regulation of potassium currents in an identified neuron of the stomatogastric ganglion of the crab Cancer borealis. J Neurosci 19:RC33.

Gould AP, Elstob PR, Brodu V (2001) Insect oenocytes: a model system for studying cell-fate specification by Hox genes. J Anat 199:25-33.

Haghighi AP, McCabe BD, Fetter RD, Palmer JE, Hom S, Goodman CS (2003) Retrograde control of synaptic transmission by postsynaptic CaMKII at the Drosophila neuromuscular junction. Neuron 39:255-267.

Hall AC, Lucas FR, Salinas PC (2000) Axonal remodeling and synaptic differentiation in the cerebellum is regulated by WNT-7a signaling. Cell 100:525-535.

Hata Y, Butz S, Sudhof TC (1996) CASK: a novel dlg/PSD95 homolog with an N-terminal calmodulin-dependent protein kinase domain identified by interaction with neurexins. J Neurosci 16:2488-2494.

Henderson JT, Georgiou J, Jia Z, Robertson J, Elowe S, Roder JC, Pawson T (2001) The receptor tyrosine kinase EphB2 regulates NMDA-dependent synaptic function. Neuron 32:1041-1056.

Hing H, Xiao J, Harden N, Lim L, Zipursky SL (1999) Pak functions downstream of Dock to regulate photoreceptor axon guidance in Drosophila. Cell 97:853-863.

Huh GS, Boulanger LM, Du H, Riquelme PA, Brotz TM, Shatz CJ (2000) Functional requirement for class I MHC in CNS development and plasticity. Science 290:2155-2159.

Husi H, Ward MA, Choudhary JS, Blackstock WP, Grant SG (2000) Proteomic analysis of NMDA receptor-adhesion protein signaling complexes. Nat Neurosci 3:661-669.

Ichtchenko K, Hata Y, Nguyen T, Ullrich B, Missler M, Moomaw C, Sudhof TC (1995) Neuroligin 1: a splice site-specific ligand for beta-neurexins. Cell 81:435-443.

Irie M, Hata Y, Takeuchi M, Ichtchenko K, Toyoda A, Hirao K, Takai Y, Rosahl TW, Sudhof TC (1997) Binding of neuroligins to PSD-95. Science 277:1511-1515.

Jan LY, Jan YN (1976) L-glutamate as an excitatory transmitter at the Drosophila larval neuromuscular junction. J Physiol 262:215-236.

Kaltschmidt B, Ndiaye D, Korte M, Pothion S, Arbibe L, Prullage M, Pfeiffer J, Lindecke A, Staiger V, Israel A, Kaltschmidt C, Memet S (2006) NF-kappaB regulates spatial memory formation and synaptic plasticity through protein kinase A/CREB signaling. Mol Cell Biol 26:2936-2946.

Katchalski-Katzir E, Kasher R, Balass M, Scherf T, Harel M, Fridkin M, Sussman JL, Fuchs S (2003) Design and synthesis of peptides that bind alpha-bungarotoxin with high affinity and mimic the three-dimensional structure of the binding-site of acetylcholine receptor. Biophys Chem 100:293-305.

Kazama H, Morimoto-Tanifuji T, Nose A (2003) Postsynaptic activation of calcium/calmodulin-dependent protein kinase II promotes coordinated pre- and postsynaptic maturation of Drosophila neuromuscular junctions. Neuroscience 117:615-625.

Koh YH, Popova E, Thomas U, Griffith LC, Budnik V (1999) Regulation of DLG localization at synapses by CaMKII-dependent phosphorylation. Cell 98:353-363.

Lahey T, Gorczyca M, Jia XX, Budnik V (1994) The Drosophila tumor suppressor gene dlg is required for normal synaptic bouton structure. Neuron 13:823-835.

Li W, Fan J, Woodley DT (2001) Nck/Dock: an adapter between cell surface receptors and the actin cytoskeleton. Oncogene 20:6403-6417.

Lisman JE, Zhabotinsky AM (2001) A model of synaptic memory: a CaMKII/PP1 switch that potentiates transmission by organizing an AMPA receptor anchoring assembly. Neuron 31:191-201.

MacLean JN, Zhang Y, Johnson BR, Harris-Warrick RM (2003) Activity-independent homeostasis in rhythmically active neurons. Neuron 37:109-120.

Malinow R, Malenka RC (2002) AMPA receptor trafficking and synaptic plasticity. Annu Rev Neurosci 25:103-126.

Manser E, Huang HY, Loo TH, Chen XQ, Dong JM, Leung T, Lim L (1997) Expression of constitutively active alpha-PAK reveals effects of the kinase on actin and focal complexes. Mol Cell Biol 17:1129-1143.

Marrus SB, Portman SL, Allen MJ, Moffat KG, DiAntonio A (2004) Differential localization of glutamate receptor subunits at the Drosophila neuromuscular junction. J Neurosci 24:1406-1415{Wagh, 2006 #1432}.

Mattson MP (2005) NF-kappaB in the survival and plasticity of neurons. Neurochem Res 30:883-893.

McDonald MJ, Rosbash M (2001) Microarray analysis and organization of circadian gene expression in Drosophila. Cell 107:567-578.

Meffert MK, Chang JM, Wiltgen BJ, Fanselow MS, Baltimore D (2003) NF-kappa B functions in synaptic signaling and behavior. Nat Neurosci 6:1072-1078.

Mellitzer G, Xu Q, Wilkinson DG (2000) Control of cell behaviour by signalling through Eph receptors and ephrins. Curr Opin Neurobiol 10:400-408.

Miller KD (1996) Synaptic economics: competition and cooperation in synaptic plasticity. Neuron 17:371-374.

Morishita W, Marie H, Malenka RC (2005) Distinct triggering and expression mechanisms underlie LTD of AMPA and NMDA synaptic responses. Nat Neurosci 8:1043-1050.

Mu Y, Otsuka T, Horton AC, Scott DB, Ehlers MD (2003) Activity-dependent mRNA splicing controls ER export and synaptic delivery of NMDA receptors. Neuron 40:581-594.

Murthy VN, Schikorski T, Stevens CF, Zhu Y (2001) Inactivity produces increases in neurotransmitter release and synapse size. Neuron 32:673-682.

Newsome TP, Schmidt S, Dietzl G, Keleman K, Asling B, Debant A, Dickson BJ (2000)

Trio combines with dock to regulate Pak activity during photoreceptor axon pathfinding in Drosophila. Cell 101:283-294.

O'Riordan KJ, Huang IC, Pizzi M, Spano P, Boroni F, Egli R, Desai P, Fitch O, Malone L, Ahn HJ, Liou HC, Sweatt JD, Levenson JM (2006) Regulation of nuclear factor kappaB in the hippocampus by group I metabotropic glutamate receptors. J Neurosci 26:4870-4879.

Olofsson B, Page DT (2005) Condensation of the central nervous system in embryonic Drosophila is inhibited by blocking hemocyte migration or neural activity. Dev Biol 279:233-243.

Packard M, Koo ES, Gorczyca M, Sharpe J, Cumberledge S, Budnik V (2002) The Drosophila Wnt, wingless, provides an essential signal for pre- and postsynaptic differentiation. Cell 111:319-330.

Paradis S, Sweeney ST, Davis GW (2001) Homeostatic control of presynaptic release is triggered by postsynaptic membrane depolarization. Neuron 30:737-749.

Parnas D, Haghighi AP, Fetter RD, Kim SW, Goodman CS (2001) Regulation of postsynaptic structure and protein localization by the Rho-type guanine nucleotide exchange factor dPix. Neuron 32:415-424.

Parrini MC, Lei M, Harrison SC, Mayer BJ (2002) Pak1 kinase homodimers are autoinhibited in trans and dissociated upon activation by Cdc42 and Rac1. Mol Cell 9:73-83.

Penzes P, Beeser A, Chernoff J, Schiller MR, Eipper BA, Mains RE, Huganir RL (2003) Rapid induction of dendritic spine morphogenesis by trans-synaptic ephrinB-EphB receptor activation of the Rho-GEF kalirin. Neuron 37:263-274.

Perez-Otano I, Ehlers MD (2005) Homeostatic plasticity and NMDA receptor trafficking. Trends Neurosci 28:229-238.

Petersen SA, Fetter RD, Noordermeer JN, Goodman CS, DiAntonio A (1997) Genetic analysis of glutamate receptors in Drosophila reveals a retrograde signal regulating presynaptic transmitter release. Neuron 19:1237-1248.

Plomp JJ, van Kempen GT, Molenaar PC (1992) Adaptation of quantal content to decreased postsynaptic sensitivity at single endplates in alpha-bungarotoxin-treated rats. J Physiol 458:487-499.

Qin G, Schwarz T, Kittel RJ, Schmid A, Rasse TM, Kappei D, Ponimaskin E, Heckmann M, Sigrist SJ (2005) Four different subunits are essential for expressing the synaptic glutamate receptor at neuromuscular junctions of Drosophila. J Neurosci 25:3209-3218.

Rasse TM, Fouquet W, Schmid A, Kittel RJ, Mertel S, Sigrist CB, Schmidt M, Guzman

A, Merino C, Qin G, Quentin C, Madeo FF, Heckmann M, Sigrist SJ (2005) Glutamate receptor dynamics organizing synapse formation in vivo. Nat Neurosci 8:898-905.

Ravdin P, Axelrod D (1977) Fluorescent tetramethyl rhodamine derivatives of alpha-bungarotoxin: preparation, separation, and characterization. Anal Biochem 80:585-592.

Reiff DF, Thiel PR, Schuster CM (2002) Differential regulation of active zone density during long-term strengthening of Drosophila neuromuscular junctions. J Neurosci 22:9399-9409.

Rich MM, Lichtman JW (1989) In vivo visualization of pre- and postsynaptic changes during synapse elimination in reinnervated mouse muscle. J Neurosci 9:1781-1805.

Richman DP, Agius MA (2003) Treatment of autoimmune myasthenia gravis. Neurology 61:1652-1661.

Rorth P (1996) A modular misexpression screen in Drosophila detecting tissue-specific phenotypes. Proc Natl Acad Sci U S A 93:12418-12422.

Sandrock AW, Jr., Dryer SE, Rosen KM, Gozani SN, Kramer R, Theill LE, Fischbach GD (1997) Maintenance of acetylcholine receptor number by neuregulins at the neuromuscular junction in vivo. Science 276:599-603.

Sanes JR, Lichtman JW (1999) Development of the vertebrate neuromuscular junction. Annu Rev Neurosci 22:389-442.

Sanes JR, Lichtman JW (2001) Induction, assembly, maturation and maintenance of a postsynaptic apparatus. Nat Rev Neurosci 2:791-805.

Scheiffele P, Fan J, Choih J, Fetter R, Serafini T (2000) Neuroligin expressed in nonneuronal cells triggers presynaptic development in contacting axons. Cell 101:657-669.

Schmucker D, Clemens JC, Shu H, Worby CA, Xiao J, Muda M, Dixon JE, Zipursky SL (2000) Drosophila Dscam is an axon guidance receptor exhibiting extraordinary molecular diversity. Cell 101:671-684.

Schuster CM, Davis GW, Fetter RD, Goodman CS (1996) Genetic dissection of structural and functional components of synaptic plasticity. I. Fasciclin II controls synaptic stabilization and growth. Neuron 17:641-654.

Schwabe T, Bainton RJ, Fetter RD, Heberlein U, Gaul U (2005) GPCR signaling is required for blood-brain barrier formation in drosophila. Cell 123:133-144.

Sekine-Aizawa Y, Huganir RL (2004) Imaging of receptor trafficking by using alpha-

bungarotoxin-binding-site-tagged receptors. Proc Natl Acad Sci U S A 101:17114-17119.

Sheng M, Pak DT (1999) Glutamate receptor anchoring proteins and the molecular organization of excitatory synapses. Ann N Y Acad Sci 868:483-493.

Shi S, Hayashi Y, Esteban JA, Malinow R (2001) Subunit-specific rules governing AMPA receptor trafficking to synapses in hippocampal pyramidal neurons. Cell 105:331-343.

Song J, Wu L, Chen Z, Kohanski RA, Pick L (2003) Axons guided by insulin receptor in Drosophila visual system. Science 300:502-505.

Speese SD, Trotta N, Rodesch CK, Aravamudan B, Broadie K (2003) The ubiquitin proteasome system acutely regulates presynaptic protein turnover and synaptic efficacy. Curr Biol 13:899-910.

Stellwagen D, Malenka RC (2006) Synaptic scaling mediated by glial TNF-alpha. Nature 440:1054-1059.

Sullivan KM, Scott K, Zuker CS, Rubin GM (2000) The ryanodine receptor is essential for larval development in Drosophila melanogaster. Proc Natl Acad Sci U S A 97:5942-5947.

Takasu MA, Dalva MB, Zigmond RE, Greenberg ME (2002) Modulation of NMDA receptor-dependent calcium influx and gene expression through EphB receptors. Science 295:491-495.

Tessier-Lavigne M, Goodman CS (1996) The molecular biology of axon guidance. Science 274:1123-1133.

Thiagarajan TC, Lindskog M, Tsien RW (2005) Adaptation to synaptic inactivity in hippocampal neurons. Neuron 47:725-737.

Tingvall TO, Roos E, Engstrom Y (2001) The GATA factor Serpent is required for the onset of the humoral immune response in Drosophila embryos. Proc Natl Acad Sci U S A 98:3884-3888.

Turrigiano GG (1999) Homeostatic plasticity in neuronal networks: the more things change, the more they stay the same. Trends Neurosci 22:221-227.

Turrigiano GG, Nelson SB (2004) Homeostatic plasticity in the developing nervous system. Nat Rev Neurosci 5:97-107.

Turrigiano GG, Leslie KR, Desai NS, Rutherford LC, Nelson SB (1998) Activity-dependent scaling of quantal amplitude in neocortical neurons. Nature 391:892-896.

Tzou P, De Gregorio E, Lemaitre B (2002) How Drosophila combats microbial infection: a model to study innate immunity and host-pathogen interactions. Curr Opin Microbiol 5:102-110.

Tzou P, Ohresser S, Ferrandon D, Capovilla M, Reichhart JM, Lemaitre B, Hoffmann JA, Imler JL (2000) Tissue-specific inducible expression of antimicrobial peptide genes in Drosophila surface epithelia. Immunity 13:737-748.

Wagh DA, Rasse TM, Asan E, Hofbauer A, Schwenkert I, Durrbeck H, Buchner S, Dabauvalle MC, Schmidt M, Qin G, Wichmann C, Kittel R, Sigrist SJ, Buchner E (2006) Bruchpilot, a protein with homology to ELKS/CAST, is required for structural integrity and function of synaptic active zones in Drosophila. Neuron 49:833-844.

Walikonis RS, Jensen ON, Mann M, Provance DW, Jr., Mercer JA, Kennedy MB (2000) Identification of proteins in the postsynaptic density fraction by mass spectrometry. J Neurosci 20:4069-4080.

Watt AJ, van Rossum MC, MacLeod KM, Nelson SB, Turrigiano GG (2000) Activity coregulates quantal AMPA and NMDA currents at neocortical synapses. Neuron 26:659-670.

Weiss EL, Bishop AC, Shokat KM, Drubin DG (2000) Chemical genetic analysis of the budding-yeast p21-activated kinase Cla4p. Nat Cell Biol 2:677-685.

Wilson RI, Nicoll RA (2001) Endogenous cannabinoids mediate retrograde signalling at hippocampal synapses. Nature 410:588-592.

Wu G, Malinow R, Cline HT (1996) Maturation of a central glutamatergic synapse. Science 274:972-976.

Wu Q, Maniatis T (1999) A striking organization of a large family of human neural cadherin-like cell adhesion genes. Cell 97:779-790.

Yu TW, Bargmann CI (2001) Dynamic regulation of axon guidance. Nat Neurosci 4 Suppl:1169-1176.

Zhang X, Poo MM (2002) Localized synaptic potentiation by BDNF requires local protein synthesis in the developing axon. Neuron 36:675-688.

Zhu MY, Wilson R, Leptin M (2005) A screen for genes that influence fibroblast growth factor signal transduction in Drosophila. Genetics 170:767-777.

Ziv NE, Garner CC (2004) Cellular and molecular mechanisms of presynaptic assembly. Nat Rev Neurosci 5:385-399.

5227R

UCSF LIBRARY

7537346

3 1378 00753 7346

For reference

Not to be taken
from the room.